



# **Wind Tunnel Investigation of the Aerodynamic Hysteresis Phenomenon on the F-4 Aircraft and its Effects on Aircraft Motion**

**J. F. Herman and E. S. Washington  
ARO, Inc.**

**September 1980**

**Final Report for Period October 1, 1978 — October 31, 1979**

Approved for public release, distribution unlimited.

**ARNOLD ENGINEERING DEVELOPMENT CENTER  
ARNOLD AIR FORCE STATION, TENNESSEE  
AIR FORCE SYSTEMS COMMAND  
UNITED STATES AIR FORCE**

## NOTICES

When U. S. Government drawings, specifications, or other data are used for any purpose other than a definitely related Government procurement operation, the Government thereby incurs no responsibility nor any obligation whatsoever, and the fact that the Government may have formulated, furnished, or in any way supplied the said drawings, specifications, or other data, is not to be regarded by implication or otherwise, or in any manner licensing the holder or any other person or corporation, or conveying any rights or permission to manufacture, use, or sell any patented invention that may in any way be related thereto.

Qualified users may obtain copies of this report from the Defense Technical Information Center.

References to named commercial products in this report are not to be considered in any sense as an indorsement of the product by the United States Air Force or the Government.

This report has been reviewed by the Office of Public Affairs (PA) and is releasable to the National Technical Information Service (NTIS). At NTIS, it will be available to the general public, including foreign nations.

## APPROVAL STATEMENT

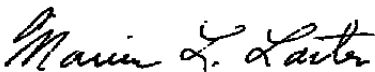
This report has been reviewed and approved.



ALVIN R. OBAL, Captain, CF  
Project Manager  
Directorate of Technology

Approved for publication:

FOR THE COMMANDER



MARION L. LASTER  
Director of Technology  
Deputy for Operations

# UNCLASSIFIED

REPORT DOCUMENTATION PAGE		READ INSTRUCTIONS BEFORE COMPLETING FORM															
1 REPORT NUMBER <b>AEDC-TR-80-10</b>	2 GOVT ACCESSION NO.	3 RECIPIENT'S CATALOG NUMBER															
4 TITLE (and Subtitle) <b>WIND TUNNEL INVESTIGATION OF THE AERO-DYNAMIC HYSTERESIS PHENOMENON ON THE F-4 AIRCRAFT AND ITS EFFECTS ON AIRCRAFT MOTION</b>		5 TYPE OF REPORT & PERIOD COVERED <b>Final Report-October 1, 1978 - October 31, 1979</b>															
7 AUTHOR(s) <b>J. F. Herman and E. S. Washington, ARO, Inc., a Sverdrup Corporation Company</b>		6 PERFORMING ORG REPORT NUMBER															
9 PERFORMING ORGANIZATION NAME AND ADDRESS <b>Arnold Engineering Development Center/DOT Air Force Systems Command Arnold Air Force Station, Tennessee 37389</b>		8 CONTRACT OR GRANT NUMBER(s)															
11 CONTROLLING OFFICE NAME AND ADDRESS <b>Arnold Engineering Development Center/DOS Air Force Systems Command Arnold Air Force Station, Tennessee 37389</b>		10 PROGRAM ELEMENT, PROJECT, TASK AREA & WORK UNIT NUMBERS <b>Program Element 65807F</b>															
14 MONITORING AGENCY NAME & ADDRESS (if different from Controlling Office)		12 REPORT DATE <b>September 1980</b>															
		13 NUMBER OF PAGES <b>92</b>															
		15 SECURITY CLASS. (of this report) <b>UNCLASSIFIED</b>															
		15a DECLASSIFICATION/DOWNGRADING SCHEDULE <b>N/A</b>															
16 DISTRIBUTION STATEMENT (of this Report)  <b>Approved for public release; distribution unlimited.</b>																	
17 DISTRIBUTION STATEMENT (of the abstract entered in Block 20, if different from Report)																	
18 SUPPLEMENTARY NOTES  <b>Available in Defense Technical Information Center (DTIC).</b>																	
19 KEY WORDS (Continue on reverse side if necessary and identify by block number) <table style="width: 100%; border: none;"> <tr> <td style="width: 33%;">hysteresis</td> <td style="width: 33%;">aerodynamic forces</td> <td style="width: 33%;">leading edges</td> </tr> <tr> <td>wind tunnel tests</td> <td>moments</td> <td></td> </tr> <tr> <td>computerized simulation</td> <td>F-4 aircraft</td> <td></td> </tr> <tr> <td>degrees of freedom</td> <td>scale models</td> <td></td> </tr> <tr> <td>static loading</td> <td>stores</td> <td></td> </tr> </table>			hysteresis	aerodynamic forces	leading edges	wind tunnel tests	moments		computerized simulation	F-4 aircraft		degrees of freedom	scale models		static loading	stores	
hysteresis	aerodynamic forces	leading edges															
wind tunnel tests	moments																
computerized simulation	F-4 aircraft																
degrees of freedom	scale models																
static loading	stores																
20 ABSTRACT (Continue on reverse side if necessary and identify by block number) <p>A wind tunnel test program and an analytical study were conducted to investigate aerodynamic hysteresis phenomena on the F-4 aircraft. The wind tunnel test was conducted in the Arnold Engineering Development Center (AEDC) Aerodynamic Wind Tunnel (4T) to investigate the source of aerodynamic hysteresis in static aerodynamic data. The wind tunnel test also provided data that were used in a motion simulation study of the effect of hysteresis</p>																	

# UNCLASSIFIED

# UNCLASSIFIED

## 20. ABSTRACT (Continued)

on predicted aircraft motion. Static longitudinal and lateral directional force and moment data and wing pressure data were obtained on a 0.05-scale model (without pylons or external stores) with various simulated leading-edge slats. These data include the effects of Mach number, angle of attack, model movement, and time dependence on the aerodynamic hysteresis characteristics. Data are presented for the Mach number range from 0.7 to 0.95 at angles of attack from -4 to 24 deg at zero deg sideslip angle and for sideslip angles from -12 to 12 deg at angles of attack of 5, 10, 15, and 20 deg. Six-degrees-of-freedom motion simulation studies were used to assess the effect of hysteresis in the rolling-moment coefficient on the prediction of aircraft motion. Simulations of various flight maneuvers were conducted both with and without hysteresis in the aerodynamic data.

# UNCLASSIFIED

## **PREFACE**

The work reported herein was conducted by the Arnold Engineering Development Center (AEDC), Air Force Systems Command (AFSC). The results of the research were obtained by ARO, Inc., AEDC Group (a Sverdrup Corporation Company), operating contractor for AEDC, AFSC, Arnold Air Force Station, Tennessee. The AEDC project manager was Mr. Alexander F. Money. The research associated with the analysis of test data and with the development of a motion simulation computer program was conducted under ARO Project Number P32F-30C. Testing was conducted from March 27 through April 5, 1979, under ARO Project Number P41C-A3. The manuscript was submitted for publication on January 25, 1980.

## CONTENTS

	<u>Page</u>
1.0 INTRODUCTION .....	7
2.0 WIND TUNNEL TEST PROGRAM APPARATUS .....	7
2.1 Test Facility and Model Support System .....	7
2.2 Test Article .....	8
2.3 Instrumentation .....	8
3.0 TEST DESCRIPTION .....	8
3.1 Test Conditions and Procedures .....	8
3.2 Data Reduction and Corrections .....	9
4.0 TEST RESULTS AND DISCUSSION .....	10
4.1 Hysteresis Characteristics in Pitch .....	10
4.2 Hysteresis Characteristics in Yaw .....	10
4.3 Data Repeatability .....	11
4.4 Time Dependence .....	11
4.5 Flow Visualization .....	12
4.6 Effect of Simulated Leading-Edge Slats .....	12
5.0 MOTION SIMULATION STUDY DESCRIPTION .....	13
5.1 General .....	13
5.2 Aerodynamic Data .....	13
5.3 Method of Analysis .....	14
6.0 STUDY RESULTS AND DISCUSSION .....	15
6.1 General .....	15
6.2 Pull-Up Maneuver .....	15
6.3 Turning Flight .....	16
6.4 Motion Sensitivity .....	17
7.0 CONCLUDING REMARKS .....	18
REFERENCES .....	18

## ILLUSTRATIONS

### Figure

1. Details and Dimensions of the F-4C Model .....	21
2. Model Installation in Tunnel 4T .....	24
3. Hysteresis Characteristics of the Clean F-4C Model in Pitch, $\beta = 0$ deg .....	27

**Figure**

**Page**

4. Typical Wing Upper Surface Pressure Measurements, $M_\infty = 0.7$ , Increasing $\alpha$ .....	33
5. Effect of Model Pitch Direction on Wing Upper Surface Pressure Distributions, $\beta = 0$ deg .....	36
6. Hysteresis Characteristics of the Clean F-4C Model in Yaw, $M_\infty = 0.9$ .....	41
7. Hysteresis Characteristics of the Rolling-Moment Coefficient at Selected Mach Numbers, $\alpha = 15$ deg .....	42
8. Effect of Model Sideslip Direction on Wing Upper Surface Pressure Distributions, $\alpha = 15$ deg, $\beta = 2$ deg .....	49
9. Wing Upper Surface Pressure Distribution Repeatability, $M_\infty = 0.9$ , $\alpha = 15$ deg, $\beta = 0$ deg .....	54
10. Effect of Initial Model Sideslip Direction on the Hysteresis Characteristics, $M_\infty = 0.9$ , $\alpha = 15$ deg .....	57
11. Wing Upper Surface Pressure Distribution Time Dependence, with Increasing Sideslip Angle, $M_\infty = 0.9$ , $\alpha = 15$ deg, $\beta = 0$ deg .....	58
12. Effect of Previous Model Attitude History on the Wing Flow Patterns of the Clean F-4C, $M_\infty = 0.9$ , $\alpha = 15$ deg, $\beta = 2$ deg .....	59
13. Effect of Slats on Wing Upper Surface Pressure Distributions with Increasing Angle of Attack, $M_\infty = 0.9$ , $\alpha = 15$ deg .....	60
14. Effect of Outboard Slat, $S_1$ , on the Rolling-Moment Coefficient, $M_\infty = 0.9$ , $\alpha = 15$ deg .....	61
15. Effect of Outboard Slat, $S_1$ , on Wing Upper Surface Pressure Distribution, $M_\infty = 0.9$ , $\alpha = 15$ deg, $\beta = 2$ deg .....	62
16. Effect of the Magnitude of Sideslip Angle and the Direction of Model Movement on the Rolling-Moment Coefficient, $M_\infty = 0.9$ , $\alpha = 15$ deg .....	63
17. Characteristics of the Rolling-Moment Coefficient in a Hysteresis Loop, $M_\infty = 0.9$ , $\alpha = 15$ deg .....	64
18. Motion Simulation Hysteresis Logics .....	65
19. Effect of Hysteresis Logic on the Aircraft Motion — Pull-Up Maneuver from Level Flight .....	66
20. Effect of $\Delta C_{\eta_H}$ Direction on the Aircraft Motion with LOGIC 1, 3-g Turning Flight .....	74
21. Effect of $\beta_M$ on the Aircraft Motion with LOGIC 1, 3-g Turning Flight .....	78
22. Effect of $\Delta C_{\eta_H}$ Direction on the Aircraft Motion with LOGIC 2, 3-g Turning Flight .....	80

FigurePage**TABLES**

1. Configuration Identification .....	84
2. Mass, Inertia, and Dimensional Characteristics of the Full-Scale F-4 Aircraft .....	85
3. Incremental Rolling-Moment Coefficient Attributable to Hysteresis .....	86

**APPENDIX**

A. EQUATIONS OF MOTION .....	87
NOMENCLATURE .....	91



## 1.0 INTRODUCTION

The flight envelope of current fighter aircraft includes maneuvers at high angles of attack at transonic speeds. The prediction of flight characteristics for these conditions must rely on flight test or wind tunnel data that may include nonlinearities and, in some cases, hysteresis, which is defined herein as the condition of dependence of data values on the past history of the model attitude. The presence of hysteresis was once attributed to model asymmetries or discrepancies that were not present on the full-scale aircraft; however, this has since been disproved (see Ref. 1).

Hysteresis in static aerodynamic data obtained in wind tunnel tests of several fighter designs has been documented in Ref. 2. The longitudinal and lateral/directional data exhibited hysteresis loops as well as large nonzero values of coefficients at zero sideslip angles. These effects were noted in the mid-to-high angle-of-attack range (from 15 to 30 deg), primarily in the transonic Mach number range. Two of the models in Ref. 2 — a 0.05-scale model of the F-4, and a 0.0417-scale F-111 model — were chosen for further tests to study the hysteresis phenomena; these tests were conducted in the Aerodynamic Wind Tunnel (4T) of the Arnold Engineering Development Center (AEDC) Propulsion Wind Tunnel (PWT) facility and are documented in Ref. 3. To investigate the cause of hysteresis, static longitudinal and lateral/directional force and moment data and wing pressure data were obtained for the F-4 model (without pylons or external stores) and with various simulated wing leading-edge slats. These data were obtained at Mach numbers from 0.7 to 0.95. Angle of attack was varied from -2 to 24 deg at zero sideslip angle, and sideslip angle was varied from -12 to 12 deg at angles of attack of 5, 10, 15, and 20 deg. Selected data from the F-4 model test are presented and discussed.

In addition, computer-generated six-degree-of-freedom motion simulation studies were used to assess the effects of rolling-moment hysteresis on the prediction of aircraft motion. Simulations of various flight maneuvers were conducted both with and without hysteresis in the aerodynamic data. Several "logics" were developed for applying the wind tunnel data in the simulation program.

## 2.0 WIND TUNNEL TEST PROGRAM APPARATUS

### 2.1 TEST FACILITY AND MODEL SUPPORT SYSTEM

The AEDC Aerodynamic Wind Tunnel (4T) is a closed-loop, continuous-flow, variable-density tunnel in which Mach number can be varied from 0.1 to 1.3 and set at discrete Mach numbers of 1.6 and 1.96 by placing nozzle inserts over the permanent sonic nozzle. At all

Mach numbers, the stagnation pressure can be varied from 300 to 3,700 psfa. The test section measures 4 ft square by 12.5 ft long, and it has perforated walls whose porosity can be varied from 0.5 to 10 percent open. It is completely enclosed in a plenum chamber from which part of the tunnel airflow can be evacuated through the perforated walls. The model support system consists of a sector and sting attachment which has a pitch angle capability of from -8 to 27 deg with respect to the tunnel centerline and a roll capability of from -180 to 180 deg about the sting centerline. (A more complete description of the tunnel may be found in Ref. 4.)

## **2.2 TEST ARTICLE**

The test article was a 0.05-scale model of the F-4C aircraft. Details of the F-4C model are shown in Fig. 1a. The left wing of the model was constructed with static pressure orifices located at two spanwise stations on the upper surface as shown in Fig. 1b. The simulated leading-edge slats that were tested with the basic wing are shown in Fig. 1c. The outboard slat,  $S_1$ , extended from the wing leading-edge notch (BL 8.00) to BL 11.03. A mid slat,  $S_2$ , extended from BL 4.75 to BL 8.00. This slat was tested in combination with  $S_1$ . A slat designated as  $S_3$  extended from the wing/fuselage junction to the wing leading-edge notch. The leading-edge slats were attached to the basic wing; no attempt was made to simulate the actual wing leading edge with slats extended. The model/slat configurations are identified in Table 1. The model stabilator was held constant at 0 deg with respect to a waterline; the model had flow-through inlet ducts. The model installation in Tunnel (4T) is shown in Fig. 2. Free boundary-layer transition was allowed on all model components throughout the test.

## **2.3 INSTRUMENTATION**

A six-component, internal strain-gage balance was used to measure the aerodynamic forces and moments on the F-4C model. Model pressure measurements were made with use of differential pressure transducers of the Tunnel (4T) pressure system.

## **3.0 TEST DESCRIPTION**

### **3.1 TEST CONDITIONS AND PROCEDURES**

Static aerodynamic data were obtained for all configurations at Mach numbers from 0.7 to 0.95 at a constant total pressure of 1,200 psfa. The nominal test conditions were

$M_\infty$	$Re \times 10^{-6}$ , per foot
0.7	2.18
0.8	2.32
0.85	2.37
0.9	2.42
0.95	2.51

The data were obtained by varying model pitch and roll angle and by utilizing computer facilities to set the model pitch and roll angles to give the required values of angle of attack and sideslip angle at a fixed test condition. Extreme care was taken throughout the test to monitor and document the model attitude history in order to correctly interpret the results when hysteresis was present in the data.

Pitch hysteresis data are static aerodynamic data that are obtained while varying the angle of attack at a constant angle of sideslip, and yaw hysteresis data are static aerodynamic data that are obtained while varying the angle of sideslip at a constant angle of attack. For pitch polars, data were obtained as the model angle of attack was varied from the minimum to the maximum angle of attack and then returned to the minimum angle. Yaw polars, with the exception of model attitude history studies, were obtained by (1) starting the model at zero deg angle of attack and sideslip angle, (2) pitching the model to the desired angle of attack at zero sideslip angle, (3) moving the model to the maximum negative sideslip angle, (4) moving to the maximum positive sideslip angle, and (5) returning to the maximum negative sideslip angle. The arrows on some of the figures indicate direction of model movement.

### 3.2 DATA REDUCTION AND CORRECTIONS

All force and moment data presented in this report are measured body axis coefficients. Moments were referenced to FS 16.217, WL 1.55, and BL 0 (see Fig. 1a).

The angle of attack and angle of sideslip were corrected for sting and balance deflections caused by aerodynamic loads. Corrections for components of weight, normally termed static tares, were also applied to the data. The model was tested both upright and inverted to provide the data to correct for the tunnel flow angularity in the pitch plane.

## 4.0 TEST RESULTS AND DISCUSSION

### 4.1 HYSTERESIS CHARACTERISTICS IN PITCH

Figure 3 presents the longitudinal characteristics of the clean F-4C model, showing the presence of aerodynamic hysteresis. Hysteresis is present for normal-force, pitching-moment, axial-force, and rolling-moment coefficients over a wide range of angles of attack and Mach numbers (see Figs. 3a, b, c, and f). The variations of wing upper surface pressure distribution with angle of attack (with increasing  $\alpha$ ) are presented in Fig. 4 at  $M_\infty = 0.7$ . Figure 5 presents the effect of model pitch direction on wing pressure distributions (clean F-4C) for  $\alpha = 15$  deg (with the exception of  $M_\infty = 0.7$ , where  $\alpha = 14$  deg). Wing pressure distributions of the outboard section (BL 9.76) were dependent on the direction of model movement for all subsonic Mach numbers ( $M_\infty = 0.7$  through 0.95). The flow separation and reattachment characteristics were also dependent on Mach number. At the higher subsonic Mach numbers ( $M_\infty = 0.85$  to 0.95), the flow on the outboard section of the wing upper surface is completely separated at  $\alpha = 15$  deg with decreasing angle of attack as shown in Figs. 5c through e. The flow separation and reattachment were not symmetrical, as indicated by the rolling-moment coefficient (see Fig. 3f).

### 4.2 HYSTERESIS CHARACTERISTICS IN YAW

The effect of yaw angle on the lateral/directional characteristics of the clean F-4C at  $M_\infty = 0.9$  is presented in Fig. 6 for various angles of attack. Hysteresis was predominant in the rolling-moment coefficient at a 15-deg angle of attack, and the value of the rolling-moment coefficient was dependent on the previous attitude history of the model (see Fig. 6c).

The effect of Mach number on the hysteresis characteristics of the rolling-moment coefficient is shown in Fig. 7 for a model angle of attack of 15 deg. Hysteresis in the rolling-moment coefficient occurred in the transonic Mach number region from  $M_\infty = 0.80$  to 0.95; the largest effects were evident at Mach numbers of 0.85 and 0.90. Figure 8 presents the effect of the direction of model sideslip (increasing or decreasing angle) on the wing upper surface pressure distributions of the clean F-4C at  $\alpha = 15$  deg and  $\beta = 2$  deg for various Mach numbers. For increasing  $\beta$ , the initial angle was -12 deg; for decreasing  $\beta$ , the initial angle was 12 deg. At Mach numbers of 0.85 or less, the flow on the outboard section of the left wing was attached on the forward half of the wing. At  $M_\infty = 0.85$ , the rolling-moment coefficient was dependent on the direction of model movement (see Fig. 7c), while the outboard wing pressure distributions for increasing and decreasing sideslip angle were very similar (see Fig. 8c), indicating that the flow on the right wing upper surface was separated

with decreasing sideslip angle. At Mach numbers of 0.9 and 0.95, the flow was separated on the outboard section of the left wing with increasing sideslip angle. With decreasing sideslip angle (decreasing from  $\beta = 12$  deg), the flow on the outboard section of the left wing was partially reattached on the forward half of the wing (see Fig. 8d). Although the flow was separated, the wing pressure distributions at  $M_\infty = 0.9$  and 0.95 do not indicate the presence of a shock system on the wing upper surface.

### 4.3 DATA REPEATABILITY

Repeatability of the aerodynamic hysteresis on the F-4C model, including force data and wing pressure distribution data, indicates that the phenomenon is not random. Figure 9 gives an example of the wing pressure distribution repeatability at  $M_\infty = 0.9$ ,  $\alpha = 15$  deg, and  $\beta = 0$  deg with increasing sideslip angle from the maximum negative value ( $\beta = -12$  deg).

The effect of initial model sideslip direction on the hysteresis characteristics for the clean F-4C, at  $M_\infty = 0.9$ ,  $\alpha = 15$  deg, is shown in Fig. 10. The model was positioned at 0 deg angle of attack and angle of sideslip at the start of each polar. The model was then pitched to  $\alpha = 15$  deg at the start of each yaw polar, and sideslip angle was either increased or decreased from  $\beta = 0$ . Figure 10a presents the effect of the direction of model movement on the rolling-moment coefficient. The rolling-moment coefficient was similar, regardless of initial model direction. Figure 10b presents wing upper surface pressure distributions at  $\beta = 2$  deg with a positive initial model direction. The wing pressure distributions for increasing (from  $\beta = -12$  deg) or decreasing (from  $\beta = 12$  deg)  $\beta$  were the same, regardless of initial model direction when hysteresis was present (see Fig. 8d).

### 4.4 TIME DEPENDENCE

The time dependence of the aerodynamic hysteresis phenomenon of the F-4C model was also investigated. Figure 11 presents wing pressure distribution data taken at selected time intervals with tunnel conditions and model attitude held constant. These conditions were  $M_\infty = 0.9$ ,  $\alpha = 15$  deg, and  $\beta = 0$  deg, with  $\beta$  increasing from the maximum negative value ( $\beta = -12$  deg). The model was initially positioned at  $\alpha = 15$  deg,  $\beta = -12$  deg. Sideslip angle was then increased in increments of two degrees as in a normal yaw polar. When the value of sideslip angle became zero, the model attitude was held constant and data were acquired over a 10-min time interval. The measured rolling-moment coefficient was constant at  $C_l \approx -0.005$ . The wing pressure distribution did not change significantly with time, and the flow at the outboard station remained separated. For the above test condition and model attitude

history, the hysteresis phenomena was not time dependent. However, the flow may be time dependent at other angles of sideslip where the flow is either separating or reattaching (e.g., Fig. 10a,  $\beta = \pm 6$  deg).

#### 4.5 FLOW VISUALIZATION

In Fig. 12, flow visualization photographs of the clean F-4C model show the effect of the previous model attitude history on the wing flow patterns during yaw polars at  $M_\infty = 0.9$ . For the oil-flow and tuft tests, the model was positioned at  $\alpha = 15$  deg and  $\beta = -12$  deg (or  $\beta = 12$  deg) at the beginning of the yaw polar. Sideslip angle was increased (or decreased) to  $\beta = 12$  deg (or  $\beta = -12$  deg) and then returned to  $\beta = -12$  deg (or  $\beta = 12$  deg). Photographs were taken at selected angles. Figures 12a and b present oil-flow and tuft photographs, taken at  $\beta = 2$  deg, for increasing and decreasing sideslip angle, respectively. The oil-flow and tuft photographs in Fig. 12a indicate flow separation on the outboard left wing. This is confirmed by the left wing pressure distribution presented in Fig. 8d. The flow patterns of Fig. 12b and the wing pressure distributions of Fig. 8d show that with decreasing  $\beta$ , the flow has reattached on the left wing, but it is now separated on the outboard right wing. Examination of the photographs shows that asymmetric flow separation initially occurs near the leading edge of the wing inboard of the wing leading-edge notch. The hysteresis phenomenon was a result of asymmetric flow separation, which was dependent on the previous model attitude history.

#### 4.6 EFFECT OF SIMULATED LEADING-EDGE SLATS

Simulated wing leading-edge slats were tested on the basic F-4 wing. The leading-edge slats were attached to the basic wing; no attempt was made to simulate the actual wing leading edge with slats extended. Figure 13 presents a comparison of wing pressure distributions for the configurations tested at  $M_\infty = 0.9$  and  $\alpha = 15$  deg with increasing  $\alpha$ . For all configurations except the basic configuration, 1, and the configuration with outboard slats only, 6, the flow on the outboard wing panel was separated near the leading edge. A comparison of the rolling-moment coefficients for configurations 1 and 6, at  $M_\infty = 0.9$  and  $\alpha = 15$  deg, is given in Fig. 14. Hysteresis in rolling-moment coefficient was not present for Configuration 6. Figure 15 presents wing upper surface pressure distributions for configurations 1 and 6, with increasing and decreasing sideslip angle, and verifies that the flow remained attached, regardless of sideslip direction, on the wing with the outer wing panel slats. Adding the outboard slat,  $S_1$ , also affected the wing pressure distribution at the inboard station. The hysteresis appears to be caused by a wing leading-edge-related separation that originates inboard of the wing leading-edge notch and that affects the flow on the wing outer panel.

## 5.0 MOTION SIMULATION STUDY DESCRIPTION

### 5.1 GENERAL

The importance of nonlinearities in predicting aircraft motion in the high angle-of-attack regime has long been recognized. Reference 5 presents the results of a study on motion prediction of the F-5E aircraft including the effects of nonlinearities and aerodynamic hysteresis phenomena. Recently, symposiums on high angle-of-attack aerodynamics and its effect on aircraft motion prediction have been held (Refs. 6, 7, and 8). The effect of aerodynamic hysteresis on aircraft motion prediction, including wing rock, has also been investigated (Ref. 9).

The motion simulation study described herein was conducted to assess the effect of hysteresis in the static rolling-moment coefficient on the predicted motion of the F-4 aircraft. The rolling-moment coefficient was used because hysteresis was most predominant in the rolling-moment coefficient. The data for all other static aerodynamic coefficients were based on data obtained for increasing angle of attack or sideslip angle. The mass, inertia, and geometric characteristics used in this investigation for the full-scale aircraft are listed in Table 2.

### 5.2 AERODYNAMIC DATA

The present study utilized measured static force and moment aerodynamic data obtained from Refs. 2, 3, and 10. Control effectiveness data, static stability derivatives, and damping derivatives were obtained from Ref. 11; all aerodynamic data were based on a rigid airplane. The effects of angle of attack and Mach number were also included in these data. Aerodynamic data were input in table look-up form and linear interpolation was used. Incremental values of rolling-moment coefficient attributable to aerodynamic hysteresis,  $\Delta C_{Hr}$ , as a function of angle of attack and Mach number based on wind tunnel data, were also tabulated (see Table 3). Model movement studies were conducted to identify the sideslip angles at which hysteresis was present. Separate yaw polars were run in either the positive or negative direction of sideslip angle at a constant angle of attack. In either case, the model attitude history was consistent. At the start of each polar, the model was positioned at 0 deg angles of attack and sideslip. The model was then pitched to  $\alpha = 15$  deg and sideslip angle was either increased or decreased from  $\beta = 0$ . Figure 16 illustrates how the rolling-moment coefficient was affected by the magnitude of sideslip angle when the model was returned to zero sideslip at  $M_\infty = 0.9$  and  $\alpha = 15$  deg. If the sideslip angle exceeded approximately  $\pm 5$  deg, then hysteresis was present, and the rolling-moment coefficient was shown to be dependent on the direction of model movement. Also, the model was initially positioned at  $\alpha = 15$  deg and  $\beta = 12$  deg with  $M_\infty = 0.9$ ; sideslip angle was decreased to -4 deg and then

increased to 4 deg. The initial position of the model caused the rolling-moment coefficient to be on a hysteresis loop. The rolling-moment coefficient remained on the hysteresis loop when sideslip angle was increased to  $\beta = 4$  deg from  $\beta = -4$  deg, as shown in Fig. 17.

### 5.3 METHOD OF ANALYSIS

The differential equations of motion are presented in Section 1.0 of the appendix. Also presented are equations defining parameters required by the six-degree-of-freedom equations. Two logics (LOGIC 1 and LOGIC 2) were formulated to characterize the rolling-moment coefficient data based on results of model movement studies and published motion simulation studies (Refs. 5 and 9). The model movement studies showed that the hysteresis characteristics of the static rolling-moment coefficient were such that the resulting  $\Delta C_{tH}$  was in a counterclockwise sense.

LOGIC 1 was used to determine whether hysteresis was present, based on the magnitude of the aircraft sideslip angle. Figure 18a, with a counterclockwise path, illustrates how  $\Delta C_{tH}$  was applied for LOGIC 1 with increasing  $\beta$  from the initial trimmed condition at point 1. If  $\beta$  exceeded the positive value of  $\beta_M$  (point 2),  $\Delta C_{tH}$  was added to the basic rolling-moment coefficient (point 3) and remained in effect until the value of  $\beta$  decreased to less than the negative value of  $\beta_M$  (point 4);  $\Delta C_{tH}$  was subtracted from the basic rolling-moment coefficient (point 5) and remained in effect until the value of  $\beta$  increased to a value greater than the positive value of  $\beta_M$  (point 6). The resulting path is hereafter referred to as LOGIC 1, counterclockwise path. Similarly, for decreasing  $\beta$  (LOGIC 1, counterclockwise path), the resulting path would be the point sequence 1-2-5-6-3-4.

LOGIC 2 was used to determine whether an increment of rolling-moment coefficient attributable to hysteresis was present, based on whether the magnitude of  $\beta_M$  was exceeded and whether its sign was dependent on the sign of the  $\dot{\beta}$  term. Figure 18b shows how  $\Delta C_{tH}$  was applied to the basic rolling-moment coefficient, thus resulting in a counterclockwise path. For LOGIC 2, if the magnitude of  $\beta_M$  was exceeded, then  $\Delta C_{tH}$  was applied through the maneuver, and the value of the rolling-moment coefficient jumped directly from the increasing  $\beta$  path to the decreasing  $\beta$  path as  $\dot{\beta}$  changed sign.

Additional logics were developed to apply  $\Delta C_{tH}$  clockwise for LOGIC 1 and LOGIC 2 as shown in Figs. 18a and b, respectively.

For the analytical simulations, the initial flight conditions were specified and the control deflections and thrust were determined to obtain trimmed flight. A control surface was then moved to begin the maneuver. The computer program was numerically integrated with time



by using a Runge-Kutta integration algorithm (Ref. 12) to predict a few initial points. After these initial points were generated, an Adams-Moulton predictor-corrector integration algorithm was used for the numerical integration at each subsequent time step. Both algorithms used a fixed time step of 0.01 sec. The computer program was written so that any of the logics described previously could be applied with the option of the absence of hysteresis effects. An examination of the computed motions for each logic, when compared to the case without hysteresis effects, indicated the effects of hysteresis.

## 6.0 STUDY RESULTS AND DISCUSSION

The primary area of investigation was aircraft maneuvers at transonic Mach numbers. Because aerodynamic hysteresis was most predominant at  $M_\infty = 0.9$ , this Mach number was used as one of the initial trimmed flight conditions for the maneuvers described in the following sections. Other flight conditions included level and 3-g turning flight. Calculated time histories were plotted with use of a 0.25-sec time interval.

### 6.1 GENERAL

Flight motion simulation studies were performed with use of the F-4C aircraft characteristics given in Table 2. The thrust and control surface deflections required for trimmed flight at an altitude of 30,000 ft and at a Mach number of 0.9 were obtained by using the aerodynamic data described in Section 5.2. For the 3-g turning flight condition, it was assumed that trimmed thrust could be obtained.

Control surface deflections for the pull-up maneuver were a stabilator ramp of -3 deg from the trimmed stabilator setting at -1 deg/sec from time equal 0 to 3 sec. The stabilator was then held constant for the duration of the maneuver. A rudder doublet of  $\pm 10$  deg with a rudder deflection rate of  $\pm 20$  deg/sec was then performed to excite the motion in the lateral plane. For turning flight, the control surface perturbation was a rudder doublet of  $\pm 10$  deg from the trim rudder setting with a deflection rate of  $\pm 20$  deg/sec to excite motion in the lateral plane.

The resulting time histories of the aircraft motion were analyzed to assess the effect of hysteresis in the static rolling-moment coefficient on predicted motion. A value of  $|\beta_M| = 5$  was used for all analyses except the  $\beta_M$  study.

### 6.2 PULL-UP MANEUVER

Figure 19 compares the effects of hysteresis logic on the aircraft motion (including the case without hysteresis) during a pull-up maneuver with a rudder doublet. Figure 19a shows

a time history of Mach number, and Figs. 19b, c, and d present angle of attack, sideslip angle, and roll angle, respectively. As expected, the aircraft slows down and angle of attack is increased for all logics. The application of LOGIC 1, with a counterclockwise  $\Delta C_{rH}$ , does not result in any significant change in the sideslip angle time history, compared to the case without hysteresis, but there is significant change in the roll angle time history (see Fig. 19d). This change in roll angle time history results from the hysteresis which is present from time  $\approx 5$  to  $\approx 10$  sec, when Mach number becomes less than 0.7 ( $\beta_M < -5$  deg,  $\alpha > 5$  deg,  $M_\infty > 0.7$ ; see Table 5). The roll-off in the negative direction is a result of being on the lower side of the hysteresis loop.

The use of LOGIC 1 with a clockwise direction results in an increase of sideslip and roll angle, compared to the case without hysteresis, between time equals 6 and 12 sec; this increase results from  $\beta$ 's exceeding  $\pm 5$  deg, which results in switching sides of the hysteresis loop. The roll-off in the positive direction results from being on the upper side of the hysteresis loop until Mach number decreases to less than 0.7, at which point no hysteresis is present.

Applying LOGIC 2 with a counterclockwise direction results in a decrease in sideslip angle oscillation and a change in the roll angle time history, compared to the case without hysteresis. This clockwise application of LOGIC 2 results in an increase in sideslip and roll angles, compared to the case having no hysteresis. In addition, the roll angle oscillation between time equal 6 and 11 sec increases because  $\Delta C_{rH}$  changes signs as  $\beta$  changes sign. The sideslip angle oscillates until Mach number decreases to below 0.7, at which hysteresis is absent in the rolling-moment coefficient.

### 6.3 TURNING FLIGHT

Flight motions were calculated by applying a rudder doublet for the aircraft initially trimmed in a 3-g turn. Figure 20 gives a comparison of the effects of how  $\Delta C_{rH}$  is applied with LOGIC 1 on the predicted aircraft motion. Traces of the calculated Mach number, the angle of attack, and the sideslip and roll angles are presented for both the cases of counterclockwise, and clockwise applications of  $\Delta C_{rH}$  and the case without hysteresis. The Mach number and angle of attack for the first 6 sec are similar. After 6 sec, for the counterclockwise case, the Mach number decreased more rapidly in comparison to the case without hysteresis, while angle of attack increased until time equaled approximately 15 sec. Beyond 15 sec, the angle of attack decreased. With clockwise application of  $\Delta C_{rH}$ , the Mach number again decreased more rapidly and the angle of attack continued to increase to an angle for which accurate data were not available,  $\gamma$ , and the calculation was discontinued. The overall sideslip and roll angle characteristics are changed significantly. The roll-off in the negative direction is a result of being on the lower side of the hysteresis loop.

The wind tunnel test results indicate that the hysteresis characteristics of the rolling-moment coefficient were such that the coefficient tended to remain on the upper or lower portion of the loop, depending on the direction of model movement and the magnitude of the sideslip angle (see Figs. 16 and 17). Based on the wind tunnel results (discussed in Section 4.7) a value of  $|\beta_M| = 5$  deg was used for the basic study. The resulting calculated motion with LOGIC 1 is a roll-off, with the direction dependent upon on which side of the hysteresis loop the simulation ended. Flight motions were calculated for a reduced value of  $\beta_M$  with LOGIC 1. Figure 21 compares the calculated motions with the counterclockwise and clockwise applications of  $\Delta C_{rH}$  for  $|\beta_M| = 5$  and 2 deg. For the counterclockwise case (Fig. 21a), there are significant differences in all of the parameters ( $M_\infty$ ,  $\alpha$ ,  $\beta$ ,  $\varphi$ ), with the roll angle dependent upon on which side of the hysteresis loop the simulation ended. In the clockwise case (Fig. 21b) with  $|\beta_M| = 2$  deg, the presence of hysteresis caused oscillations in sideslip and roll angle, while for the clockwise application with  $|\beta_M| = 5$  deg, the hysteresis caused a roll-off in the negative direction. A comparison of the calculated motions using LOGIC 1 (with both counterclockwise and clockwise application of  $\Delta C_{rH}$ ) and the effect of the magnitude of  $\beta_M$  clearly demonstrates the importance of how static aerodynamic hysteresis is interpreted and applied in motion simulation calculations. It should be remembered that the static wind tunnel data show that hysteresis was present with a counterclockwise direction and that the magnitude of  $|\beta_M|$  was approximately 5 deg (see Fig. 10).

LOGIC 2 is used in additional flight motion calculations in which the sign of  $\Delta C_{rH}$  is dependent on the sign of  $\dot{\beta}$  once  $|\beta_M|$  has been exceeded. A comparison of the effect of how  $\Delta C_{rH}$  is applied with LOGIC 2 on the predicted aircraft motion is given in Fig. 22. A comparison of the case without hysteresis and the case of counterclockwise application of  $\Delta C_{rH}$  reveals the following: For the case with hysteresis present, the Mach number decreased more rapidly as the angle of attack tended to increase more rapidly to approximately 12 deg at time equal to 11 seconds. There were significant differences in the sideslip and roll damping, as hysteresis caused increased damping. Comparing the case without hysteresis and the case of the clockwise application of  $\Delta C_{rH}$  shows the following: For the case with hysteresis, the Mach number tended to remain near the initial condition ( $M_\infty = 0.9$ ), while the angle of attack, sideslip angle, and roll angle oscillated with significantly reduced damping.

#### 6.4. MOTION SENSITIVITY

The analysis described in the previous sections was based on a six-degree-of-freedom motion simulation computer program that was modified to include aerodynamic hysteresis in the static rolling-moment coefficient. The initial analysis was made with use of LOGIC 1

and LOGIC 2 with a counterclockwise application of  $\Delta C_{tH}$ . This counterclockwise direction was based on static wind tunnel test data; the application of  $\Delta C_{tH}$  resulted in increased yaw and roll damping. Clockwise application of  $\Delta C_{tH}$  resulted in hysteresis-induced motion.

## 7.0 CONCLUDING REMARKS

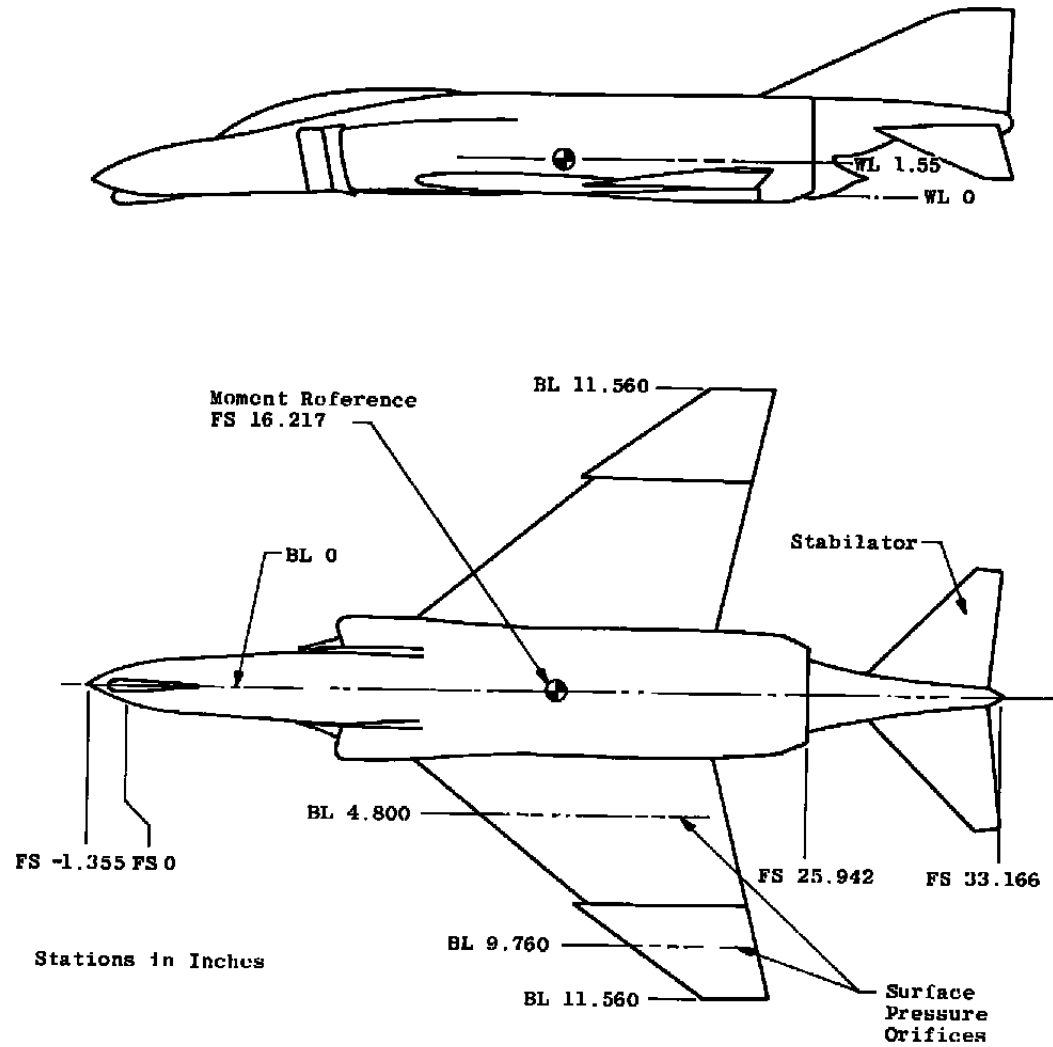
In this investigation of the effects of the hysteresis phenomenon with the F-4, the following were observed:

1. The results of wind tunnel tests with a 0.05-scale F-4 model showed that aerodynamic hysteresis was present in the static longitudinal and lateral/directional data. Hysteresis occurred primarily in the rolling-moment coefficient but was also present in the pitching-moment and normal-force coefficients. The static aerodynamic characteristics were dependent on the model attitude history and were repeatable for identical  $\alpha/\beta$  sweeps in the wind tunnel.
2. The hysteresis phenomenon exhibited in the aerodynamic data was reflected in the flow over the wing of the F-4 model.
3. Flight motion simulations in which the hysteresis characteristics of the rolling-moment coefficient were modeled on the direction of the static wind tunnel data produced indications of increases in yaw and roll damping.
4. Flight motion simulations with the hysteresis characteristics of the rolling-moment coefficient modeled against the direction of the static wind tunnel data resulted in hysteresis-induced oscillating motion with decreases in yaw and roll damping.
5. Based on the preceding two observations, it can be concluded that flight simulations using limited static wind tunnel data can be misleading, particularly in regard to hysteresis effects associated with the rolling-moment coefficient.

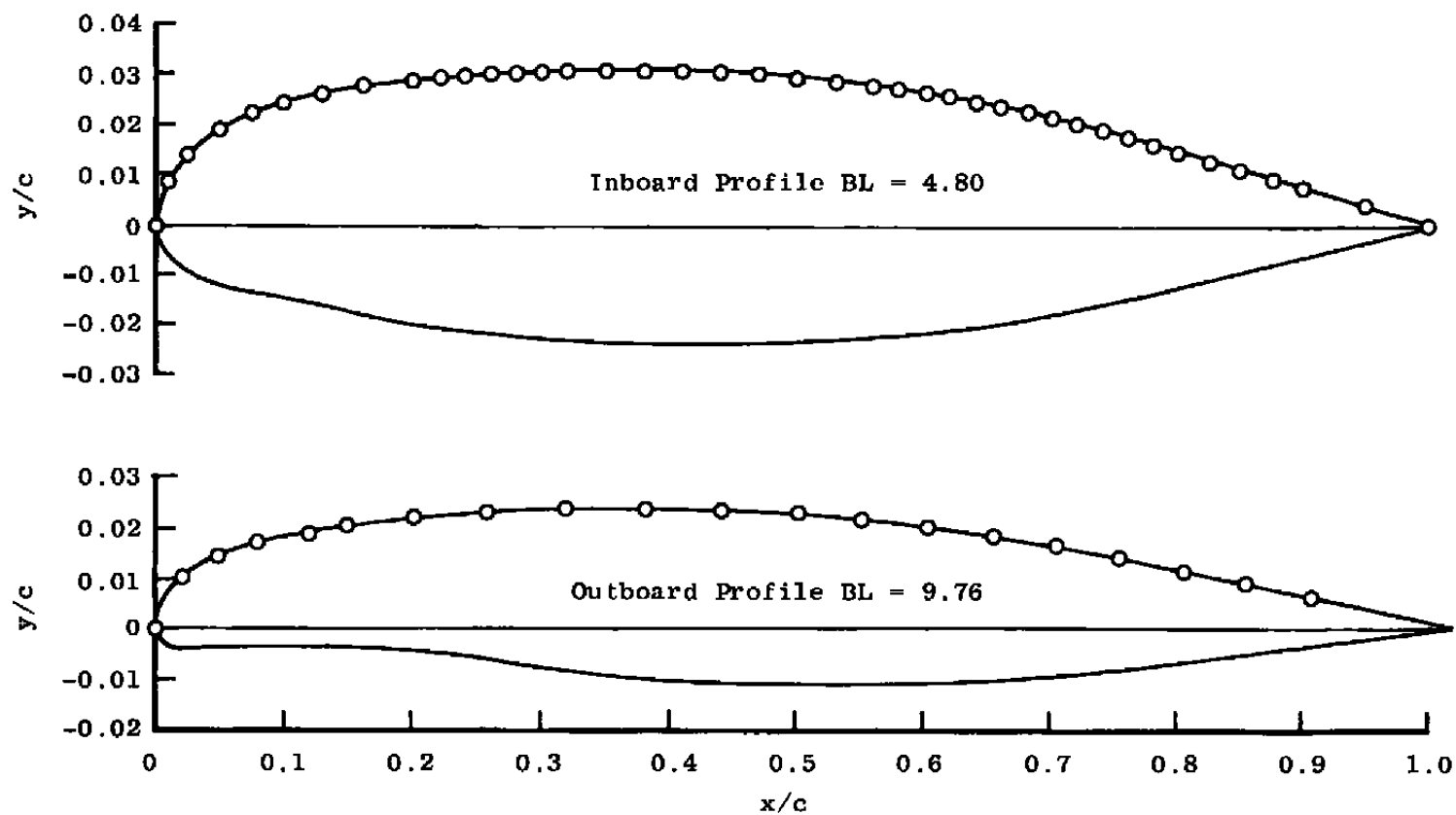
## REFERENCES

1. Titiriga, A., Jr., Ackerman, J. S., and Skow, A. M. "Design Technology for Departure Resistance of Fighter Aircraft." In *AGARD Conference Proceedings No. 199 on Stall/Spin Problems of Military Aircraft*. Papers presented at the Flight Mechanics Panel Specialists' Meeting, von Karman Institute, Rhode Saint Genese, Belgium, November 18—21, 1975. June 1976.

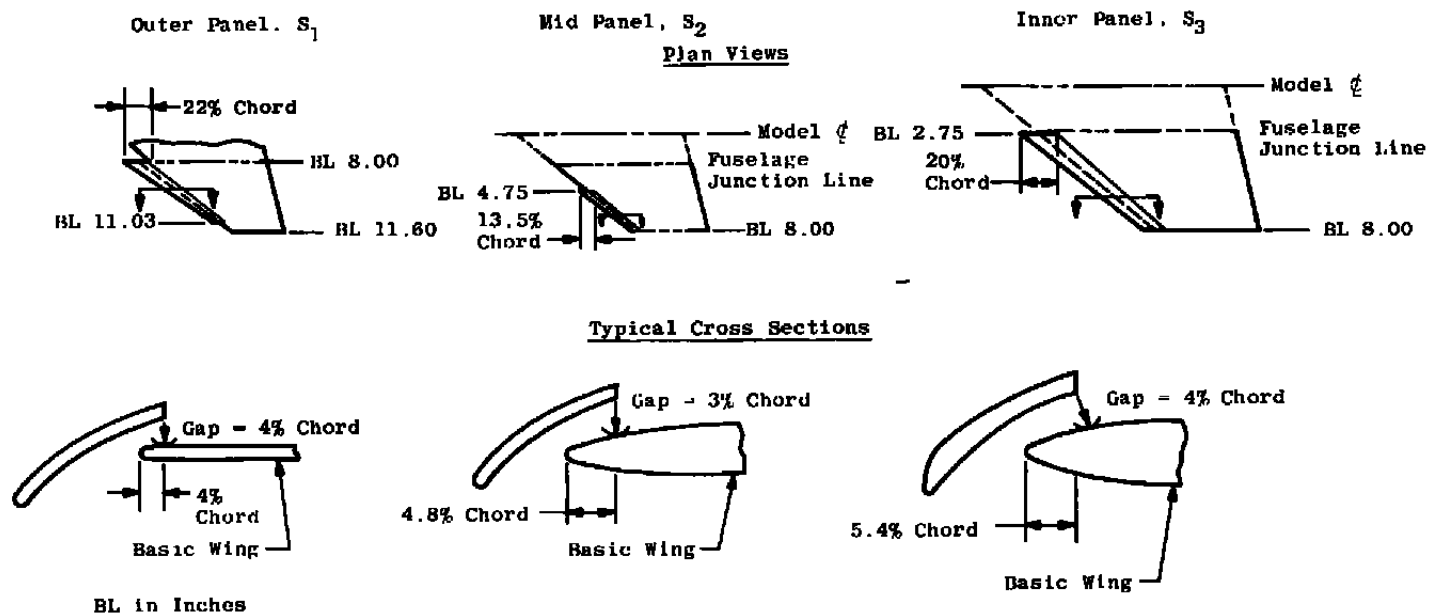
2. Herman, J. F. "Wind Tunnel Measurements of Hysteresis in the Static Aerodynamic Characteristics of Aircraft." AEDC-TR-79-47 (ADB040999L), September 1979.
3. Herman, Joseph F. "Wind Tunnel Test to Investigate Aerodynamic Hysteresis Phenomena of the F-4 and F-111 Aircraft Models." AEDC-TSR-79-P27, May 1979.
4. *Test Facilities Handbook*. Eleventh edition. "Propulsion Wind Tunnel Facility, Vol. 4." Arnold Engineering Development Center, Arnold Air Force Station, Tennessee, June 1979.
5. Cord, Thomas J. "Hysteresis Induced Wing Rock." AFDL-TM-75-76-FGC, June 1975.
6. *AGARD Conference Proceedings No. 199 on Stall/Spin Problems of Military Aircraft*. June 1976.
7. *AGARD Conference Proceedings No. 235 on Dynamic Stability Parameters*. Papers presented at the Fluid Dynamics Panel Symposium, Athens, Greece, May 22—24, 1978. November 1978.
8. *AGARD Conference Proceedings No. 247 on High Angle of Attack Aerodynamics*. Papers presented at the Fluid Dynamics Panel Symposium, Sandefjord, Norway, October 4—6, 1978. January 1979.
9. Schmidt, L. V. "Wing Rock Due to Aerodynamic Hysteresis." *Journal of Aircraft*, Vol. 16, No. 3, March 1979, pp. 129-133.
10. Ray, Edward J. and Hollingsworth, Eddie G. "Subsonic Characteristics of a Twin-Jet Swept-Wing Fighter Model with Maneuvering Devices." NASA TN-D-6921, January 1973.
11. "Model F/RF-4B-C Aerodynamic Derivatives." McDonnell Aircraft Corporation Report 9842. Revised December 10, 1971.
12. Diesel, John W., Taylor, Javin M., Culver, Calvin O., Davies, John H., Cramer, William P. "Modularized Six-Degree-of-Freedom (MOD6DF) Computer Program. Vols. 1 and 2." Litton Systems, Inc., Guidance and Control System Division, Woodland Hills, California.



a. General arrangement  
 Figure 1. Details and dimensions of the F-4C model.

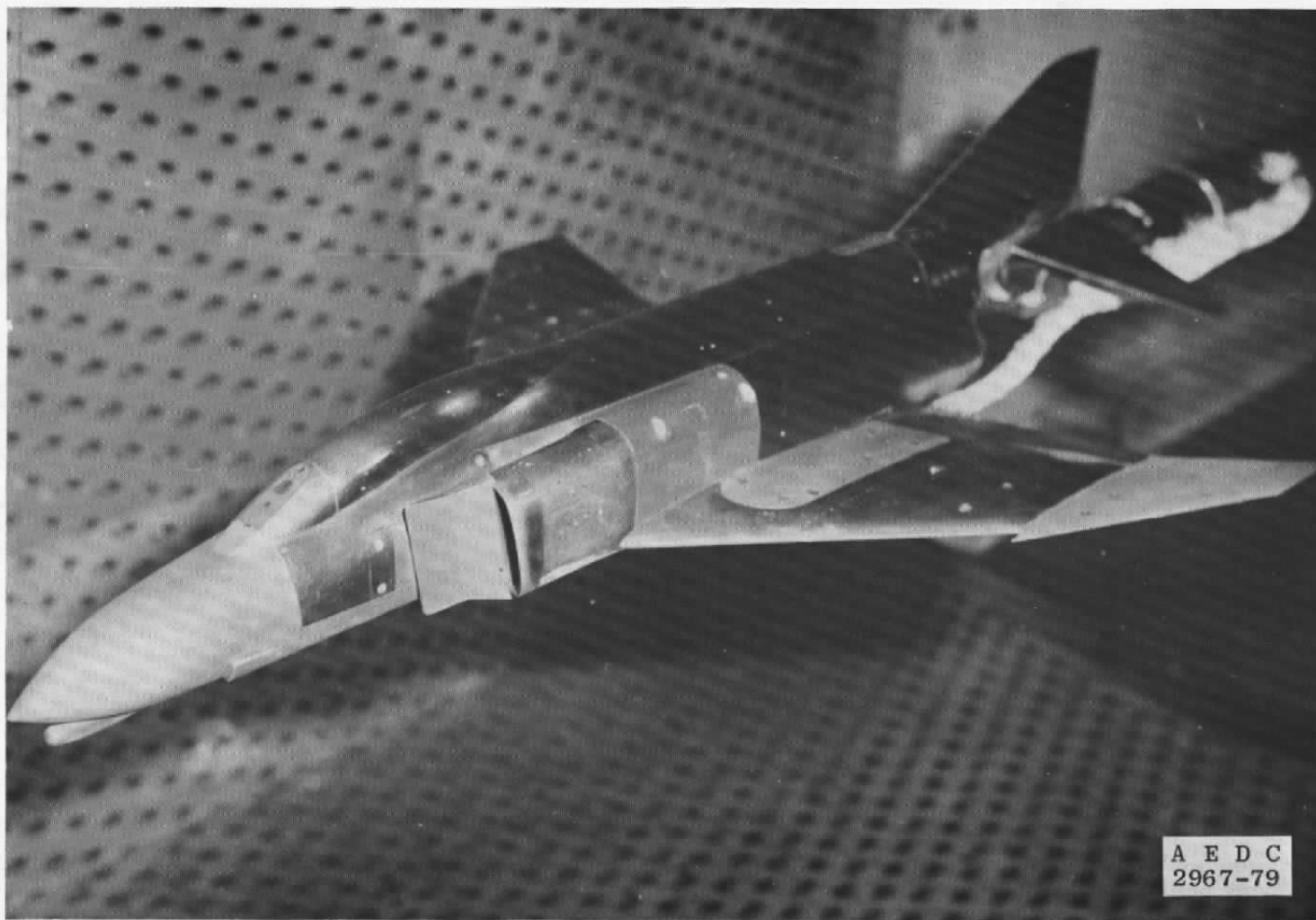


b. Wing cross section of pressure orifice locations  
Figure 1. Continued.

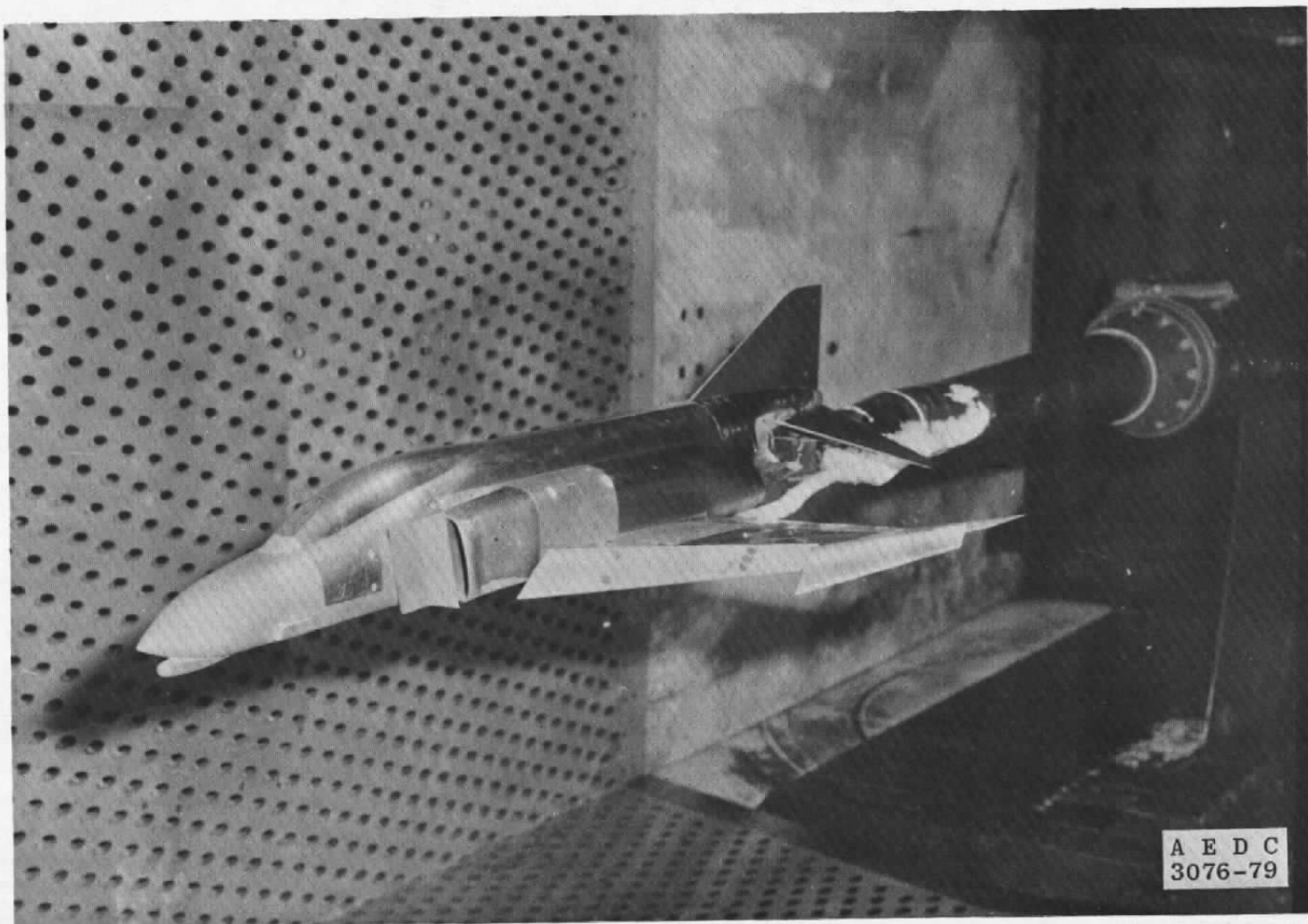


c. Simulated leading-edge slats: plan views and  
typical cross sections  
Figure 1. Concluded.

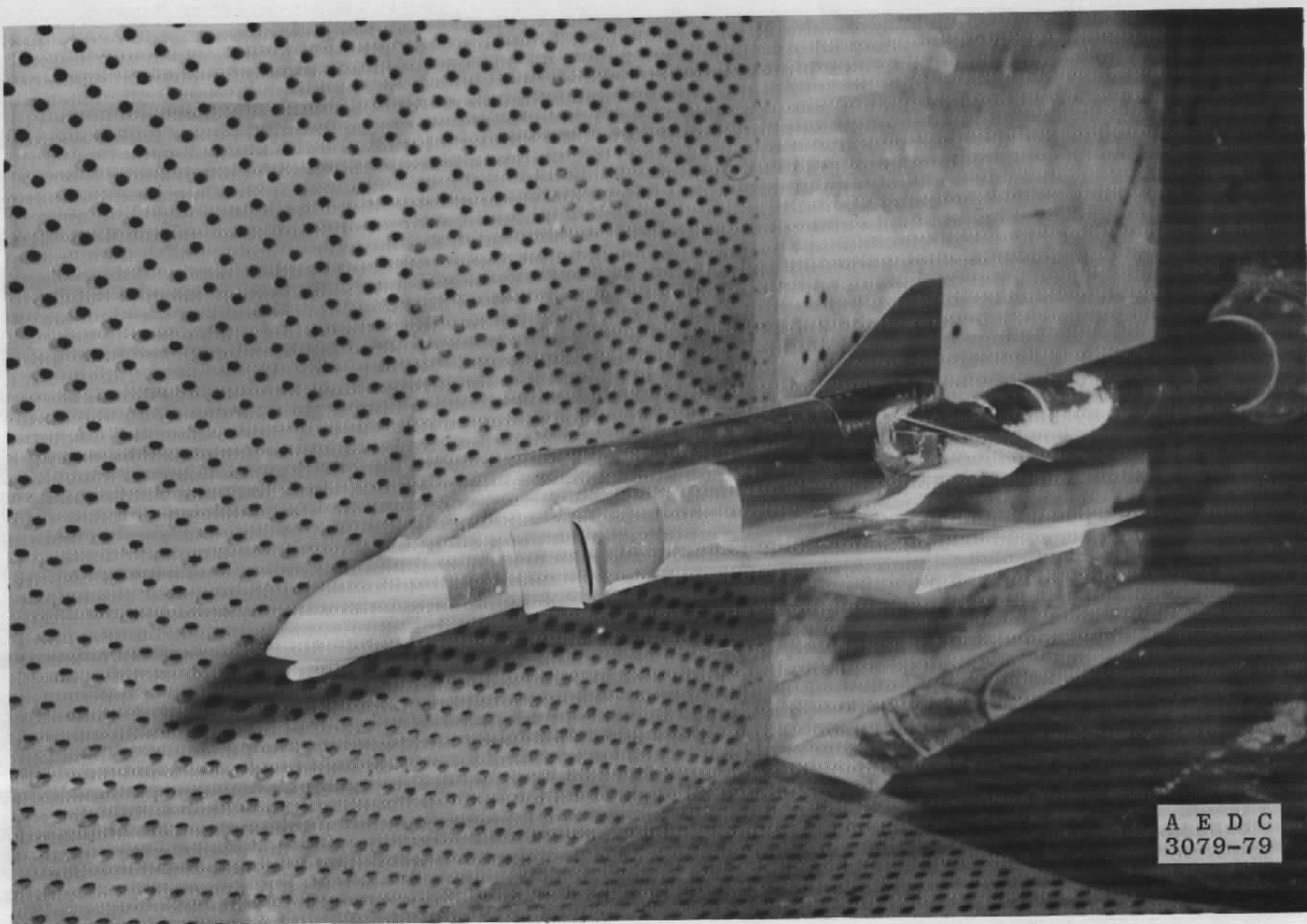




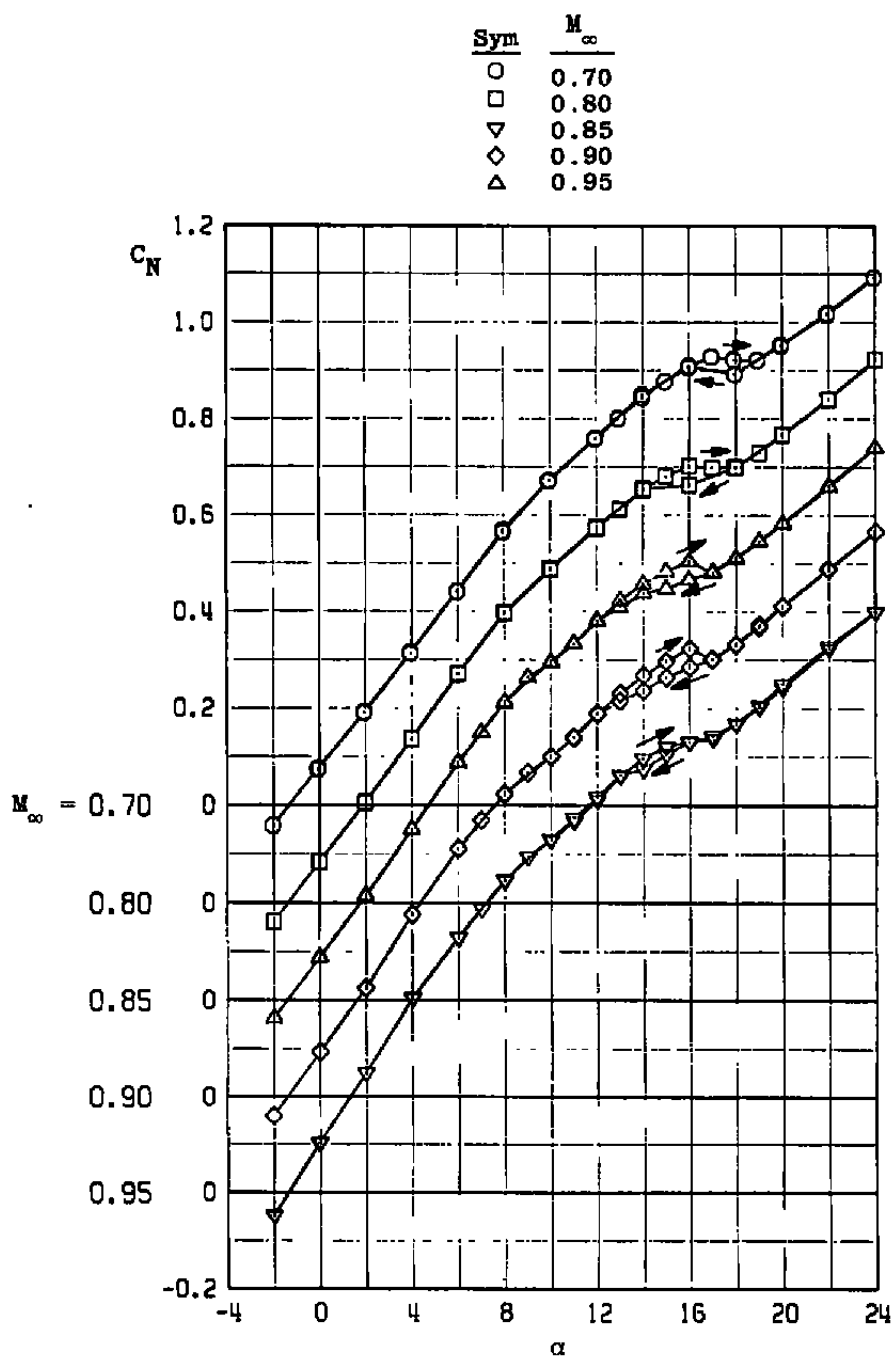
a. F-4C, Configuration 1  
Figure 2. Model installation in Tunnel 4T.



b. F-4C, Configuration 2  
Figure 2. Continued.



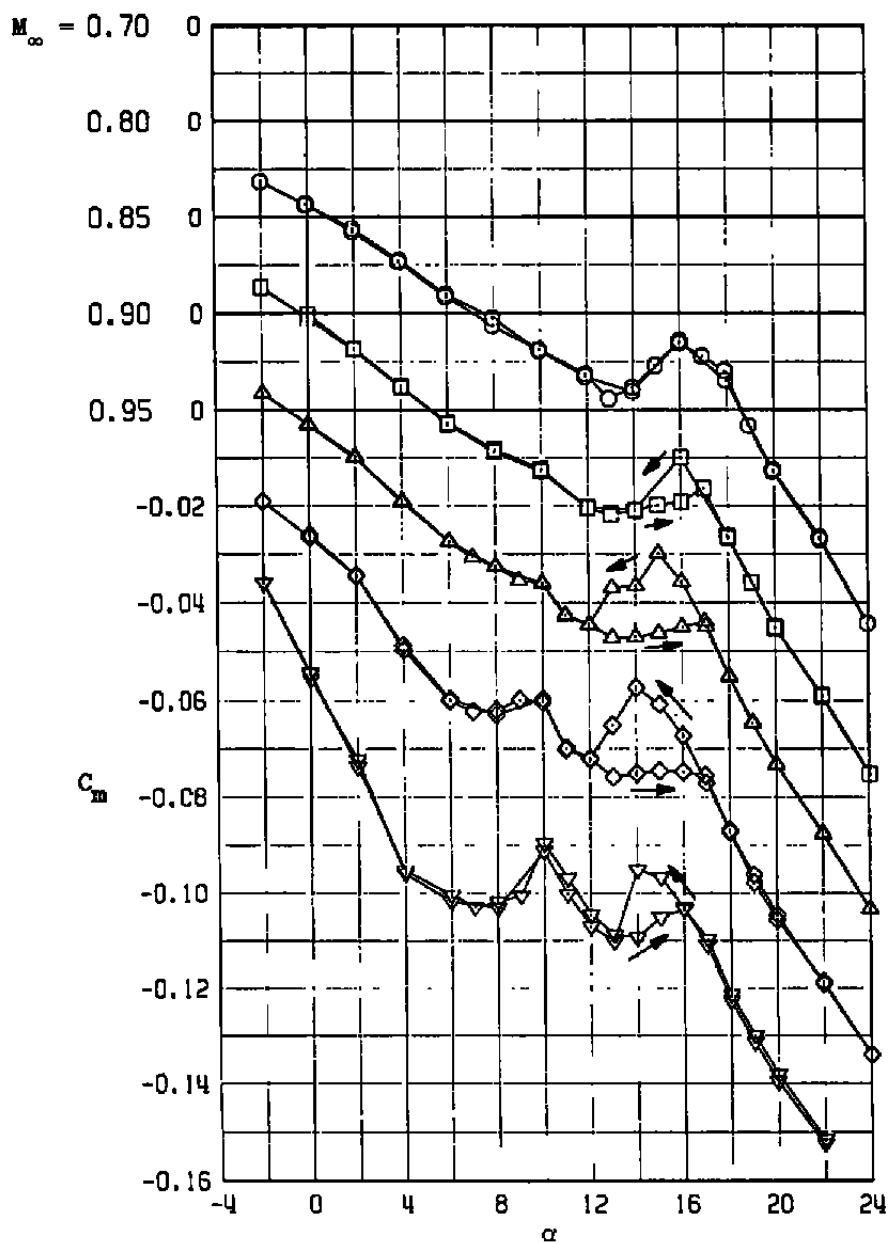
c. F-4C, Configuration 6  
Figure 2. Concluded.



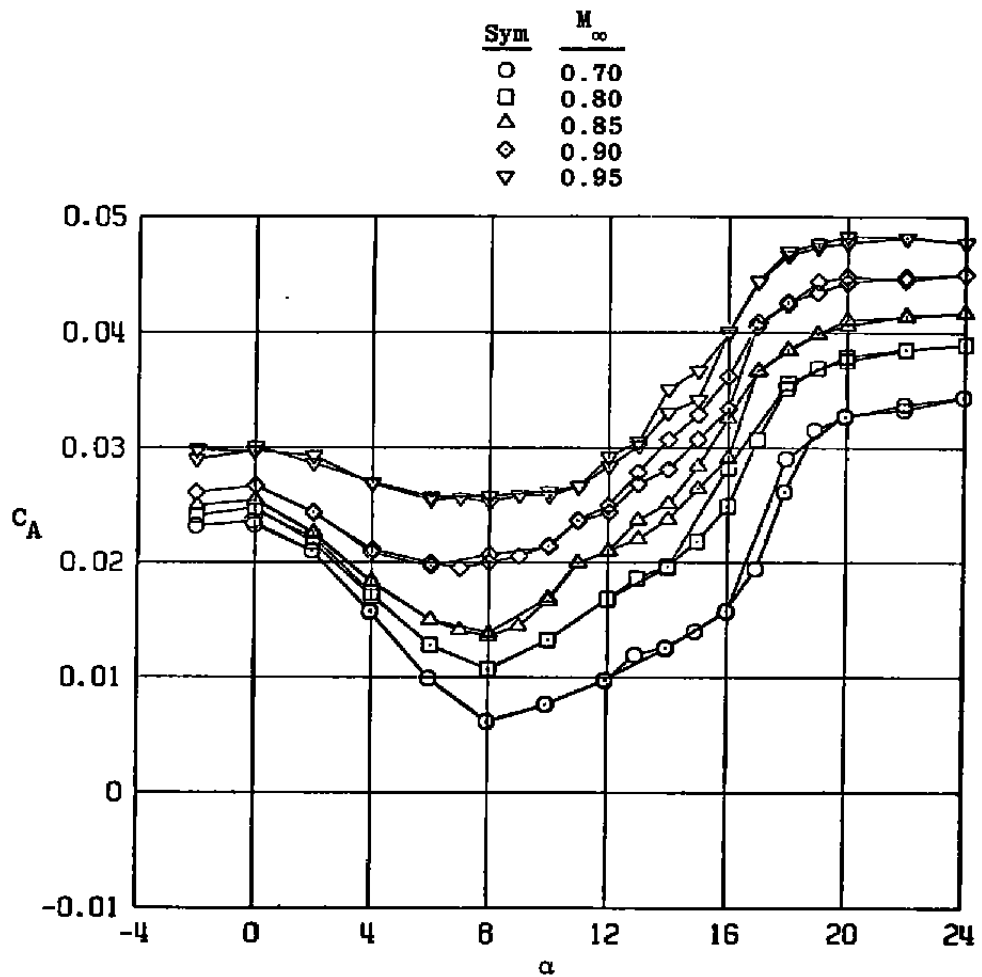
a. Normal-force coefficient

Figure 3. Hysteresis characteristics of the clean F-4C model in pitch,  $\beta = 0^\circ$ .

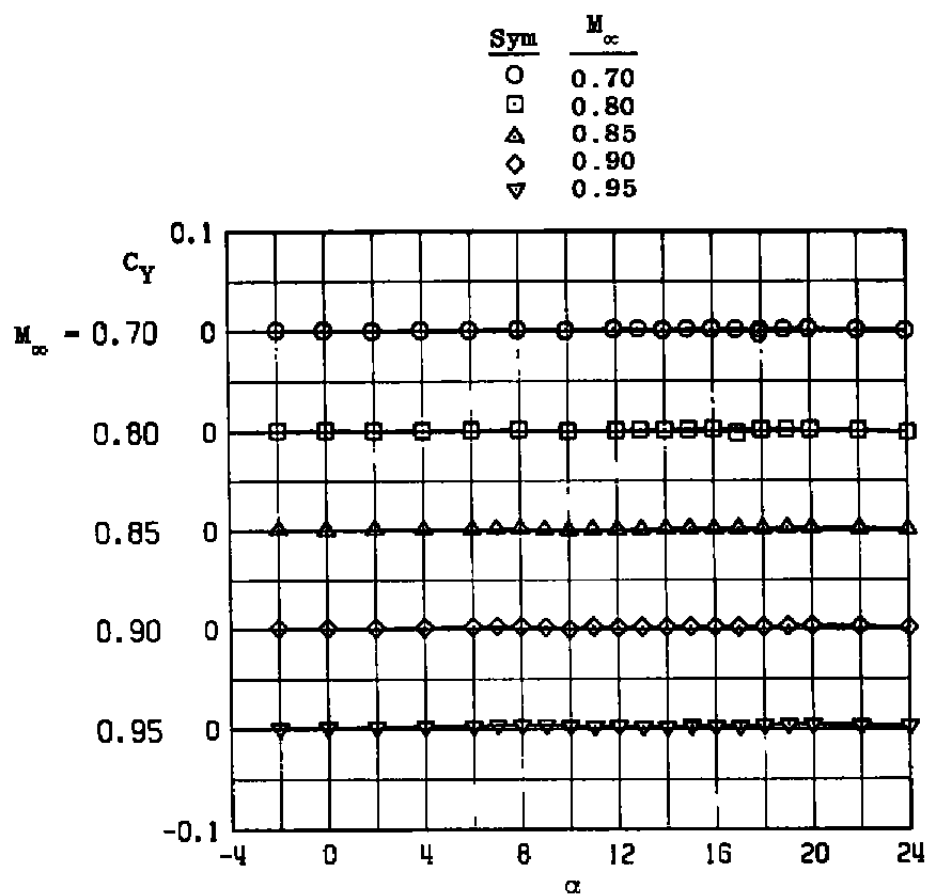
<u>Sym</u>	<u><math>M_\infty</math></u>
○	0.70
□	0.80
▽	0.85
◇	0.90
△	0.95



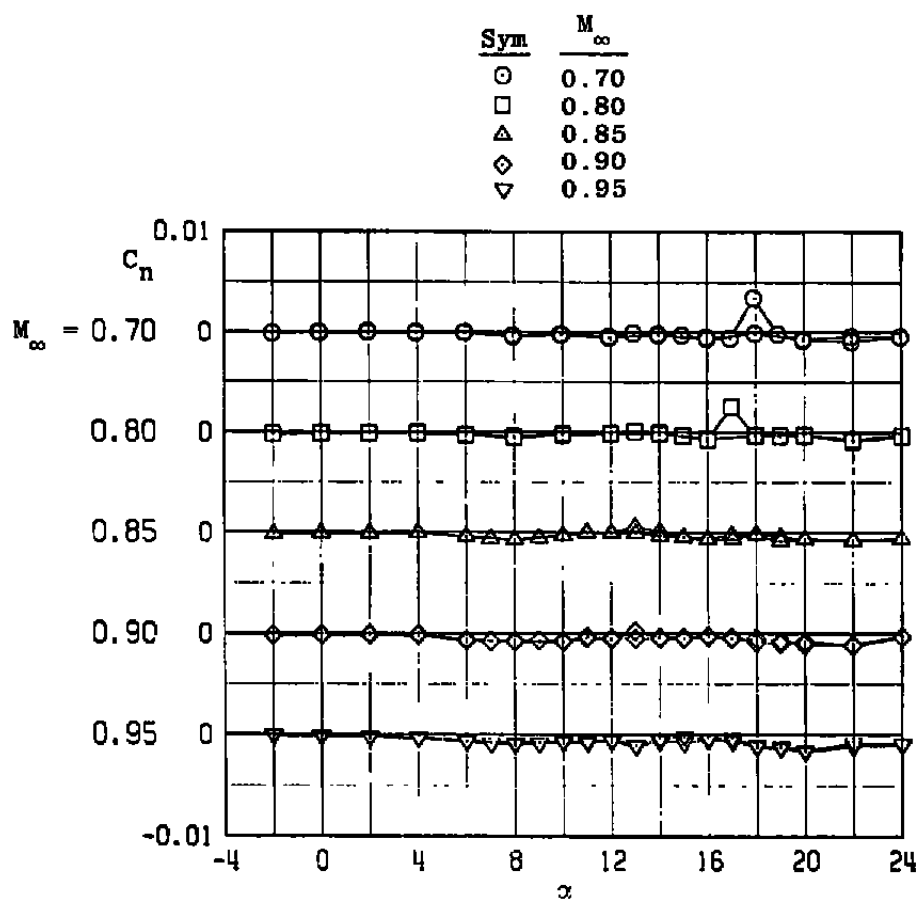
b. Pitching-moment coefficient  
Figure 3. Continued.



c. Axial-force coefficient  
Figure 3. Continued.

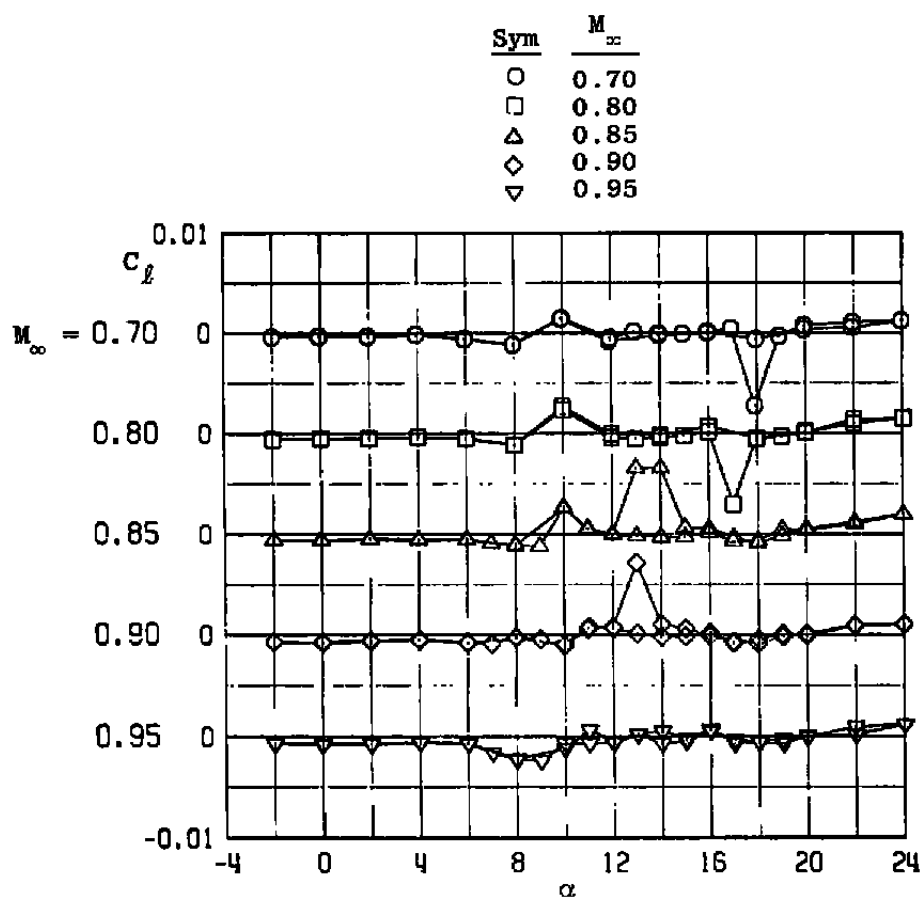


d. Side-force coefficient  
Figure 3. Continued.

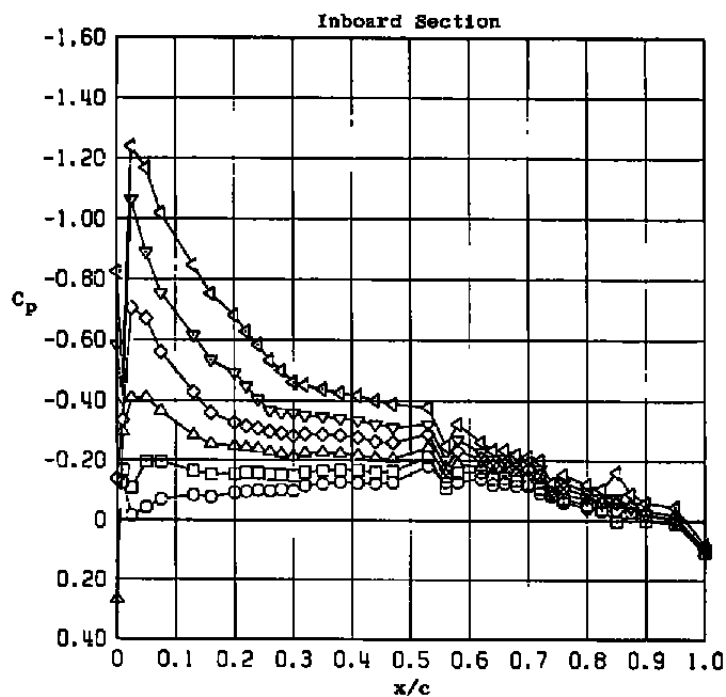
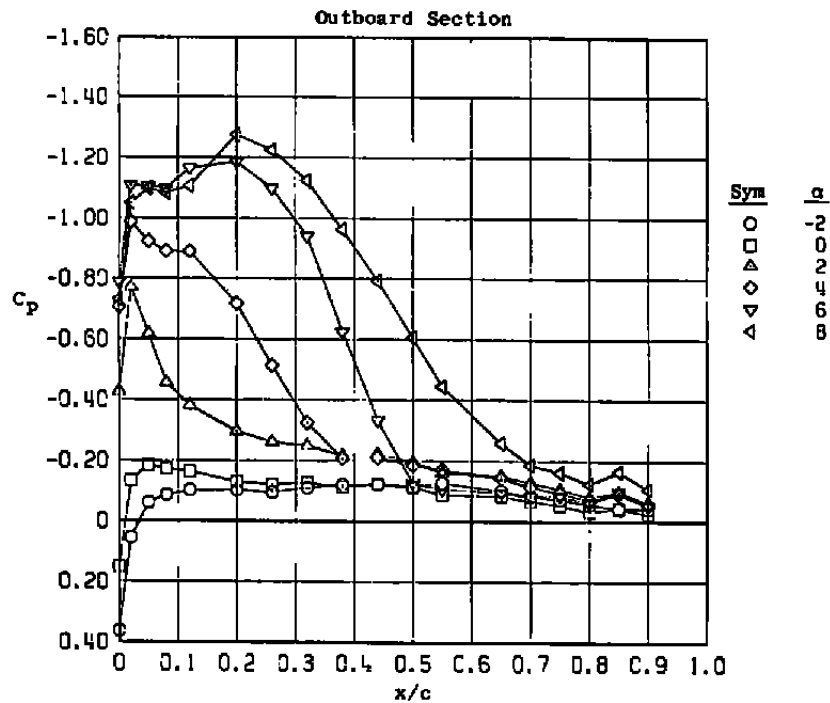


e. Yawing-moment coefficient  
Figure 3. Continued.



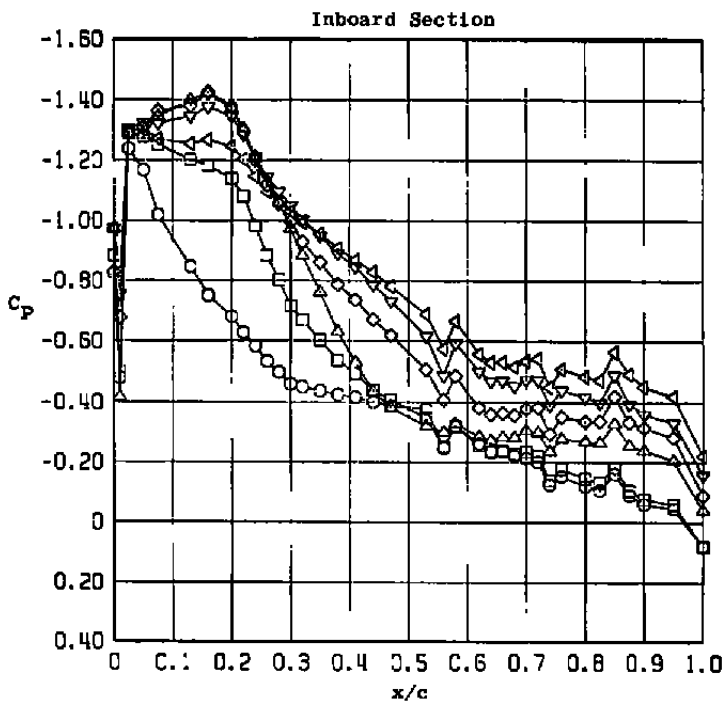
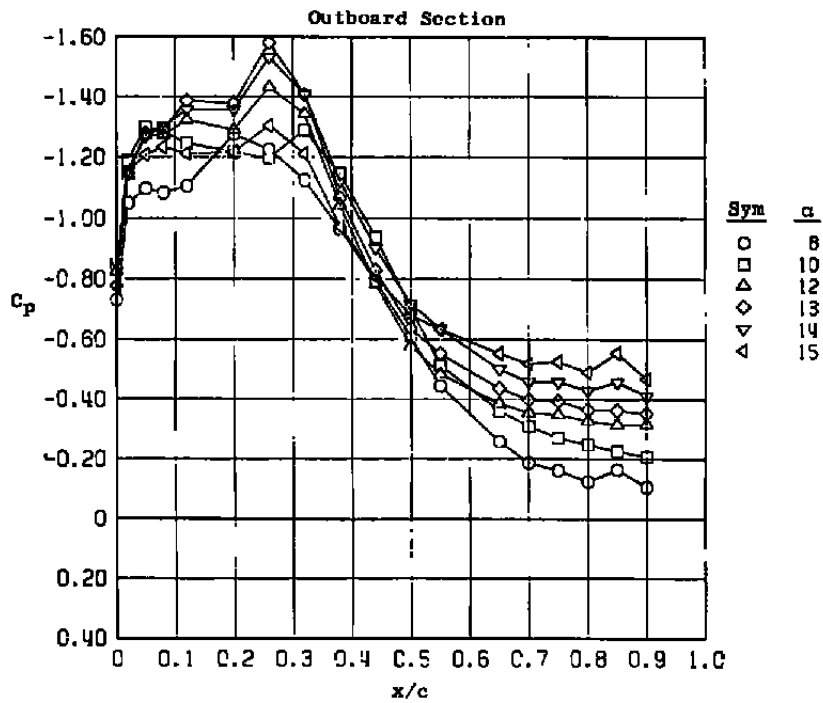


f. Rolling-moment coefficient  
Figure 3. Concluded.

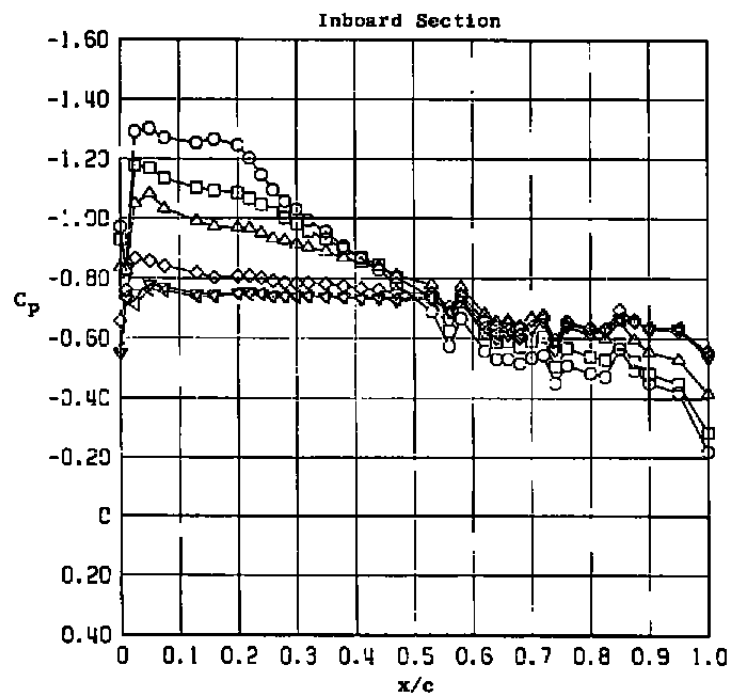
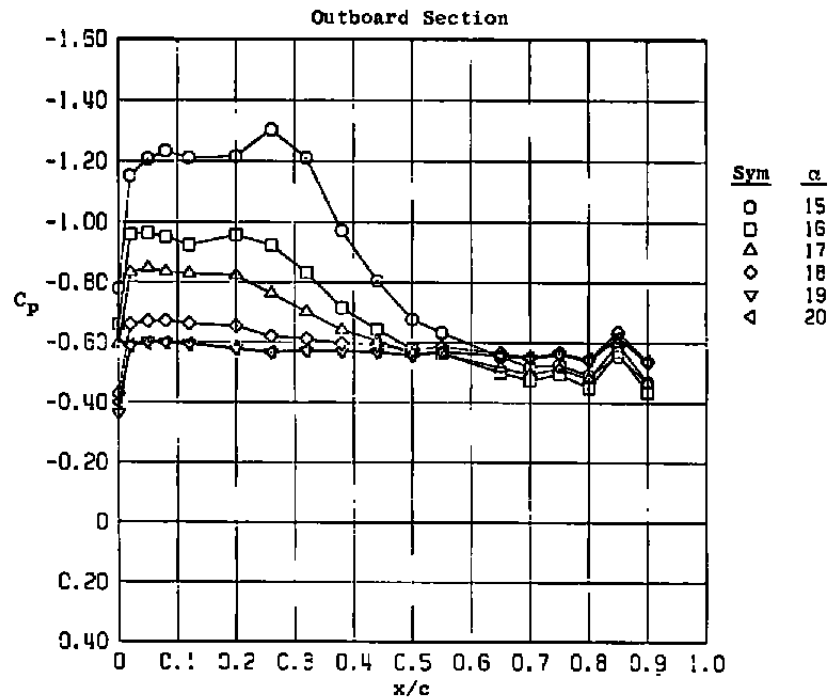


a.  $\alpha = 2$  to 8 deg

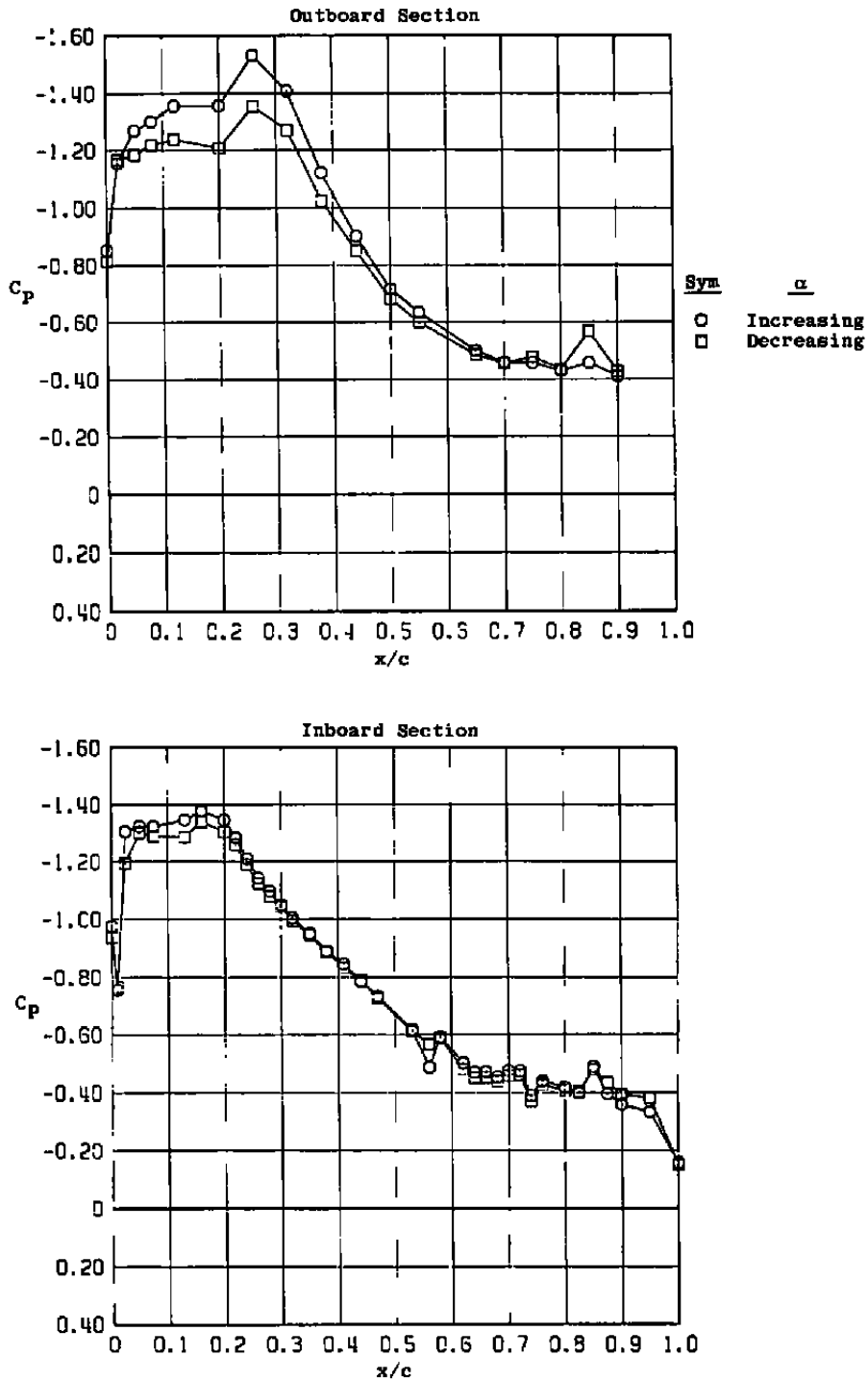
Figure 4. Typical wing upper surface pressure measurements,  $M_\infty = 0.7$ , increasing  $\alpha$ .



**b.  $\alpha = 8$  to 15 deg**  
**Figure 4. Continued.**

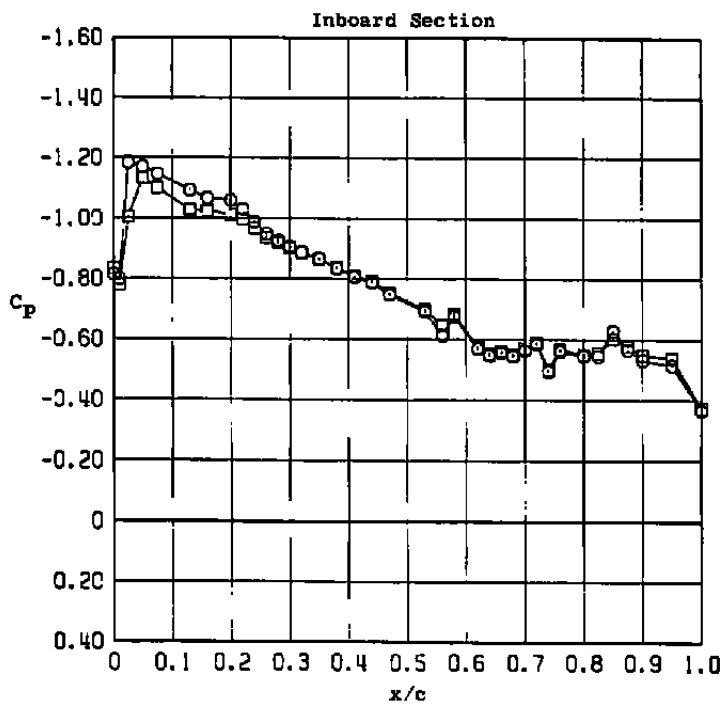
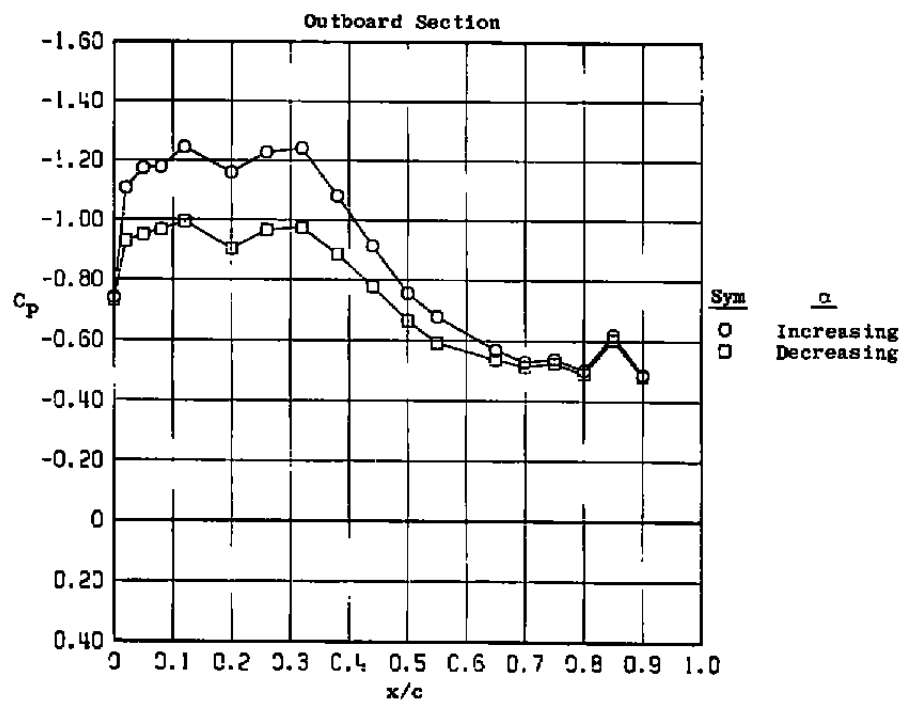


c.  $\alpha = 15$  to  $20$  deg  
**Figure 4. Concluded.**



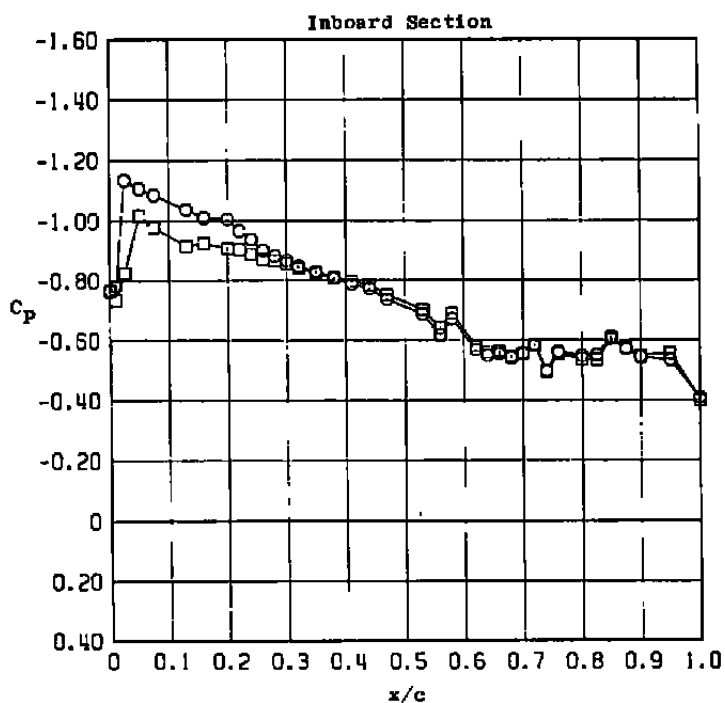
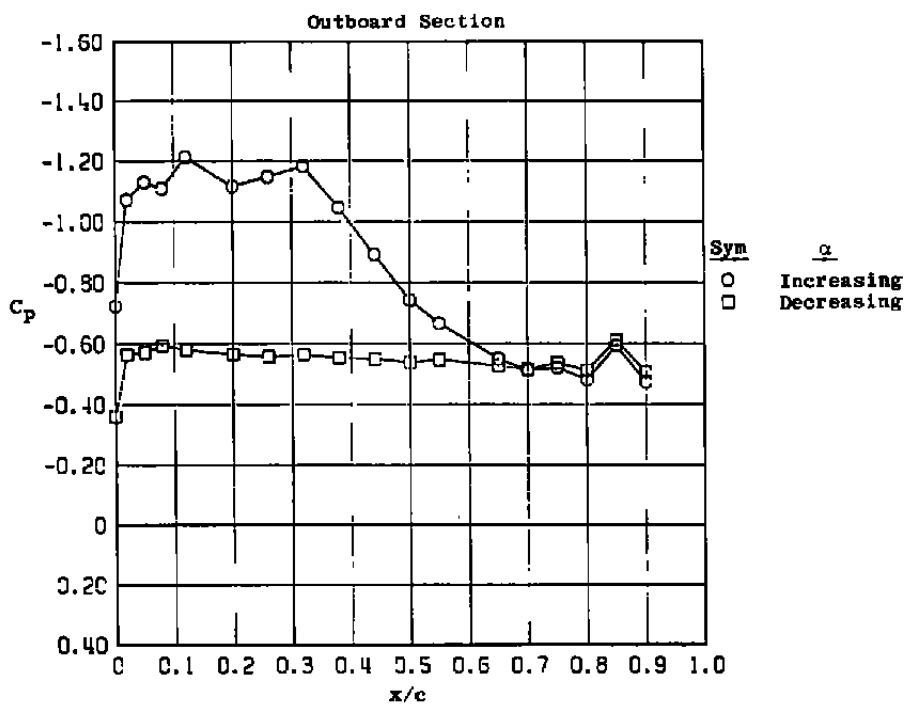
a.  $M_\infty = 0.7$ ,  $\alpha = 14^\circ$

**Figure 5. Effect of model pitch direction on wing upper surface pressure distributions,  $\beta = 0^\circ$ .**

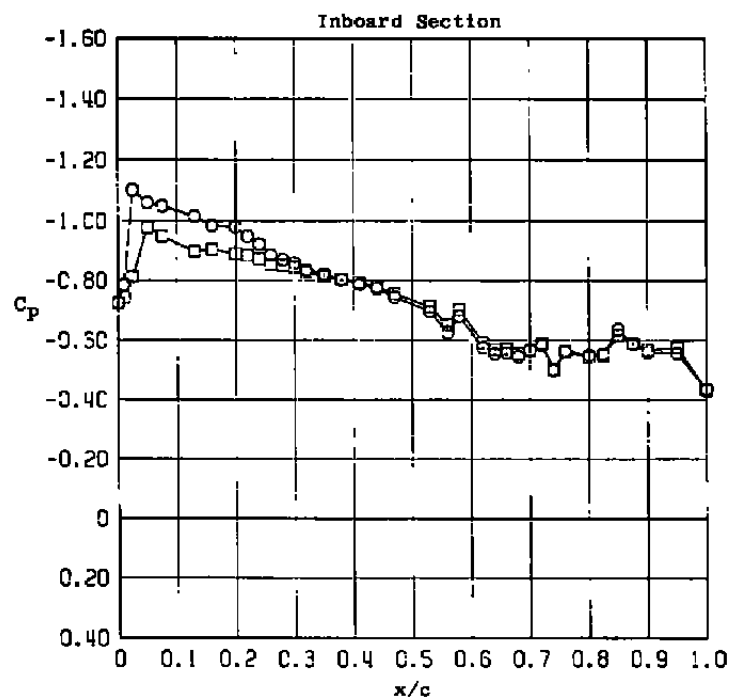
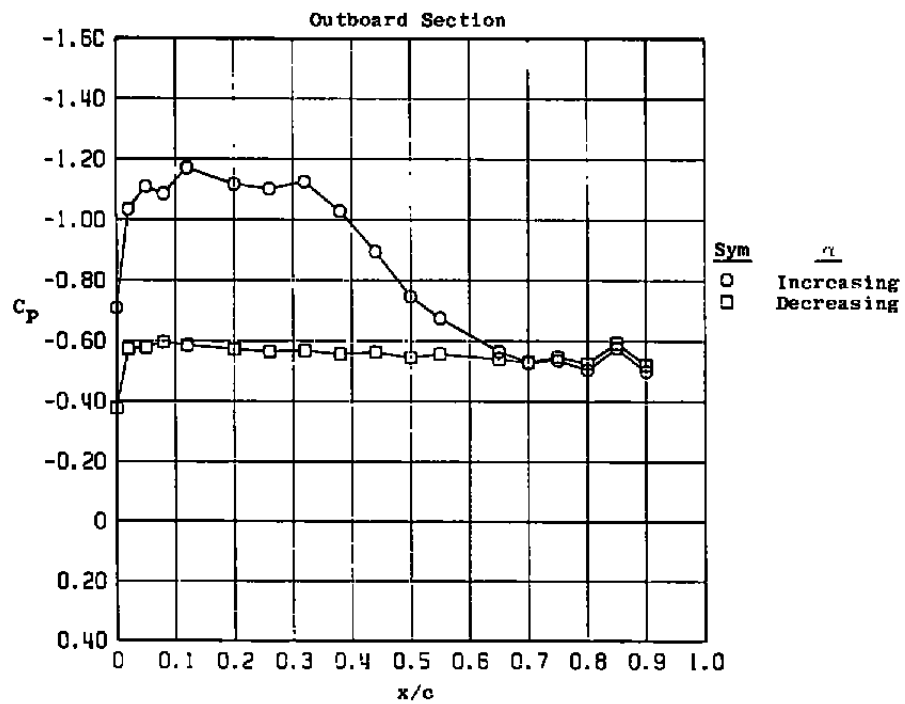


b.  $M_\infty = 0.8$ ,  $\alpha = 15^\circ$

Figure 5. Continued.

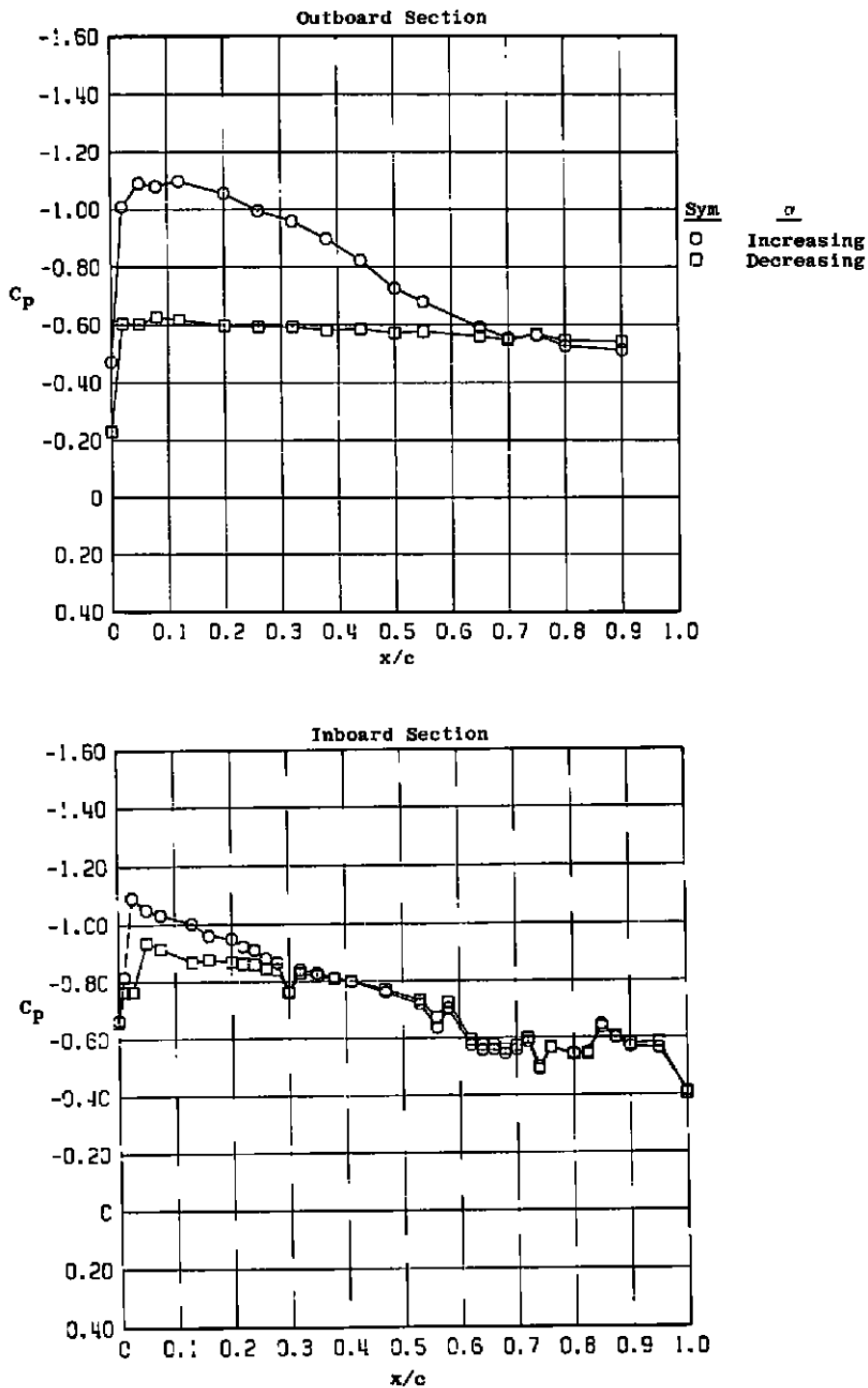


c.  $M_\infty = 0.85$ ,  $\alpha = 15^\circ$   
Figure 5. Continued.

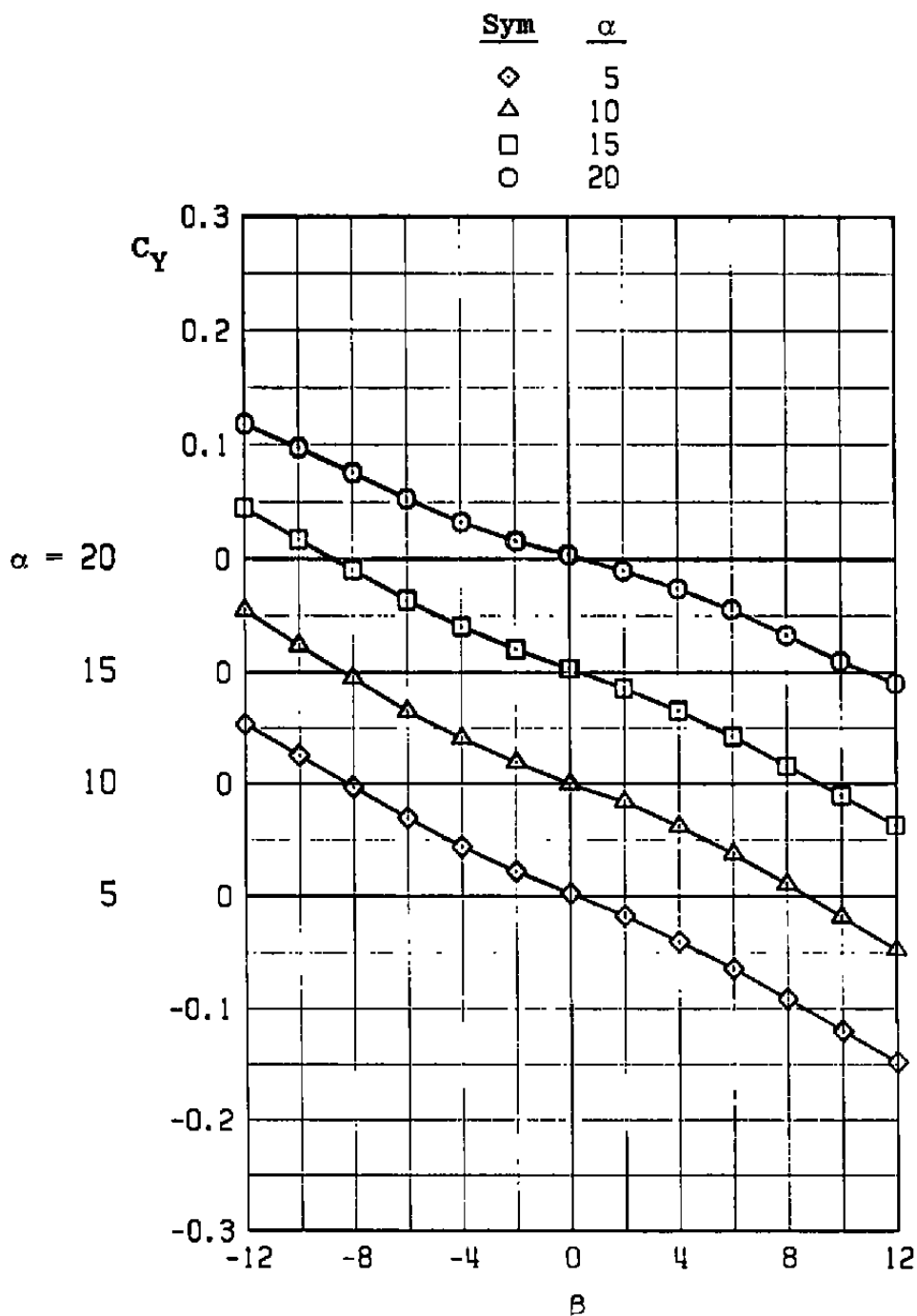


d.  $M_\infty = 0.9$ ,  $\alpha = 15^\circ$   
 Figure 5. Continued.



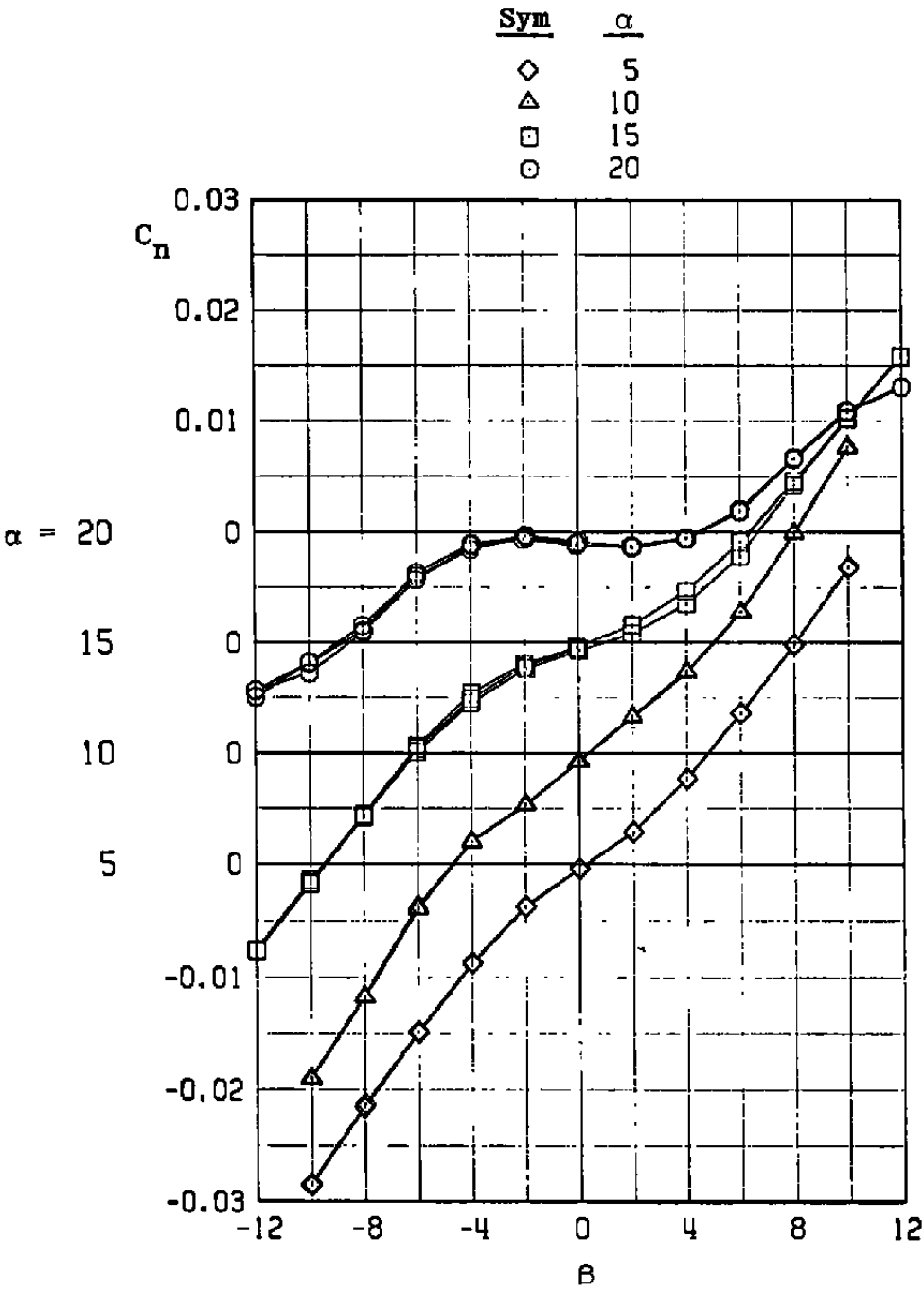


e.  $M_\infty = 0.95$ ,  $\alpha = 15^\circ$   
 Figure 5. Concluded.

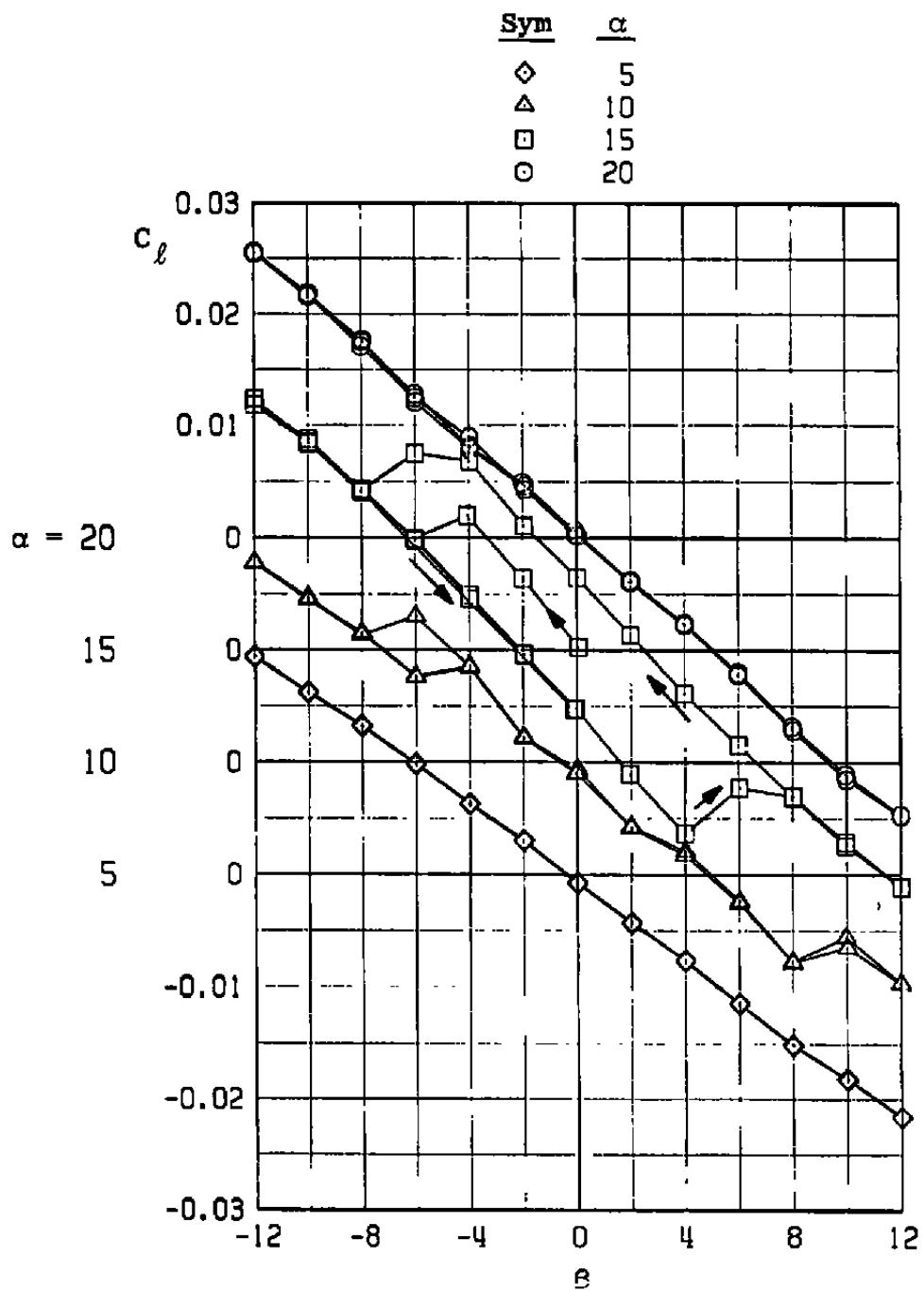


a. Side-force coefficient

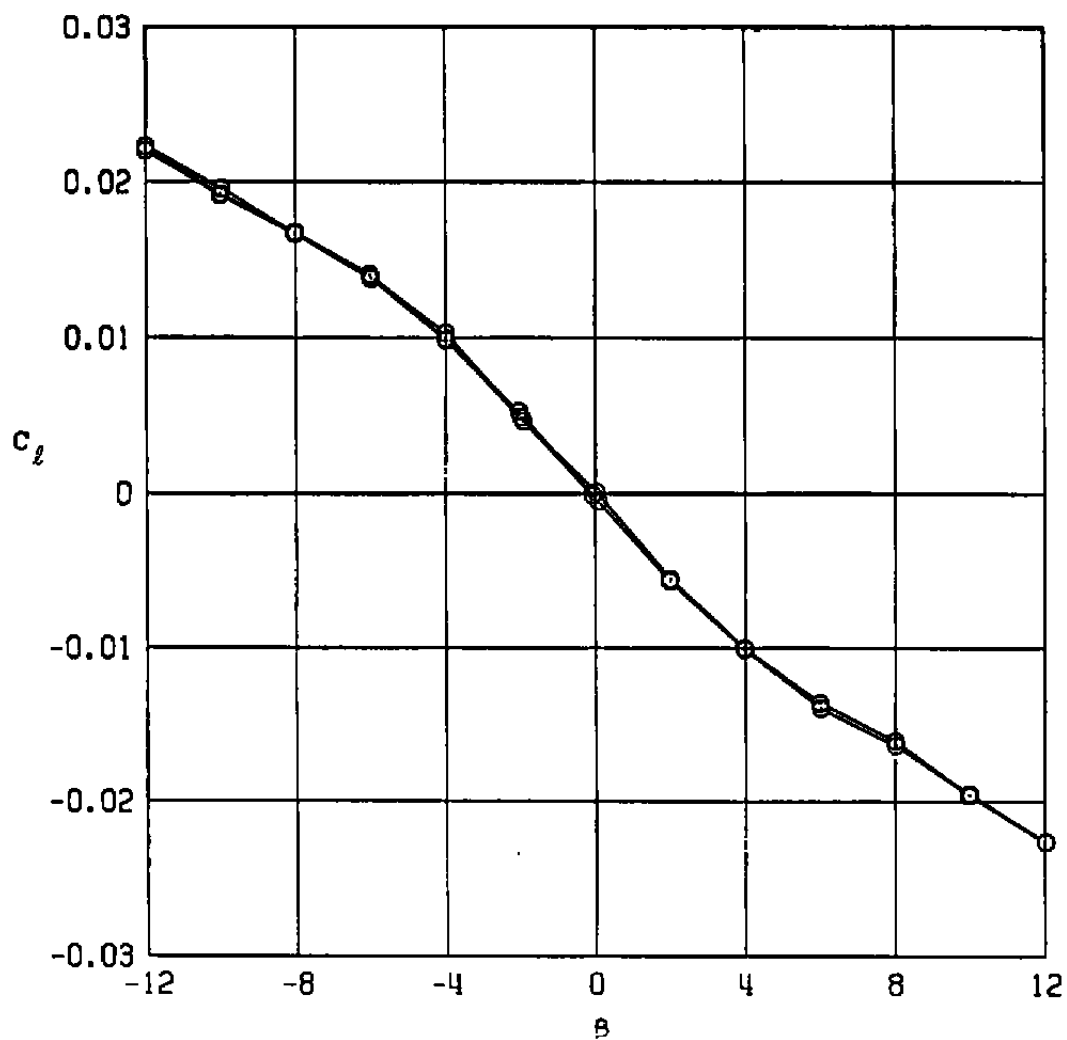
Figure 6. Hysteresis characteristics of the clean F-4C model in yaw,  $M_\infty = 0.9$ .



b. Yawing-moment coefficient  
Figure 6. Continued.

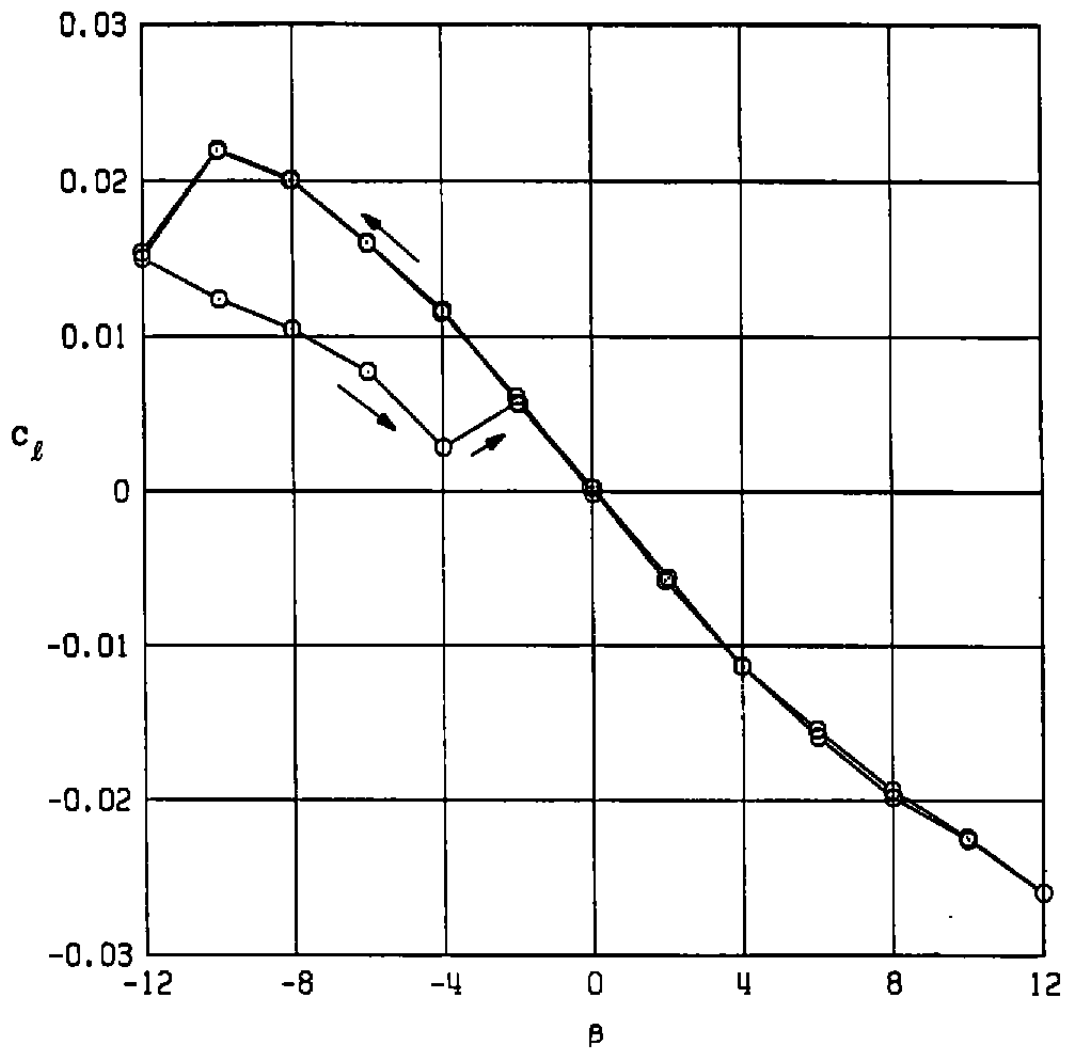


c. Rolling-moment coefficient  
Figure 6. Concluded.

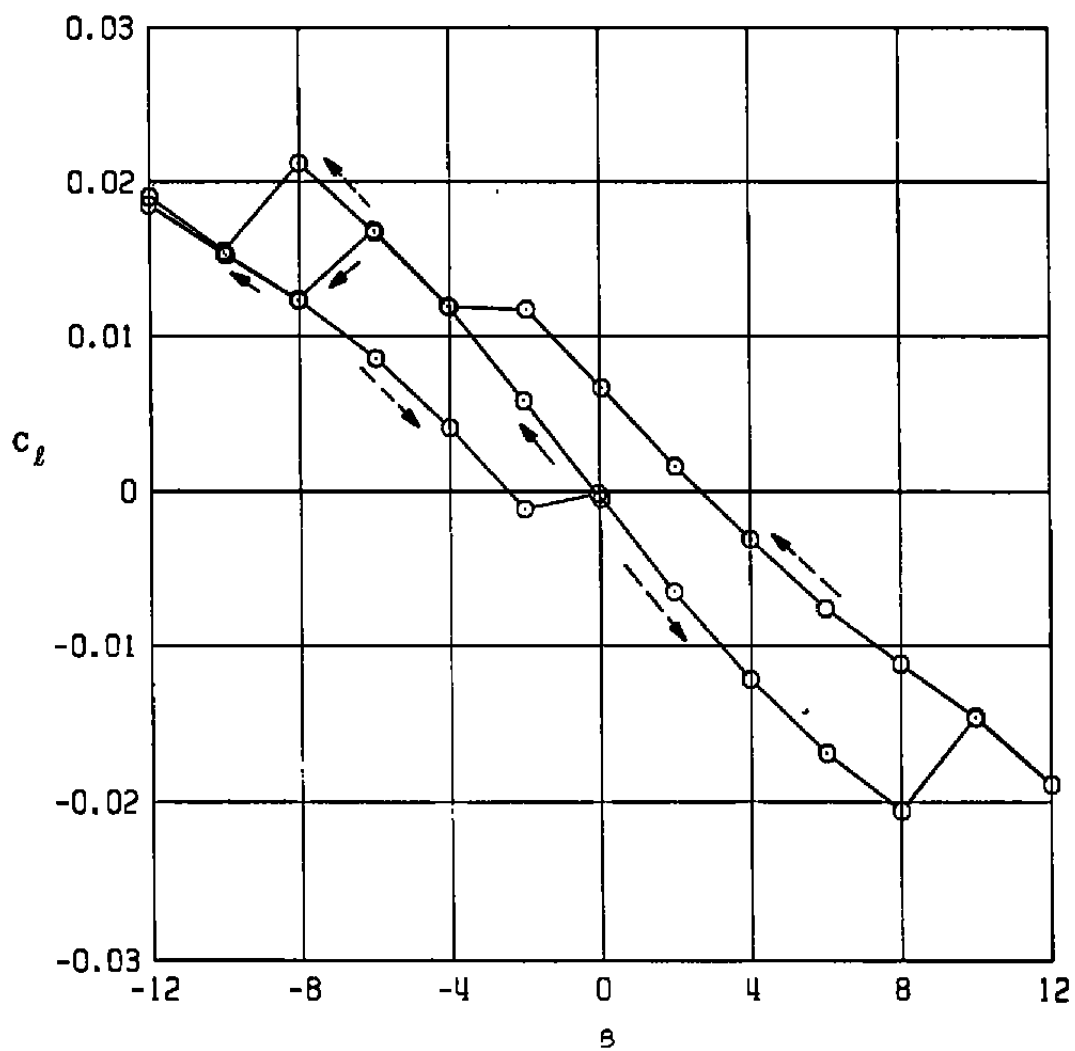


a.  $M_\infty = 0.7$

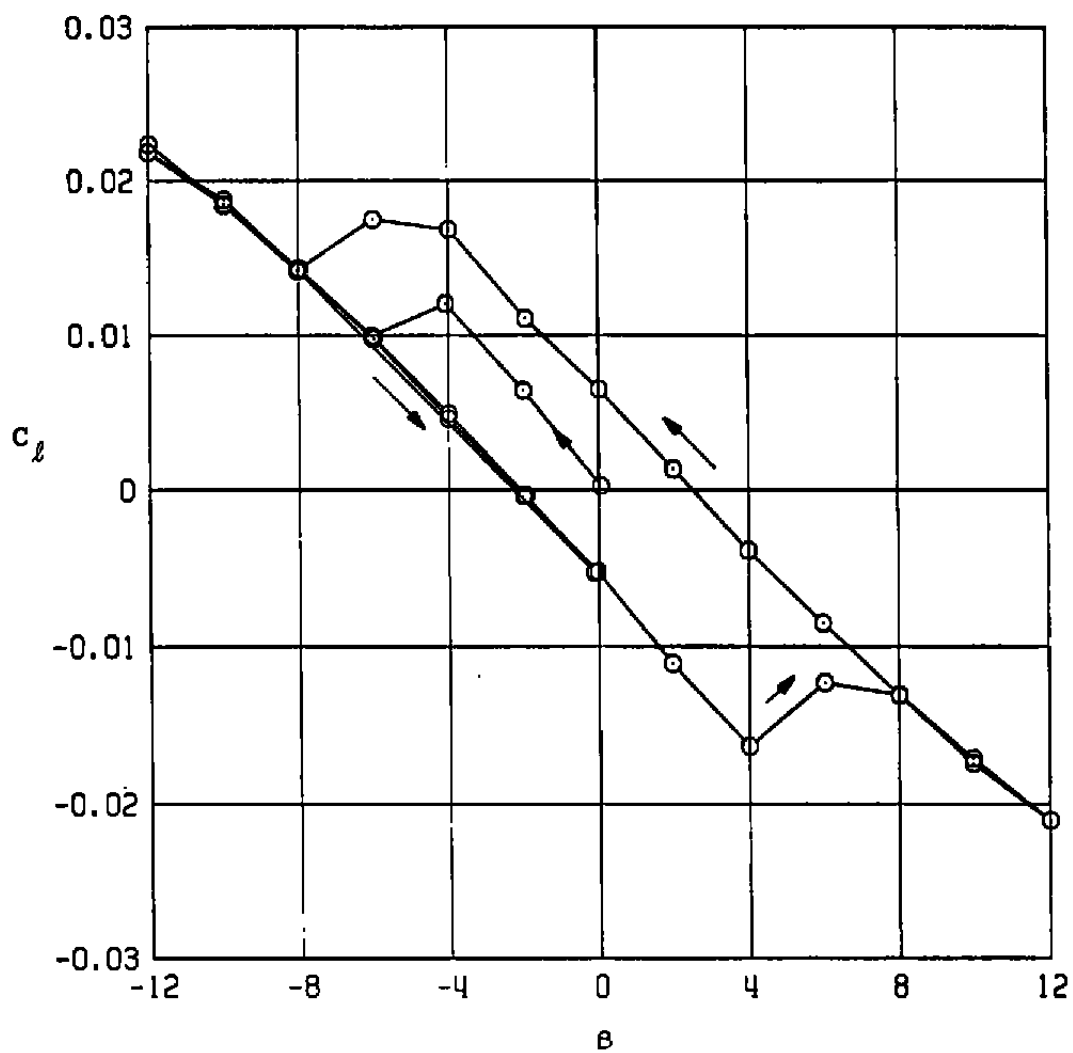
Figure 7. Hysteresis characteristics of the rolling-moment coefficient at selected Mach numbers,  $\alpha = 15^\circ$ .



b.  $M_\infty = 0.8$   
Figure 7. Continued.

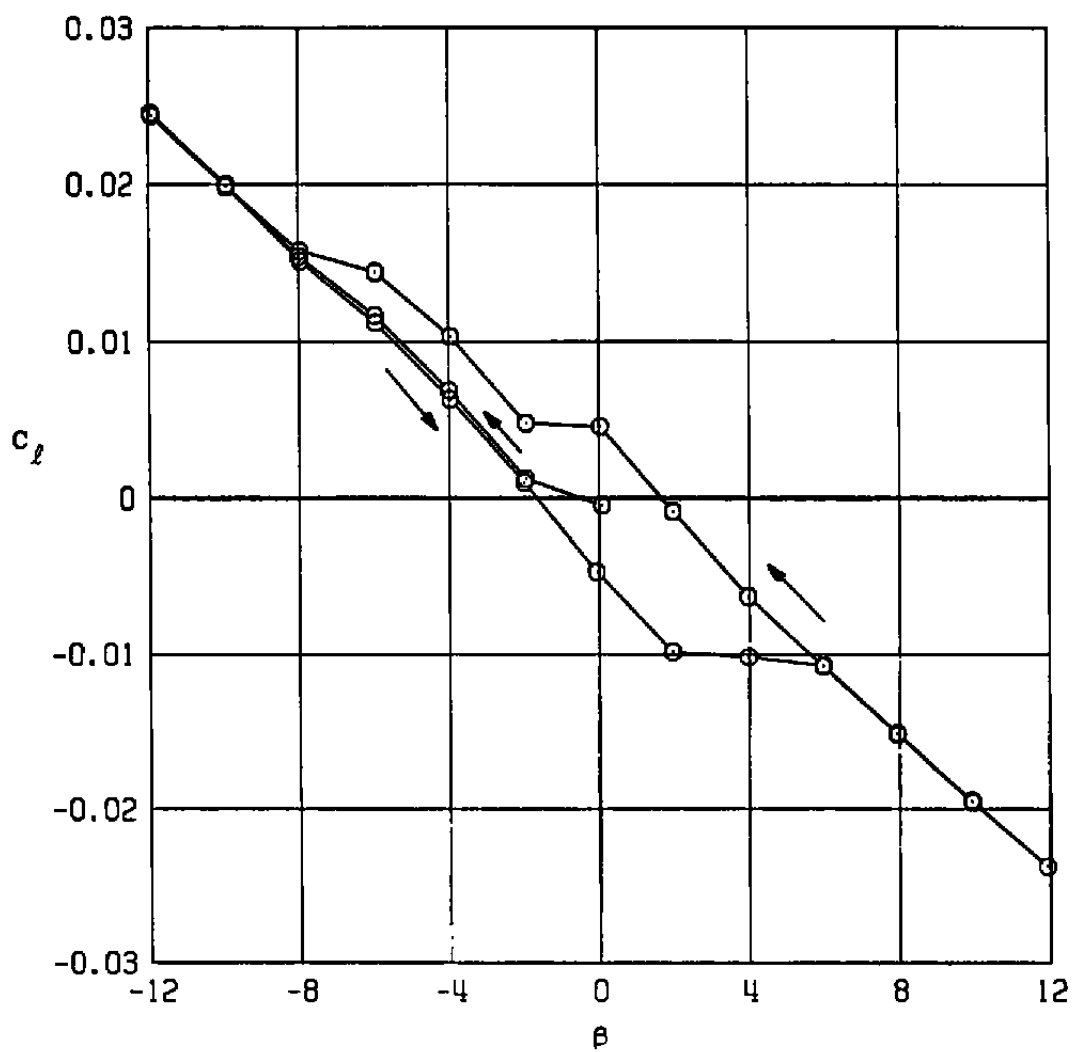


c.  $M_\infty = 0.85$   
Figure 7. Continued.

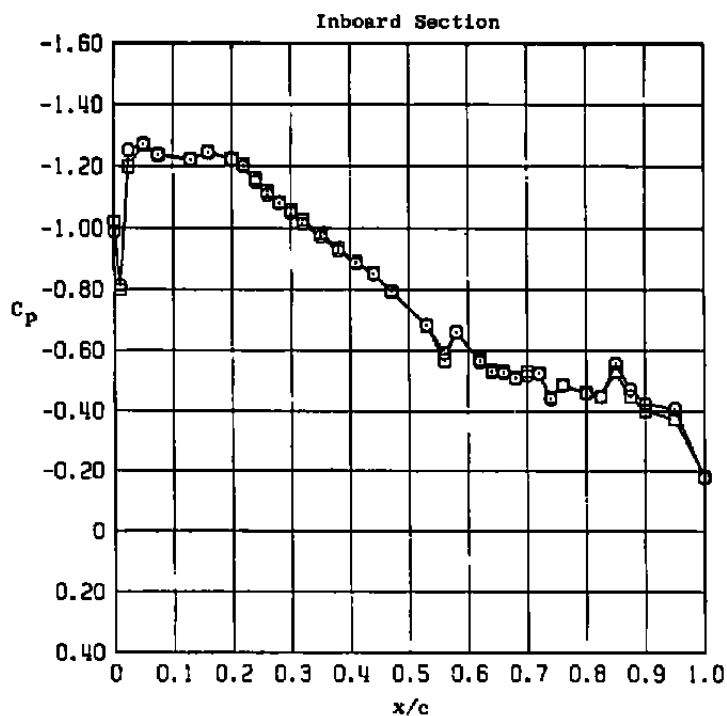
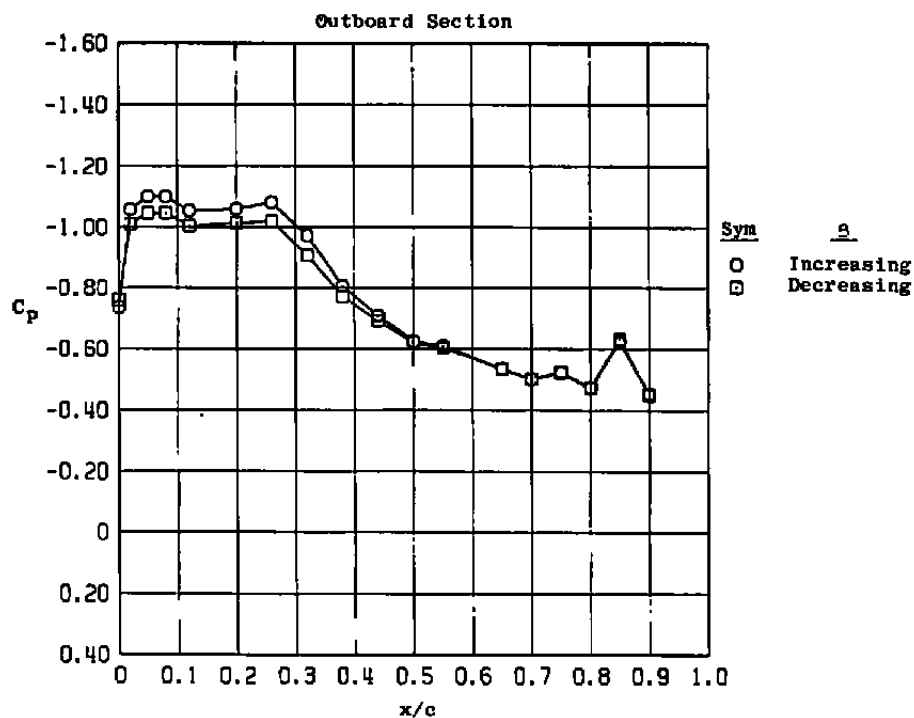


d.  $M_\infty = 0.9$   
Figure 7. Continued.



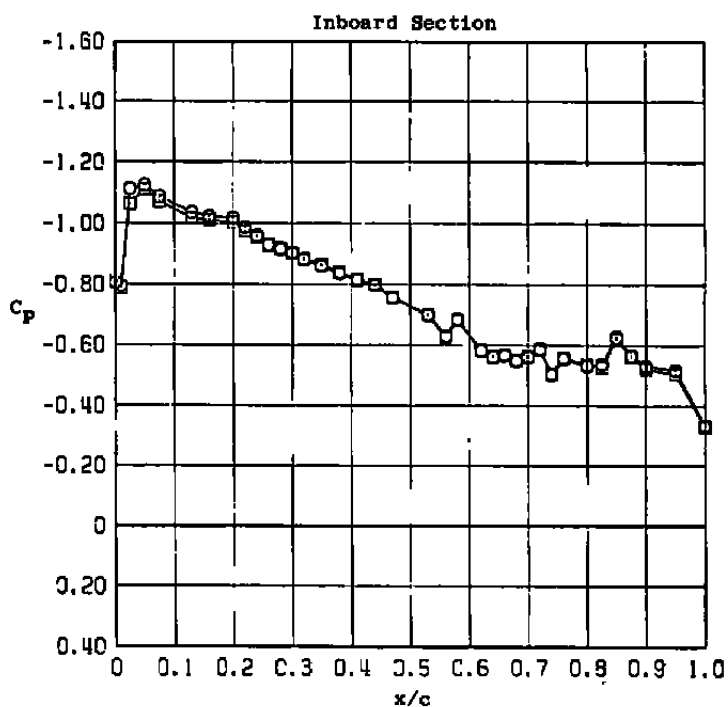
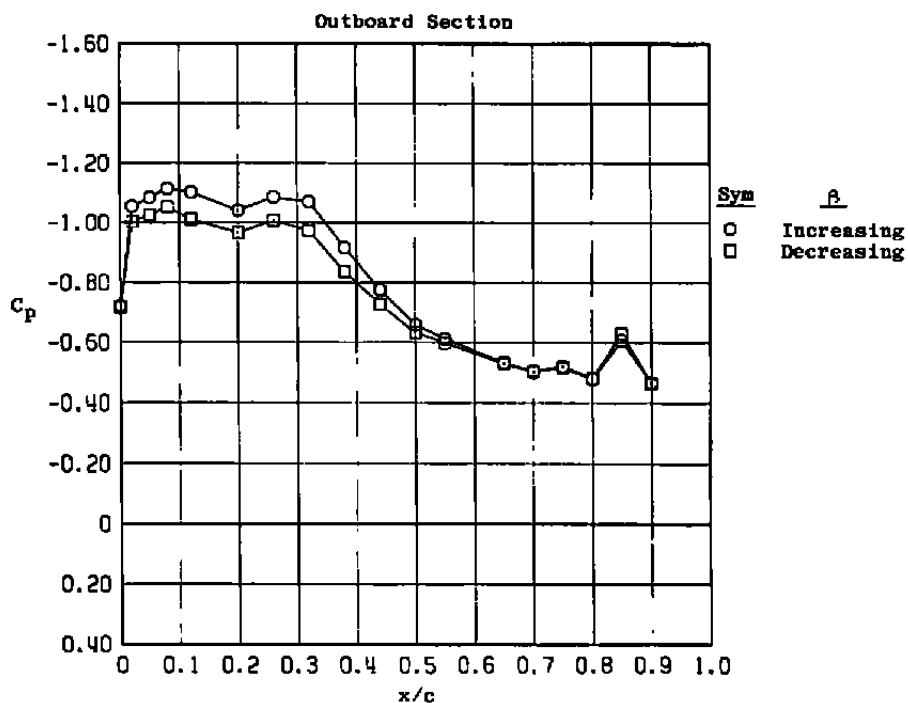


e.  $M_\infty = 0.95$   
Figure 7. Concluded.

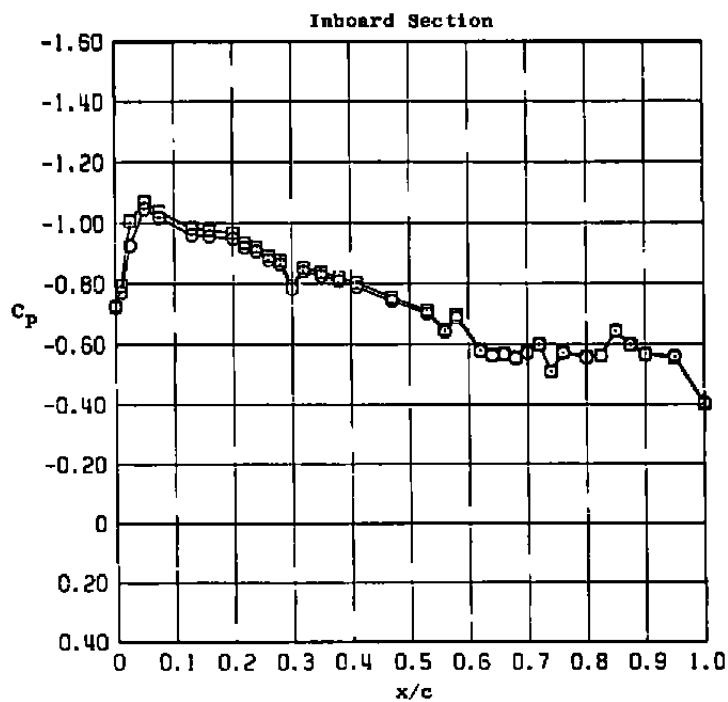
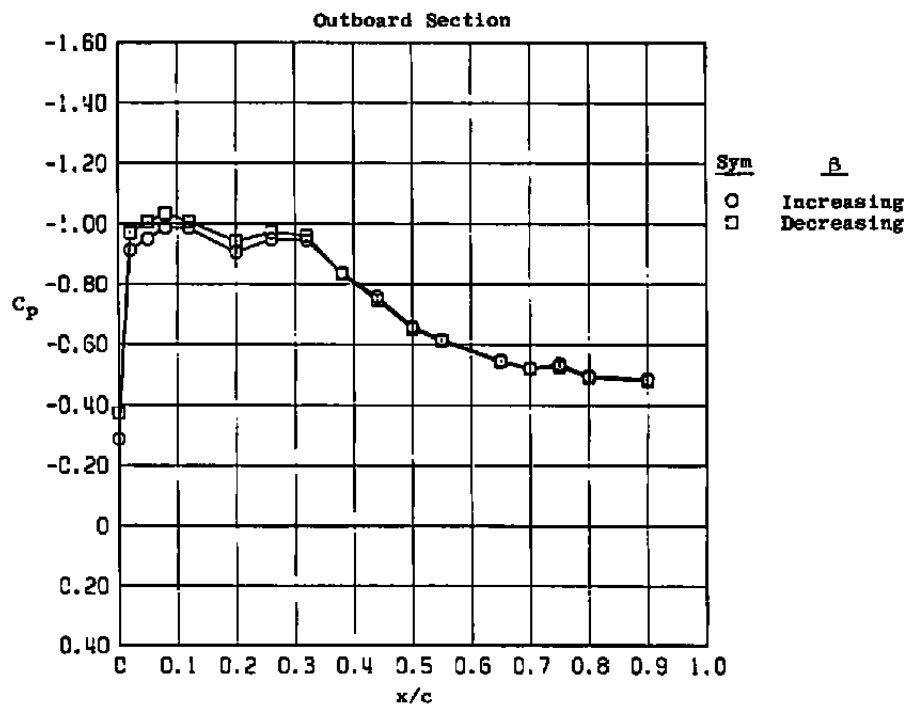


a.  $M_\infty = 0.7$

**Figure 8. Effect of model sideslip direction on wing upper surface pressure distributions,  $\alpha = 15$  deg,  $\beta = 2$  deg.**

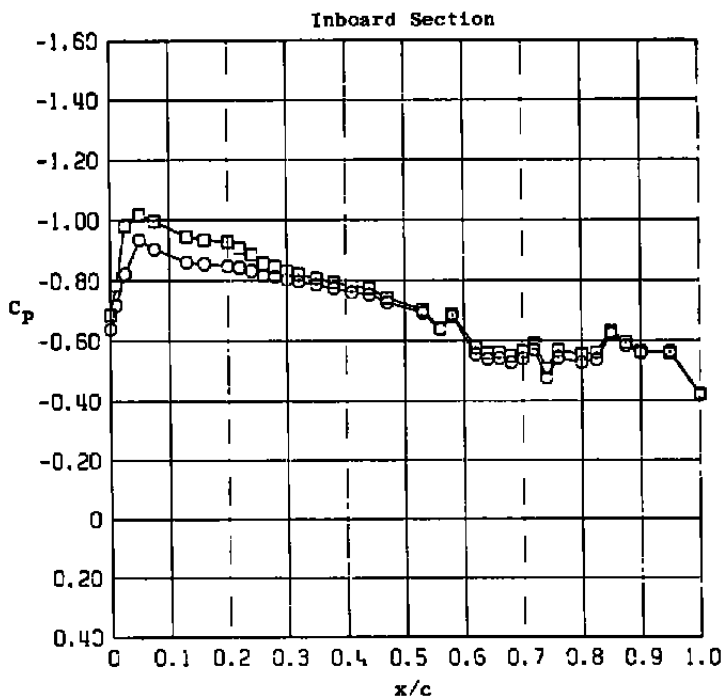
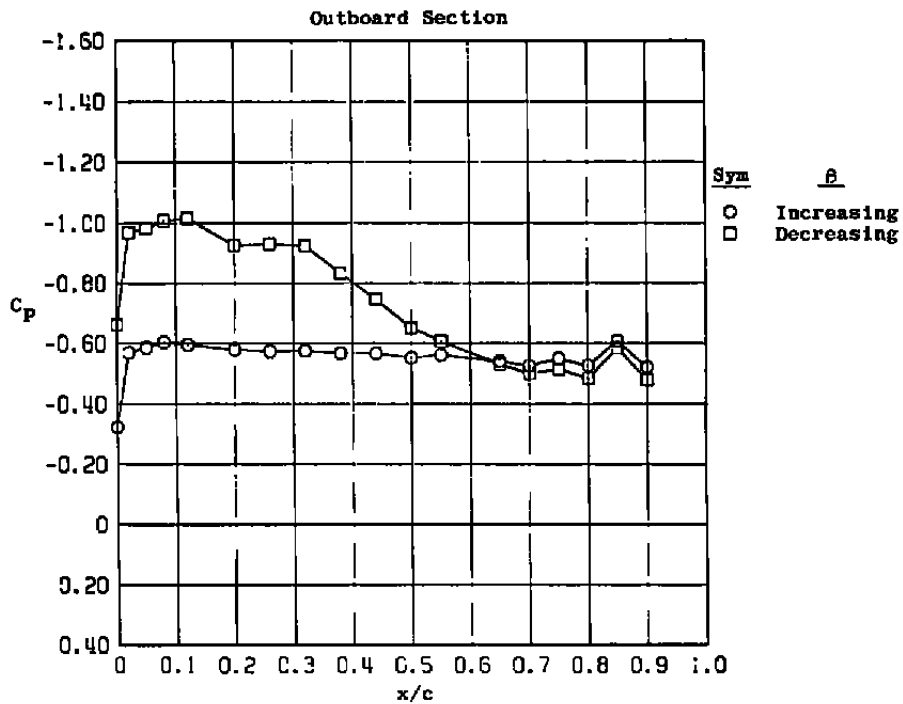


b.  $M_\infty = 0.8$   
 Figure 8. Continued.

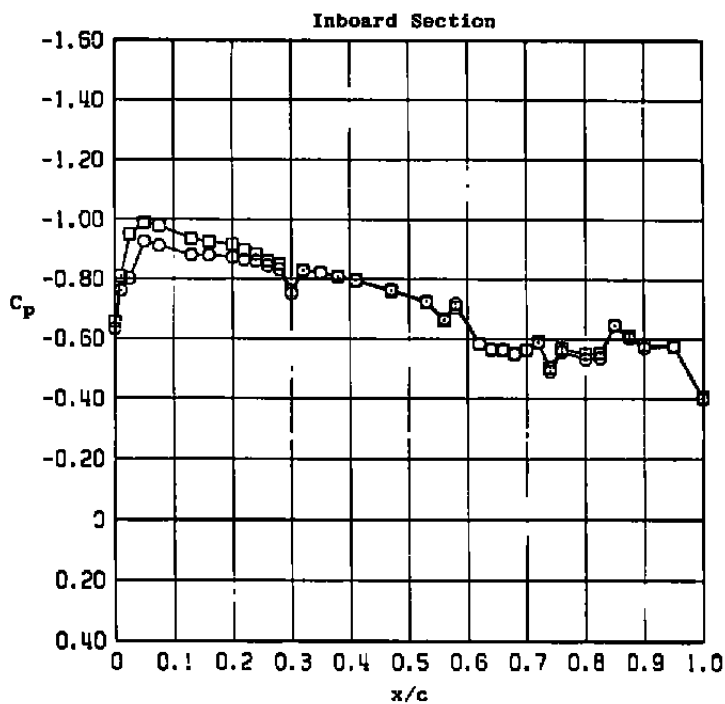
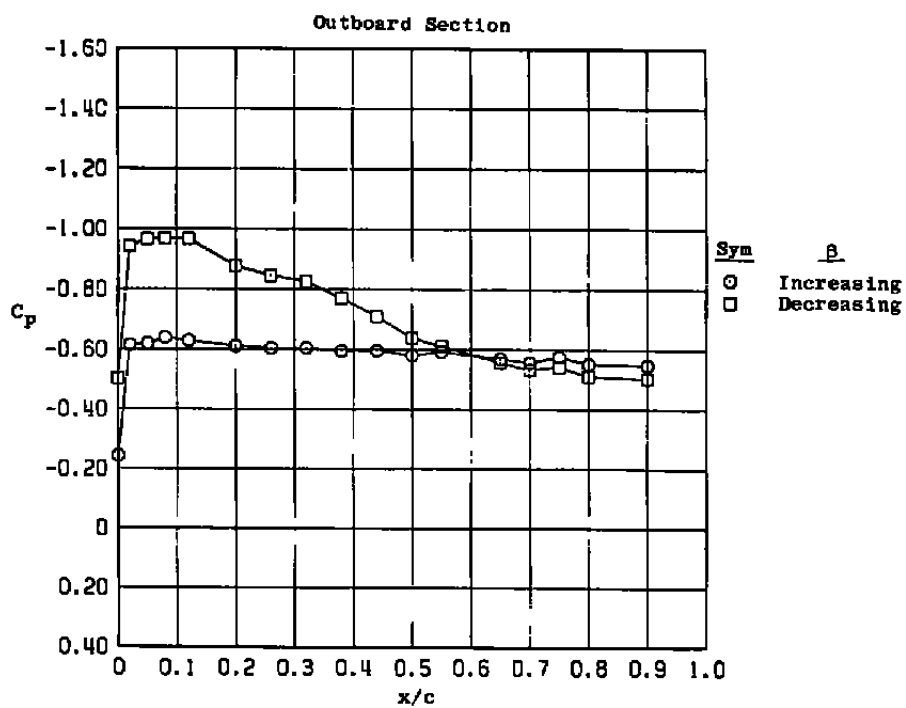


c.  $M_\infty = 0.85$

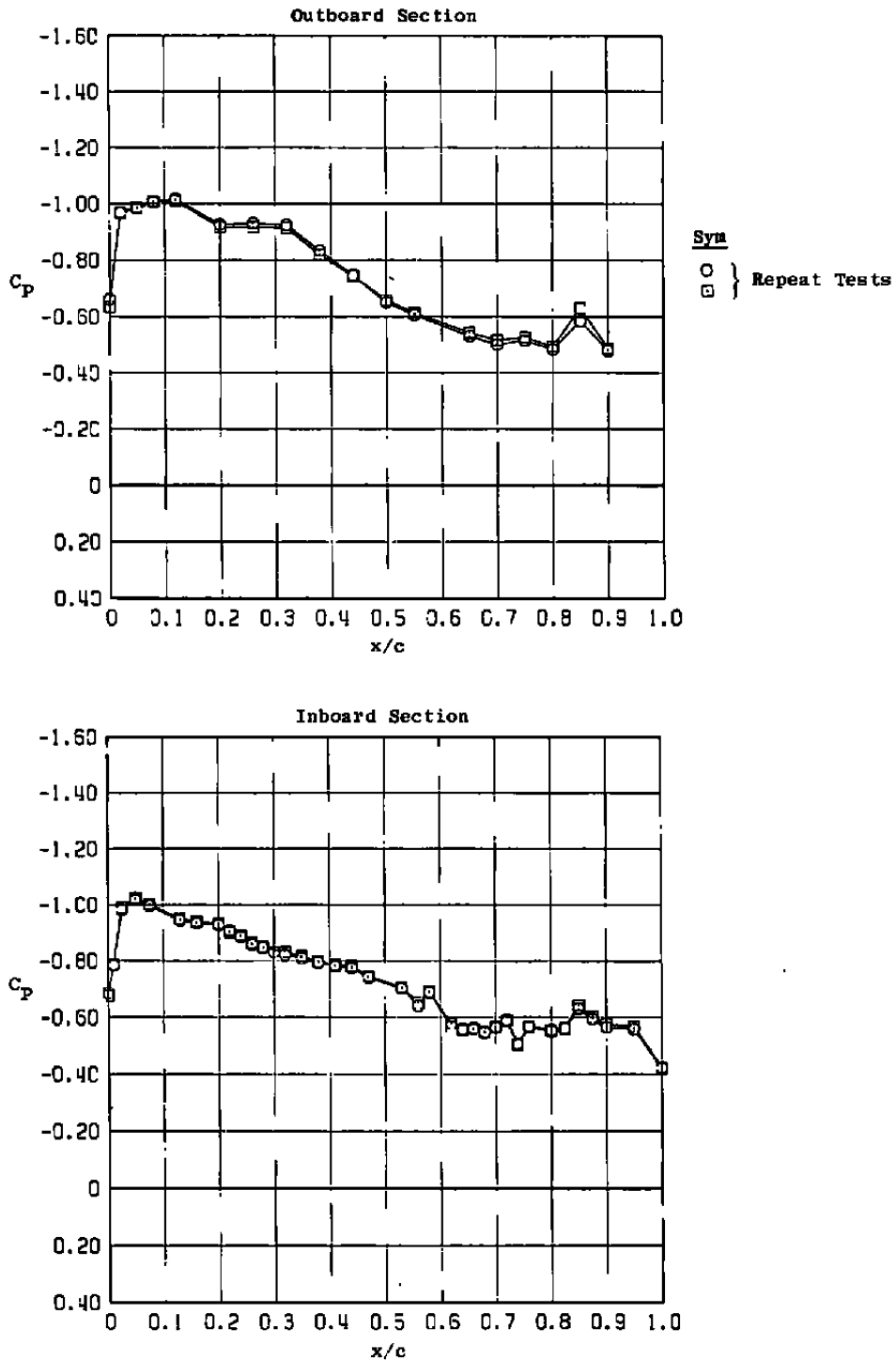
Figure 8. Continued.



d.  $M_\infty = 0.9$   
Figure 8. Continued.

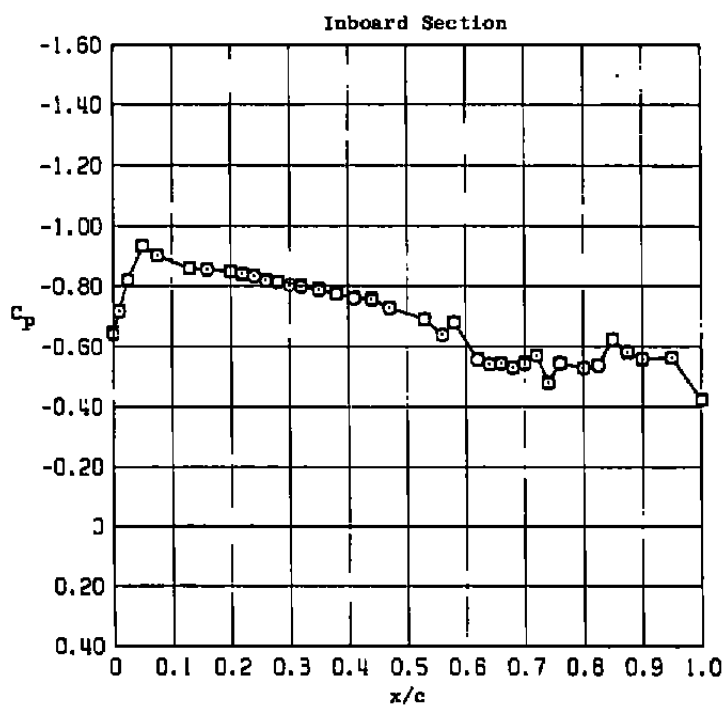
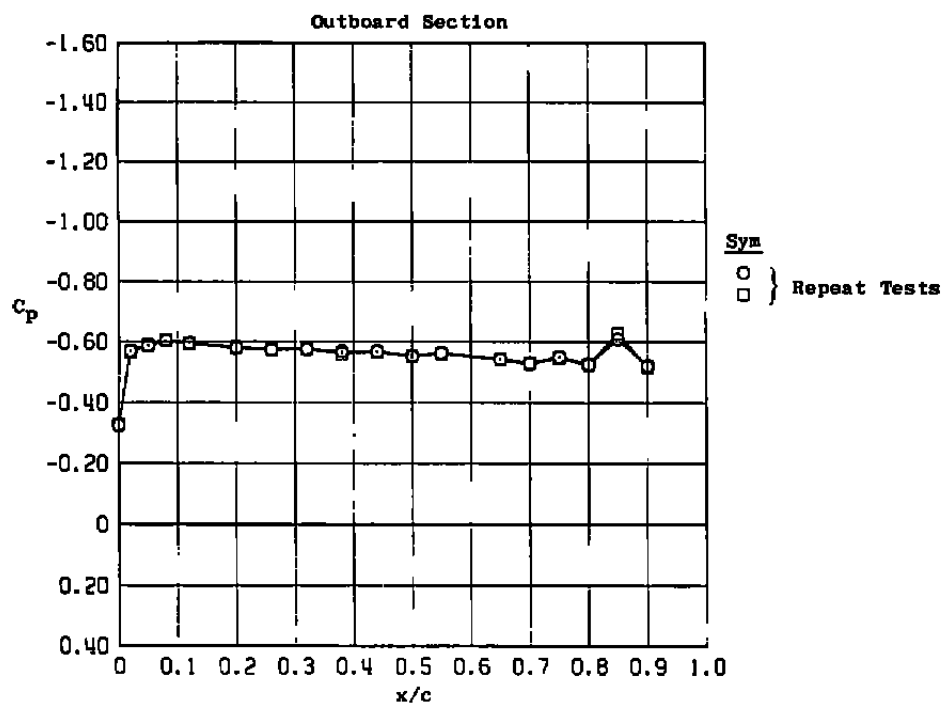


e.  $M_\infty = 0.95$   
 Figure 8. Concluded.



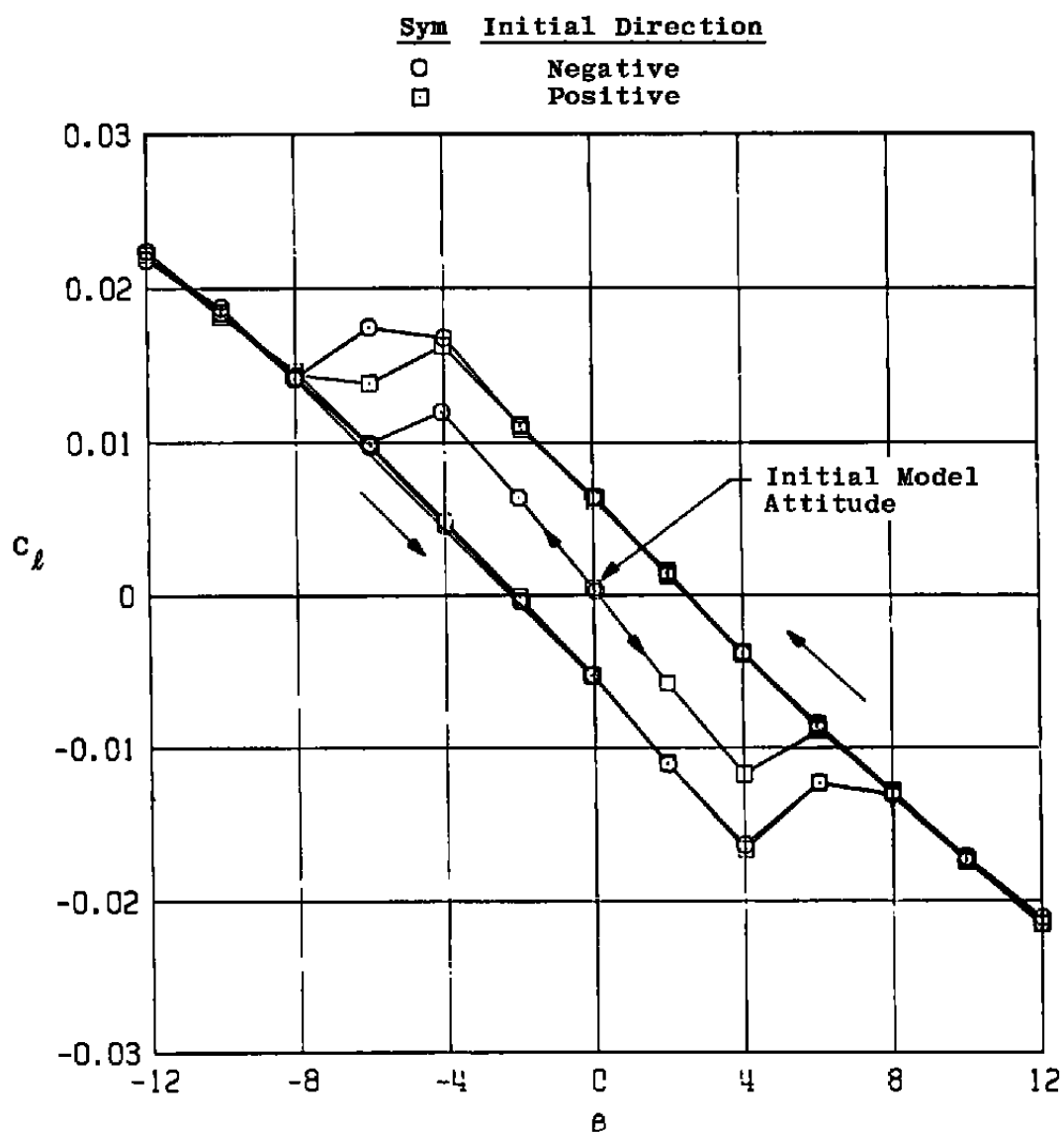
a. Decreasing  $\beta$ , from maximum positive angle

**Figure 9. Wing upper surface pressure distribution repeatability,  
 $M_\infty = 0.9$ ,  $\alpha = 15$  deg,  $\beta = 0$  deg.**



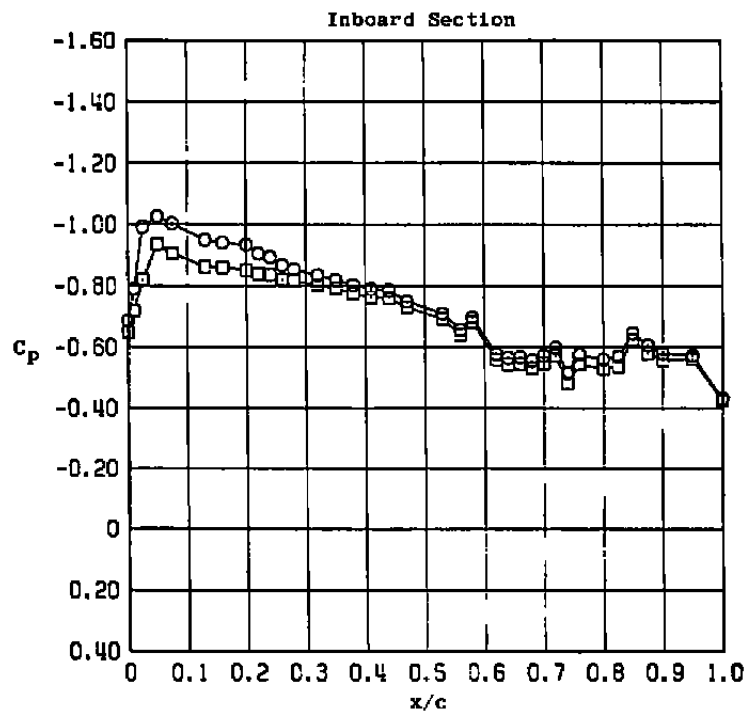
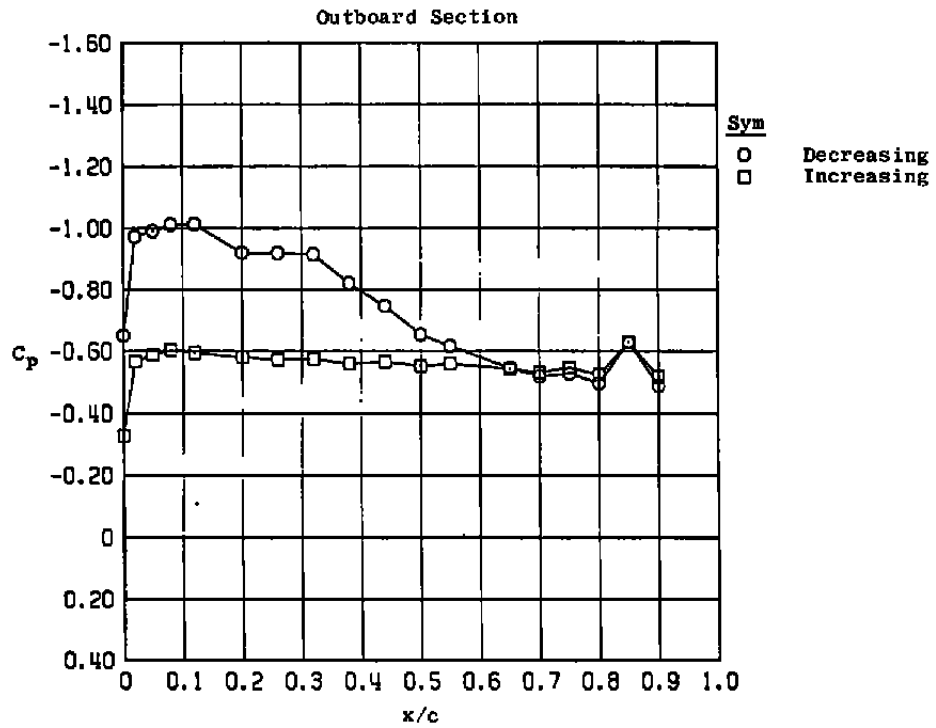
**b. Increasing  $\beta$ , from maximum negative angle  
Figure 9. Concluded.**





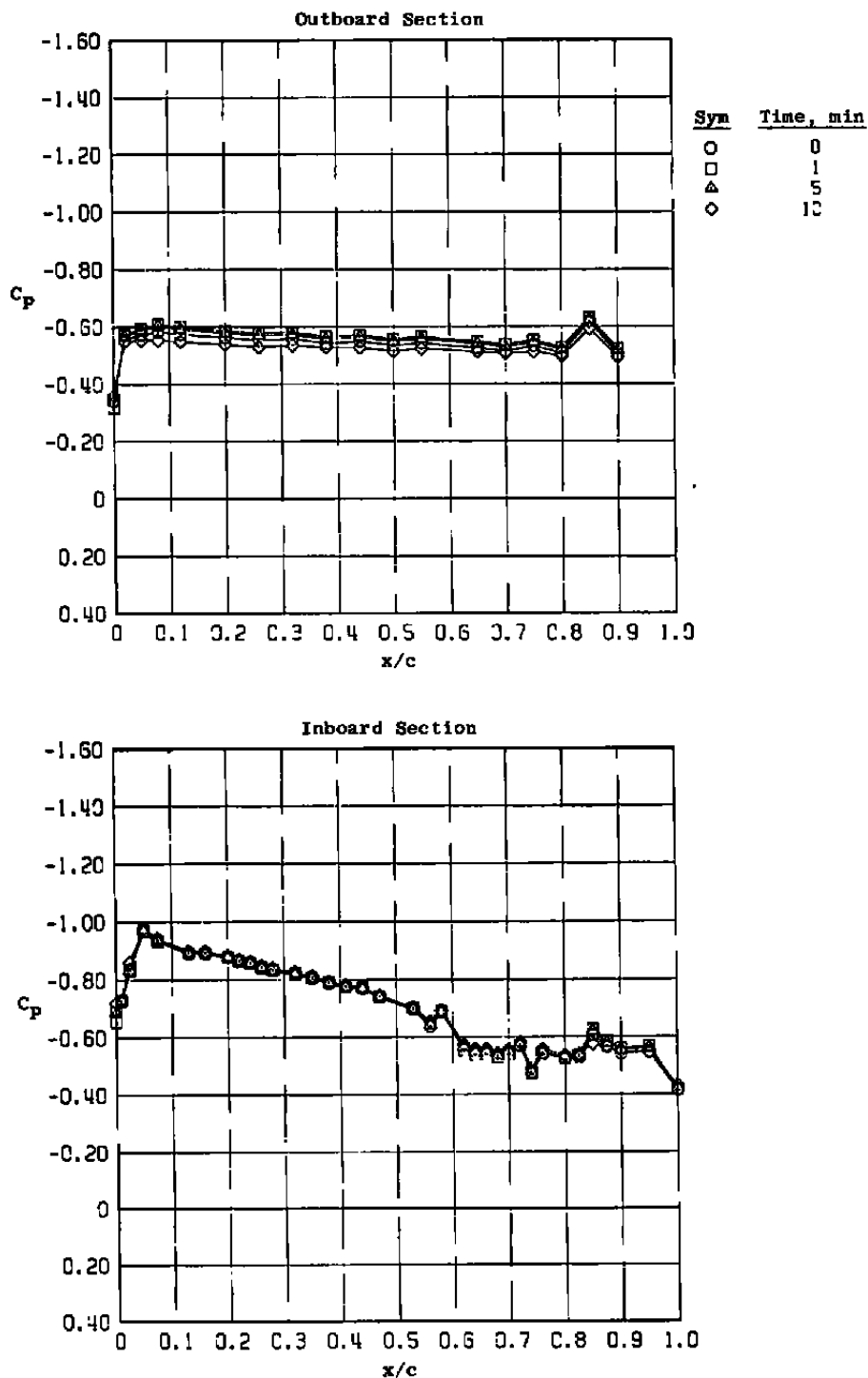
a. Rolling-moment coefficient

Figure 10. Effect of initial model sidesslip direction on the hysteresis characteristics,  $M_\infty = 0.9$ ,  $\alpha = 15$  deg.



b. Wing upper surface pressure distribution;  $\alpha = 15$  deg,  
 $\beta = 2$  deg; initial direction positive

Figure 10. Concluded.



**Figure 11. Wing upper surface pressure distribution time dependence, with increasing sideslip angle,  $M_\infty = 0.9$ ,  $\alpha = 15$  deg,  $\beta = 0$  deg.**

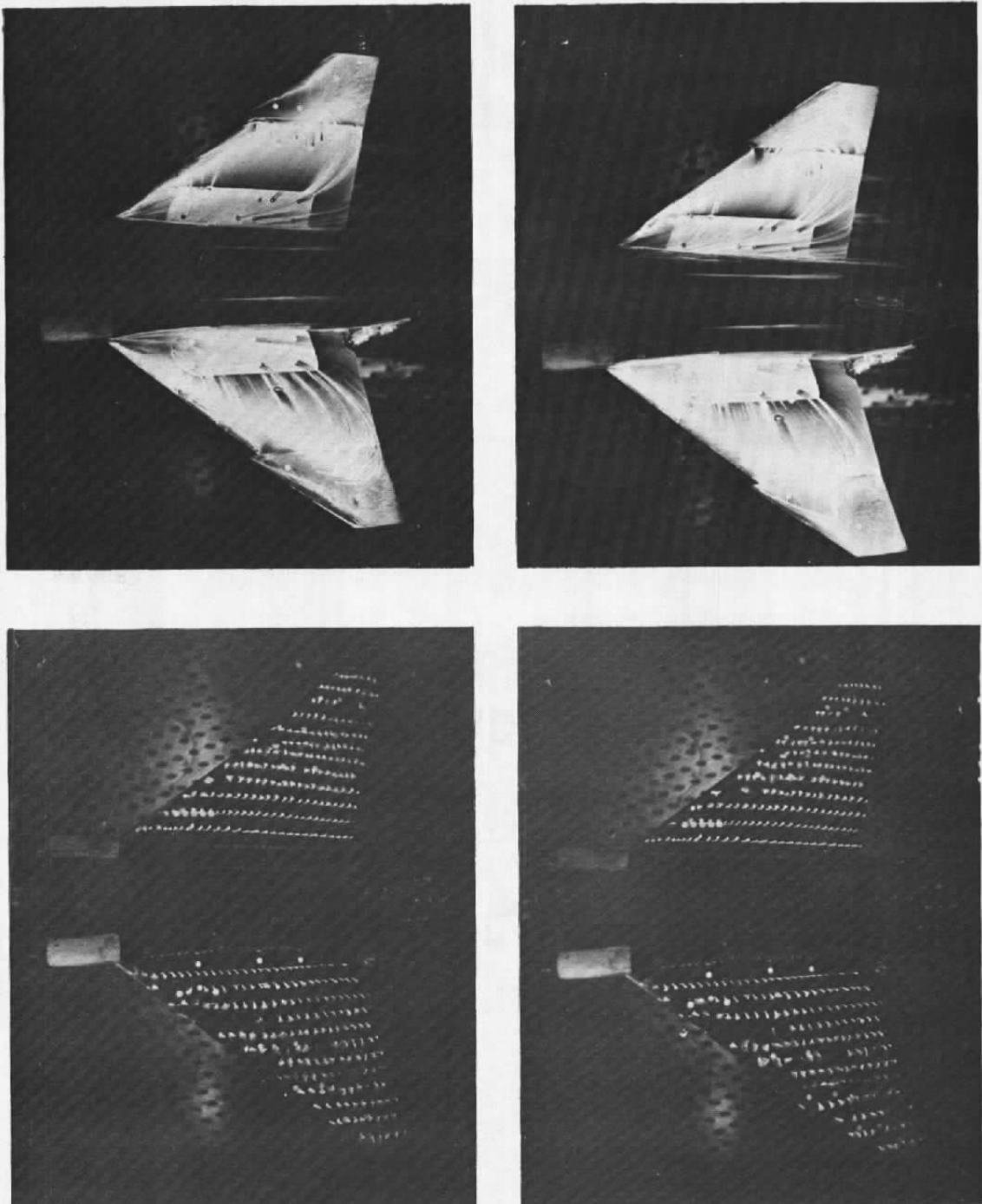
a. Increasing  $\beta$ b. Decreasing  $\beta$ 

Figure 12. Effect of previous model attitude history  
on the wing flow patterns of the clean F-4C  
 $M_\infty = 0.9$ ,  $\alpha = 15$  deg,  $\beta = 2$  deg.

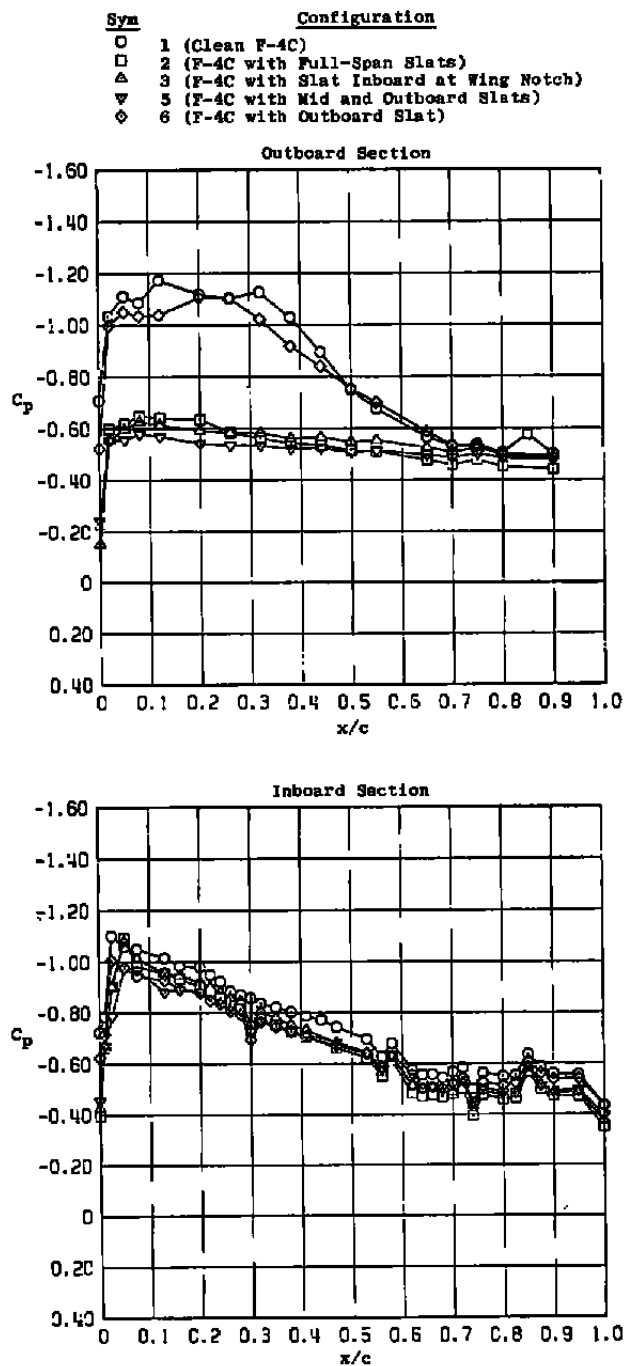


Figure 13. Effect of slats on wing upper surface pressure distributions with increasing angle of attack,  $M_\infty = 0.9$ ,  $\alpha = 15^\circ$ .

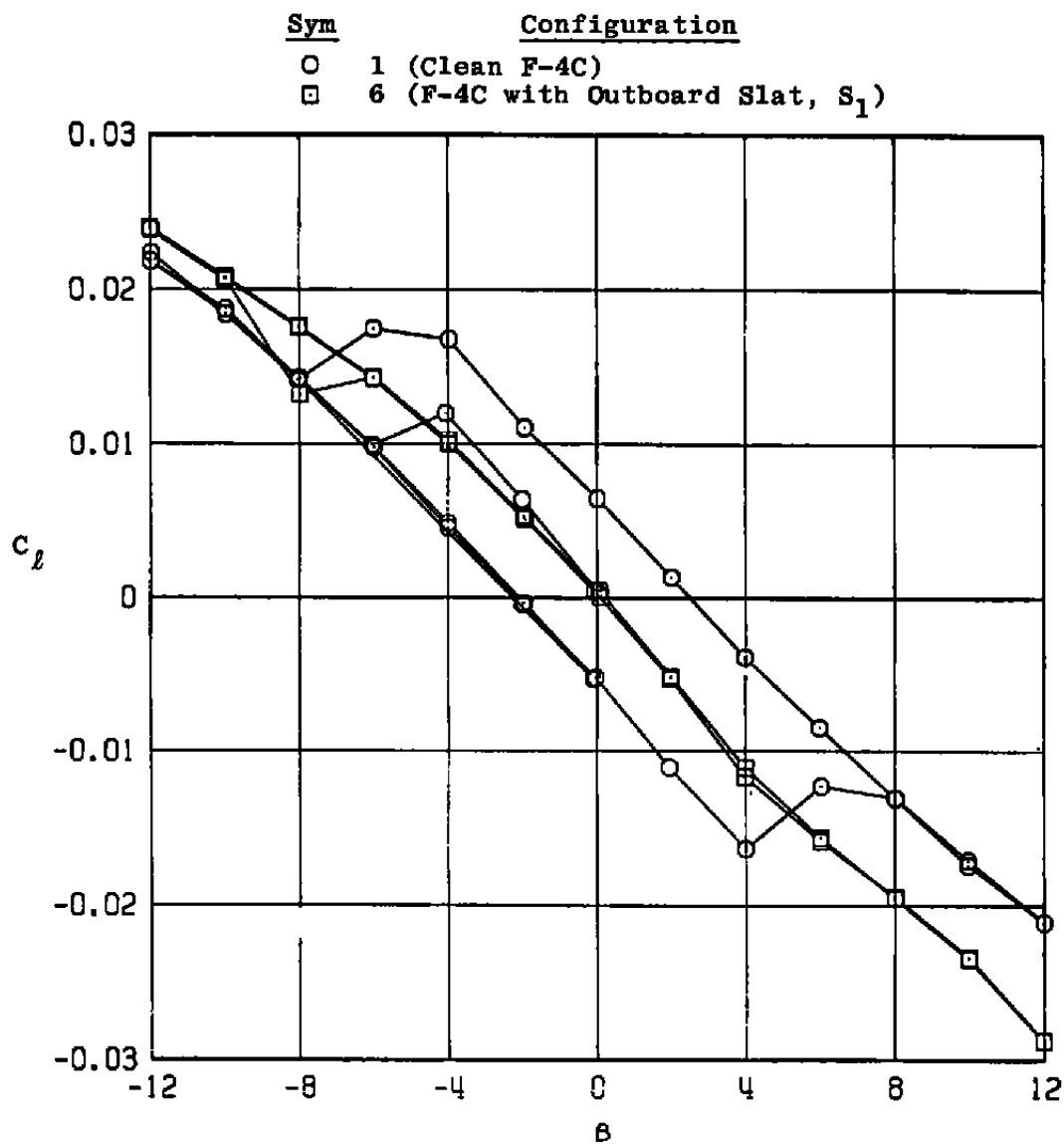


Figure 14. Effect of outboard slat,  $S_1$ , on the rolling-moment coefficient,  $M_\infty = 0.9$ ,  $\alpha = 15$  deg.

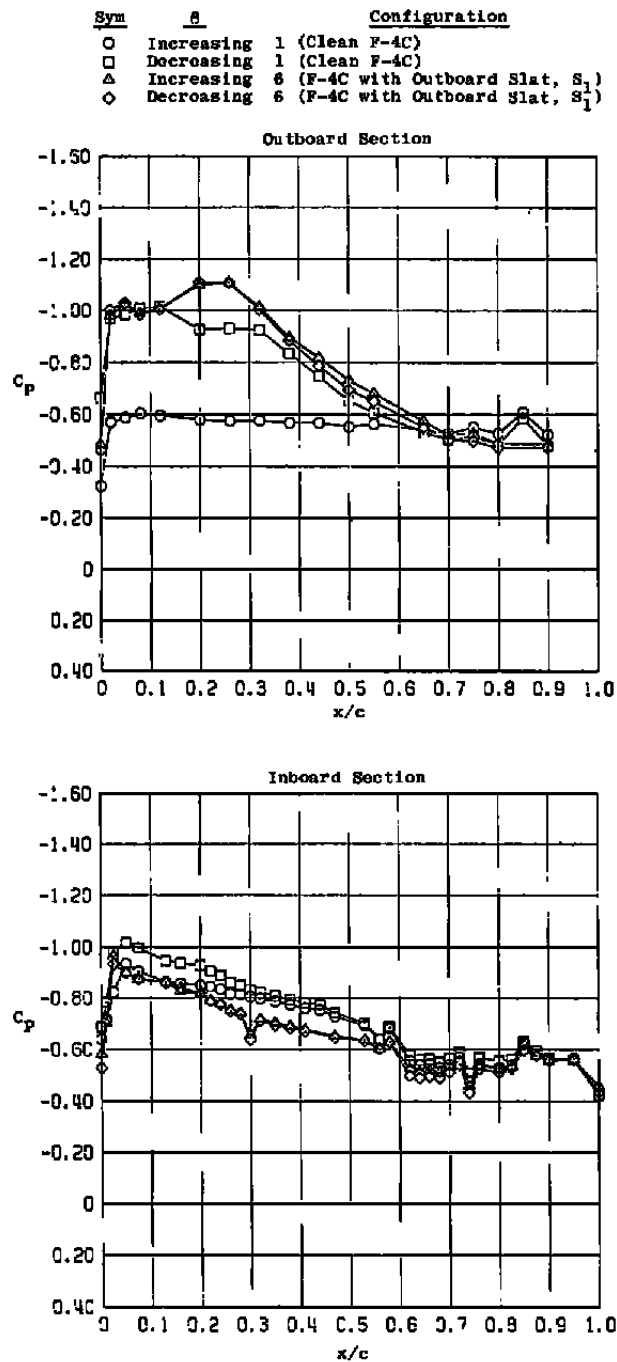


Figure 15. Effect of outboard slat,  $S_1$ , on wing upper surface pressure distribution,  $M_\infty = 0.9$ ,  $\alpha = 15$  deg,  $\beta = 2$  deg.

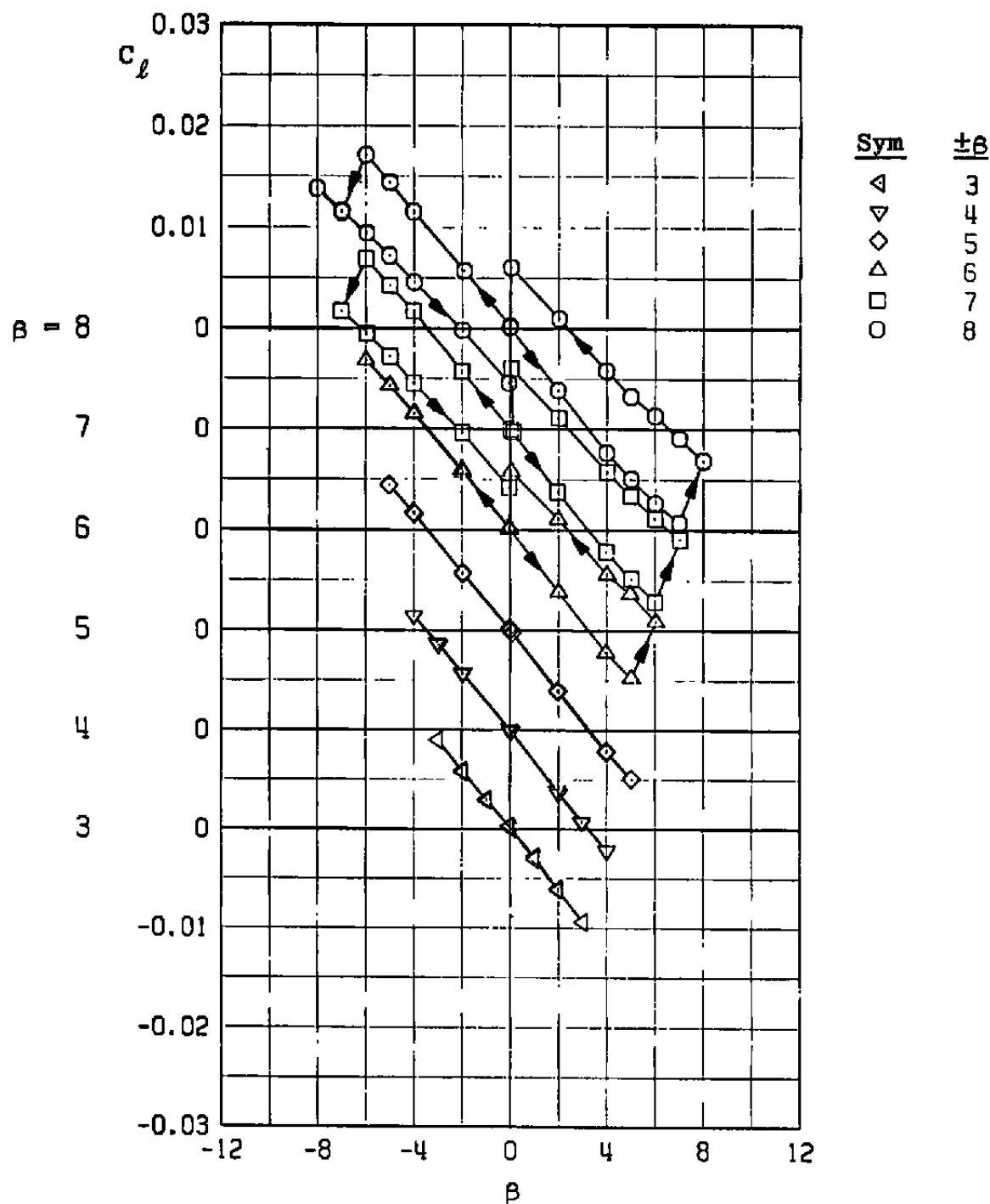


Figure 16. Effect of the magnitude of sideslip angle and the direction of model movement on the rolling-moment coefficient,  $M_\infty = 0.9$ ,  $\alpha = 15$  deg.



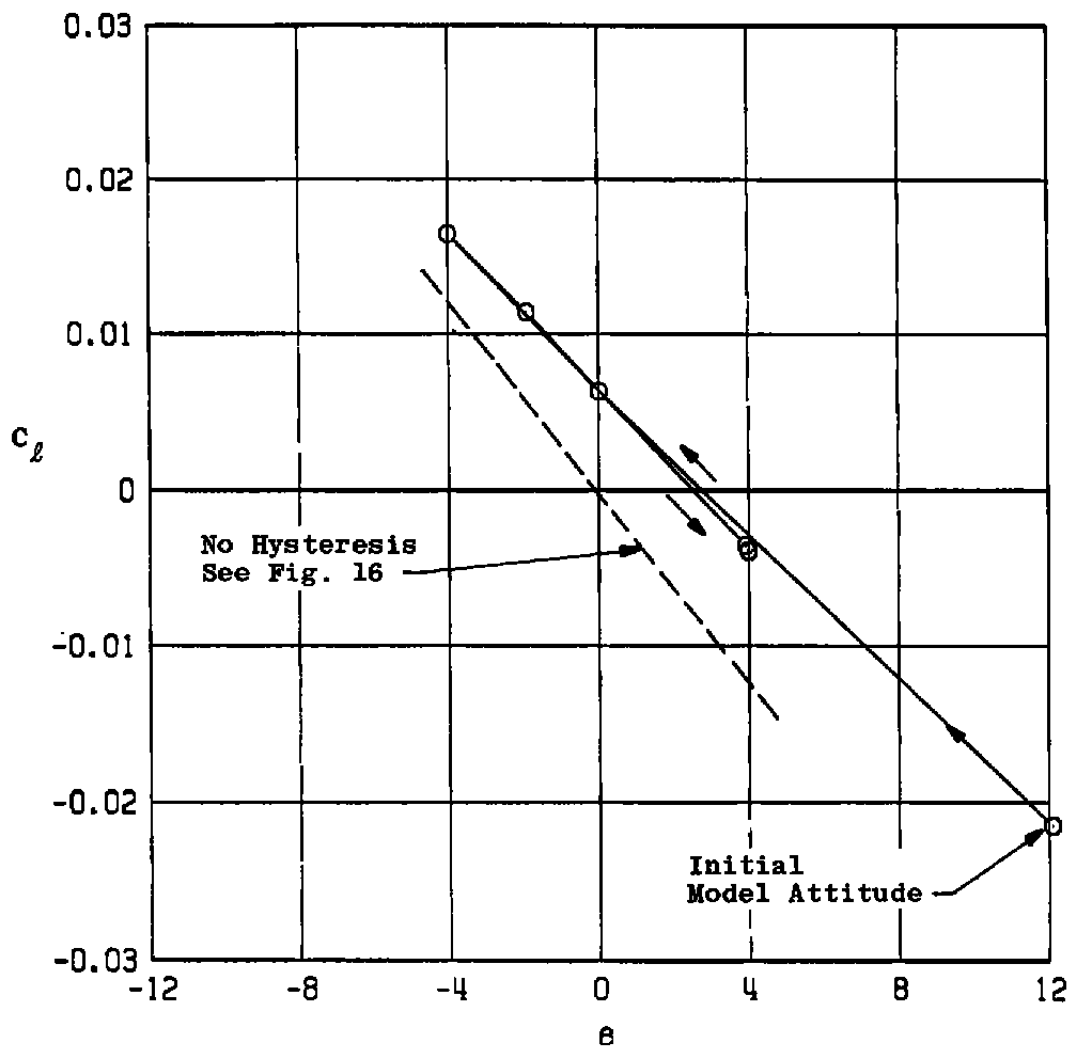
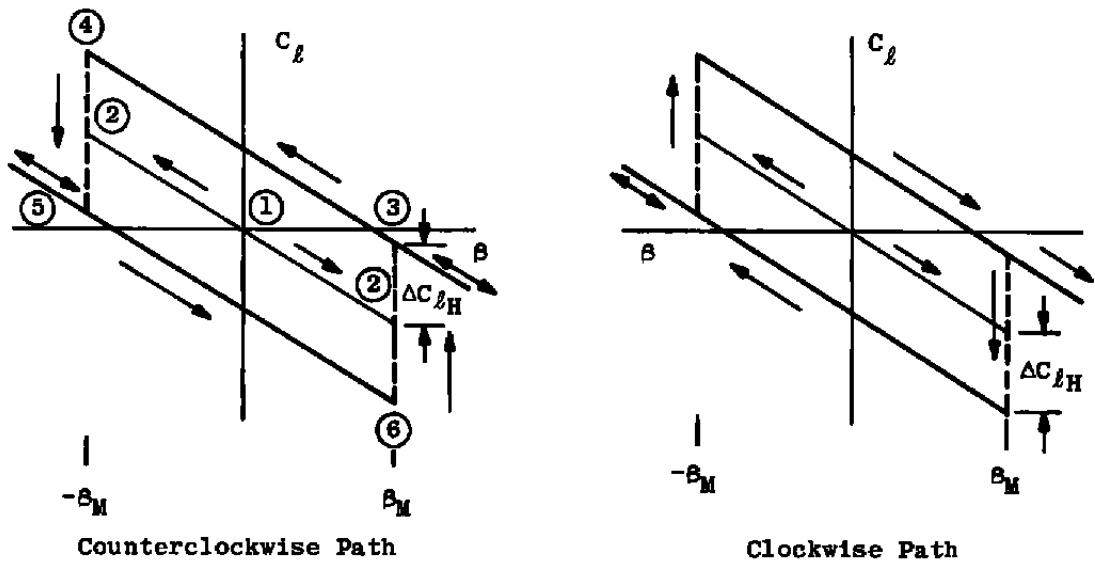
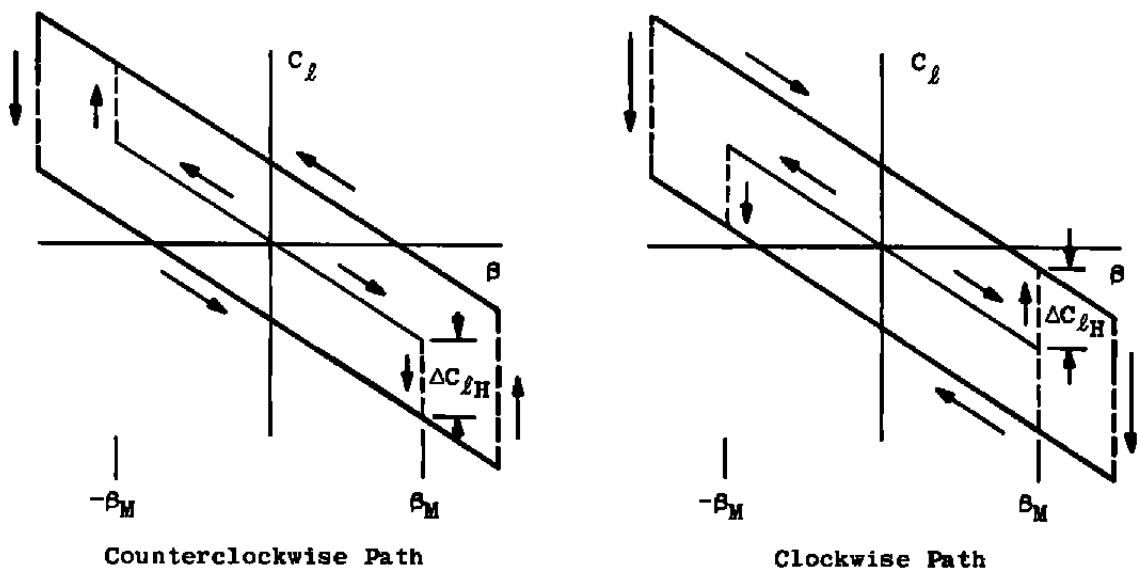


Figure 17. Characteristics of the rolling-moment coefficient in a hysteresis loop,  $M_\infty = 0.9$ ,  $\alpha = 15$  deg.

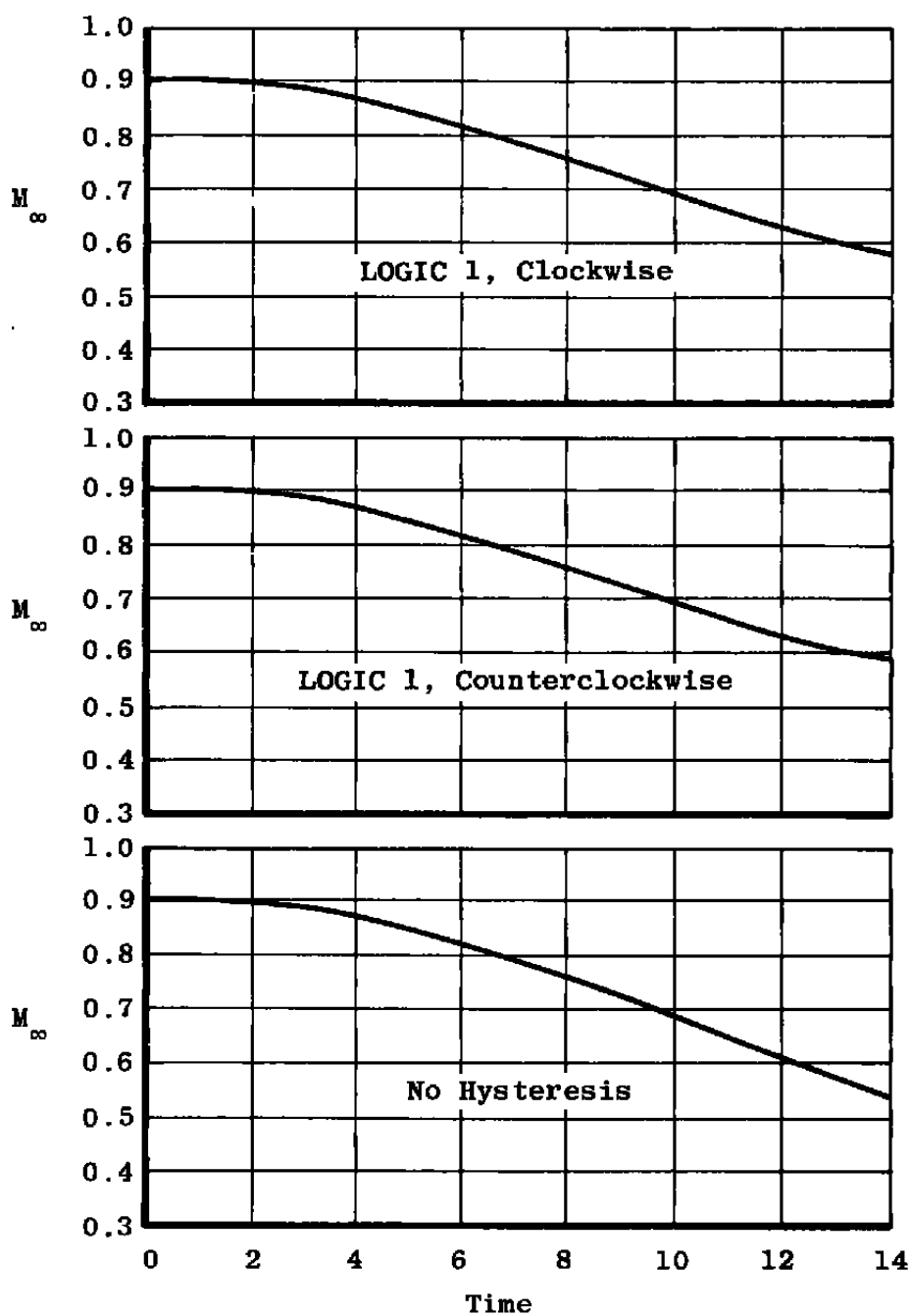


a. LOGIC 1



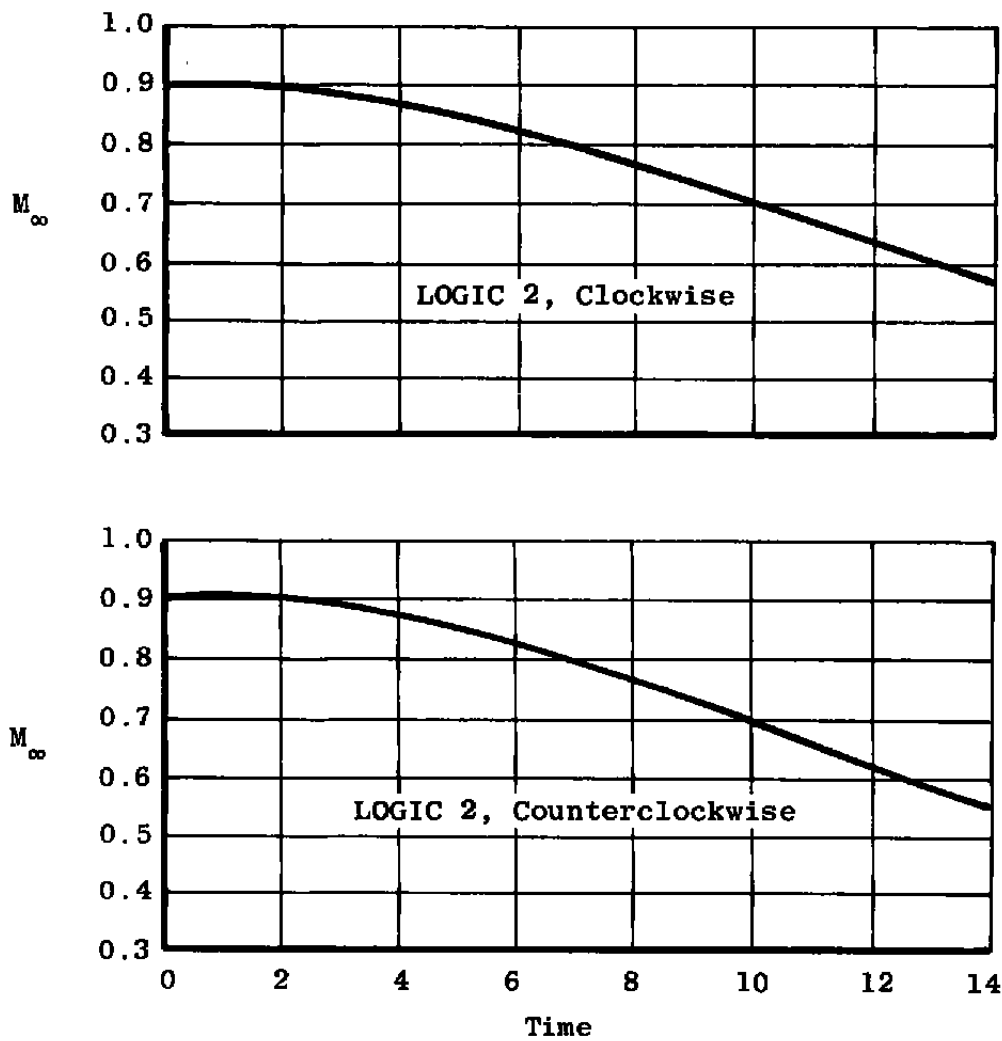
b. LOGIC 2

Figure 18. Motion simulation hysteresis logics.

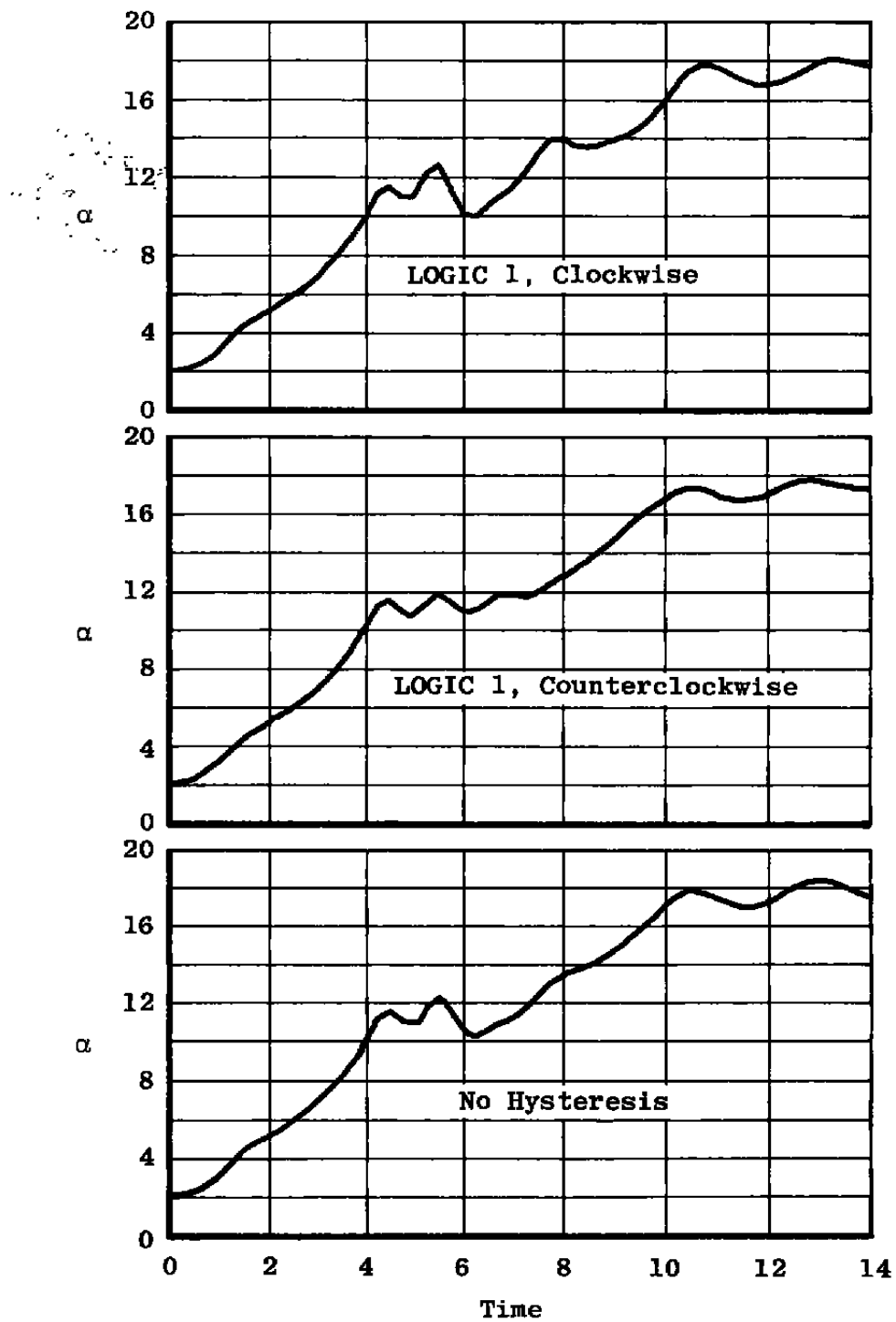


a. Mach number

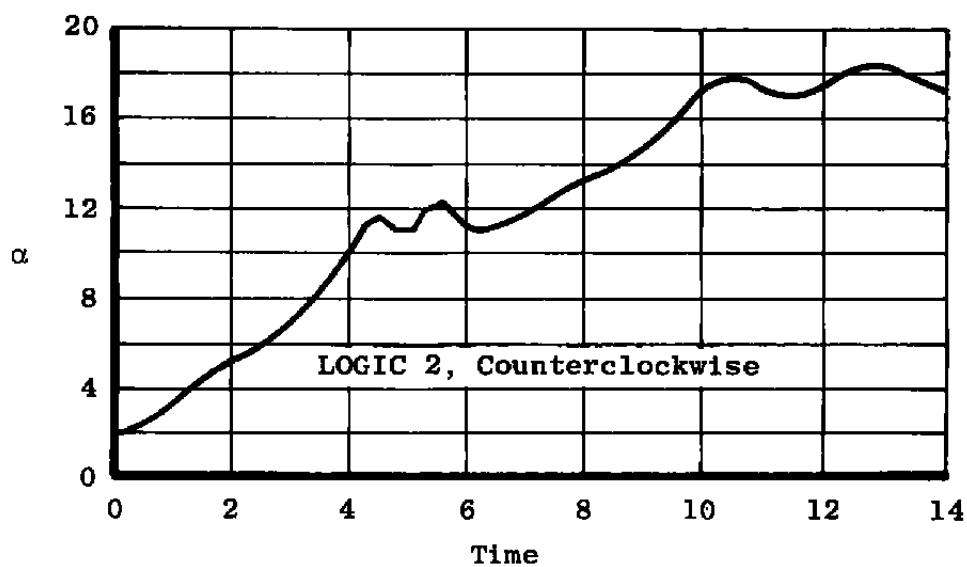
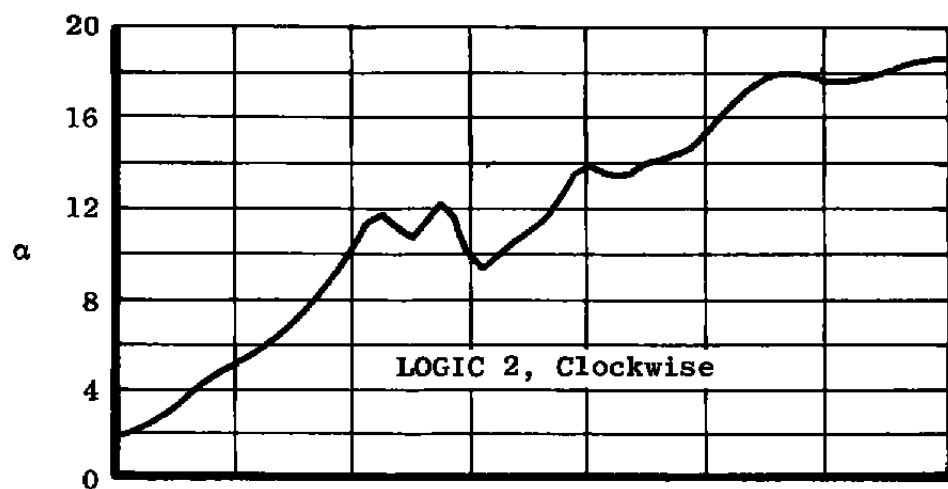
Figure 19. The effect of hysteresis logic on the aircraft motion—pull-up maneuver from level flight.



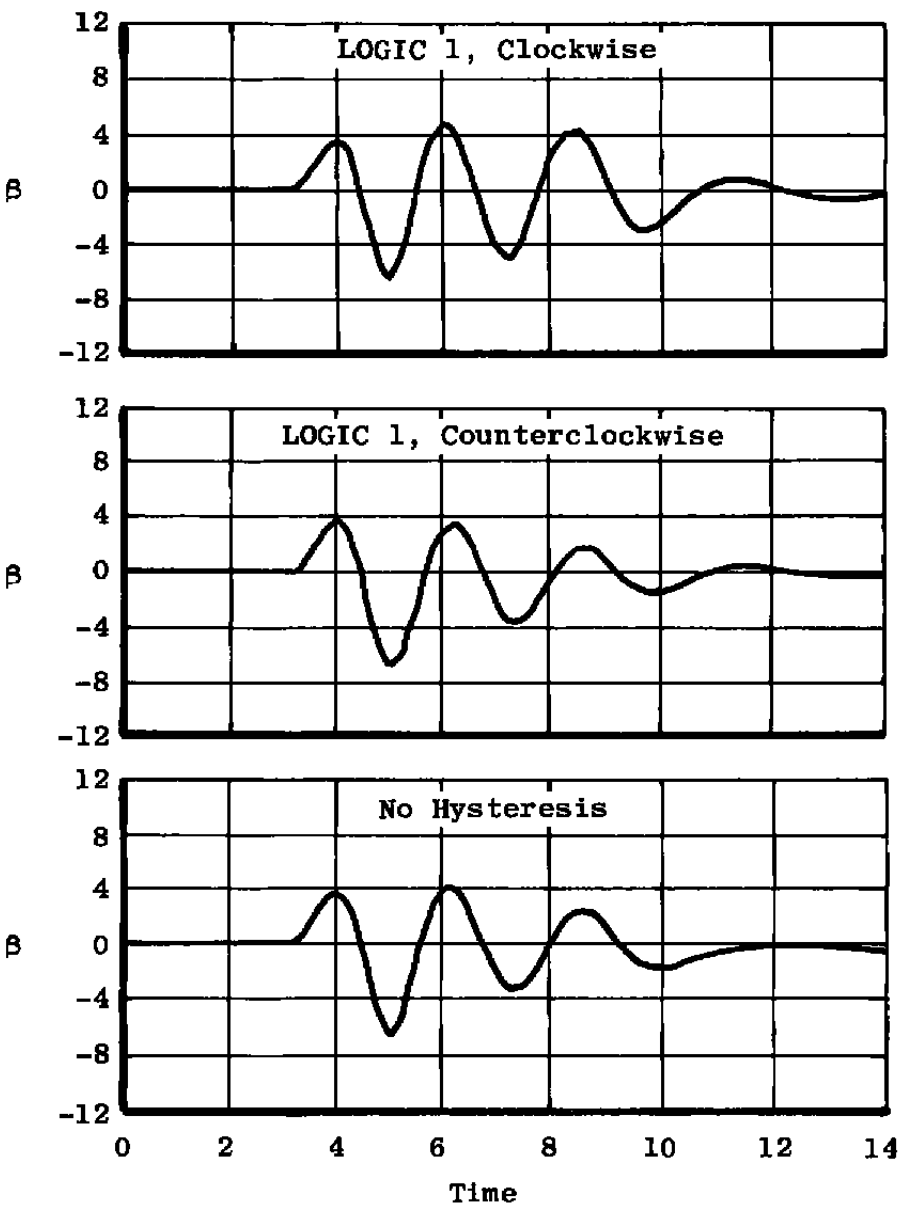
a. Concluded  
Figure 19. Continued.



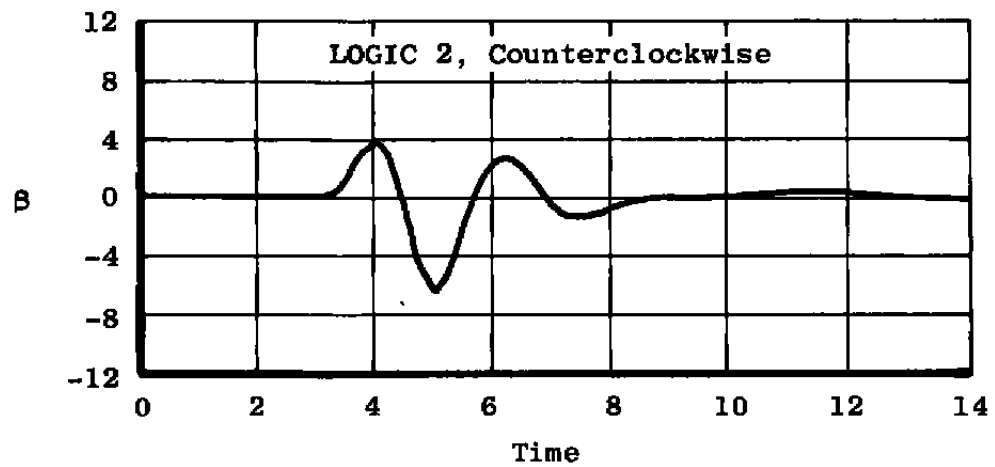
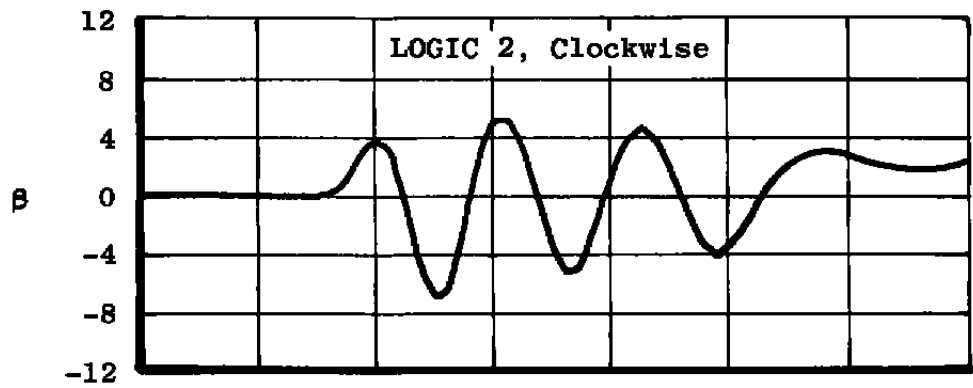
b. Angle of attack  
Figure 19. Continued.



b. Concluded  
Figure 19. Continued.

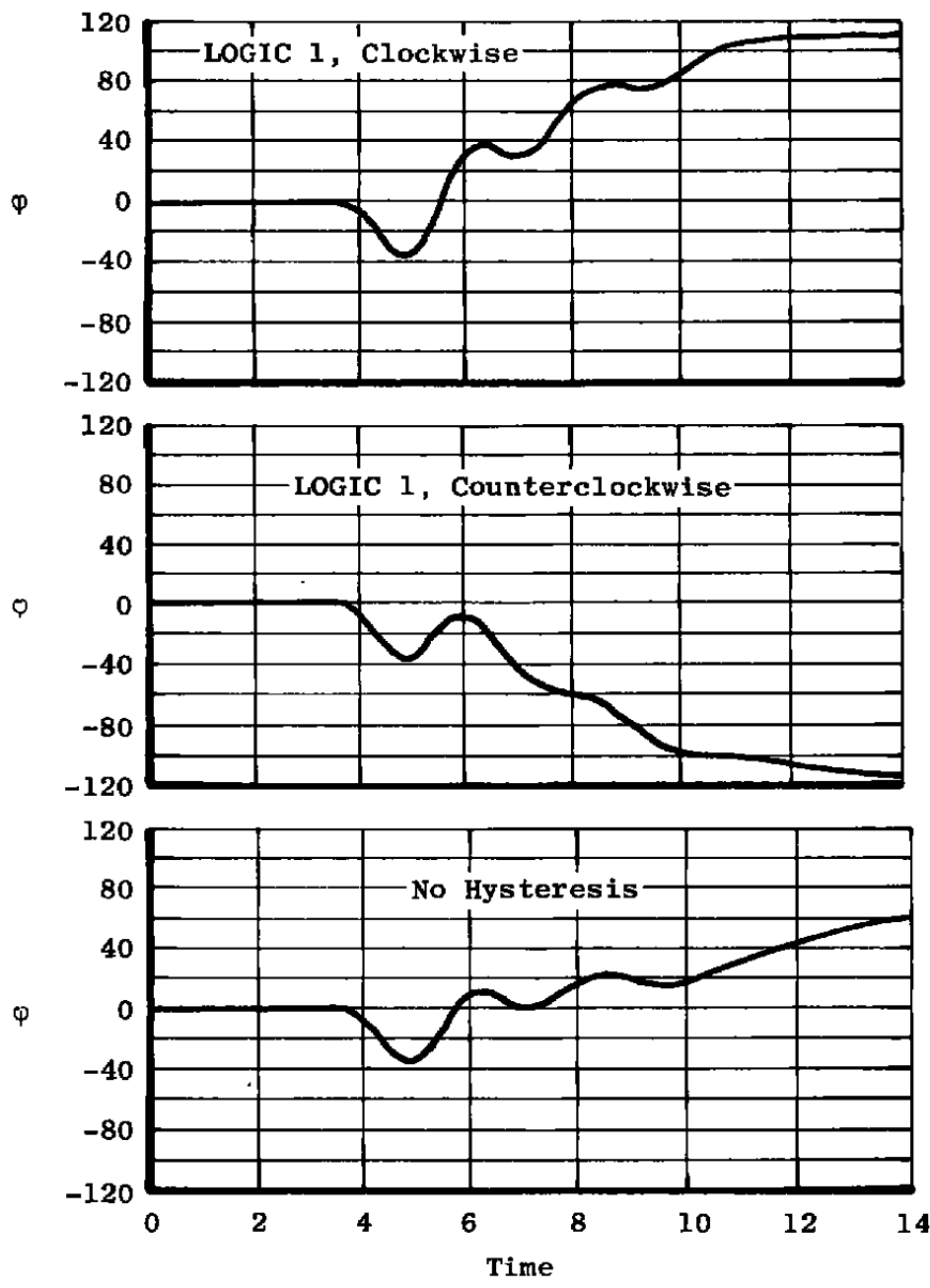


c. Sideslip angle  
Figure 19. Continued.

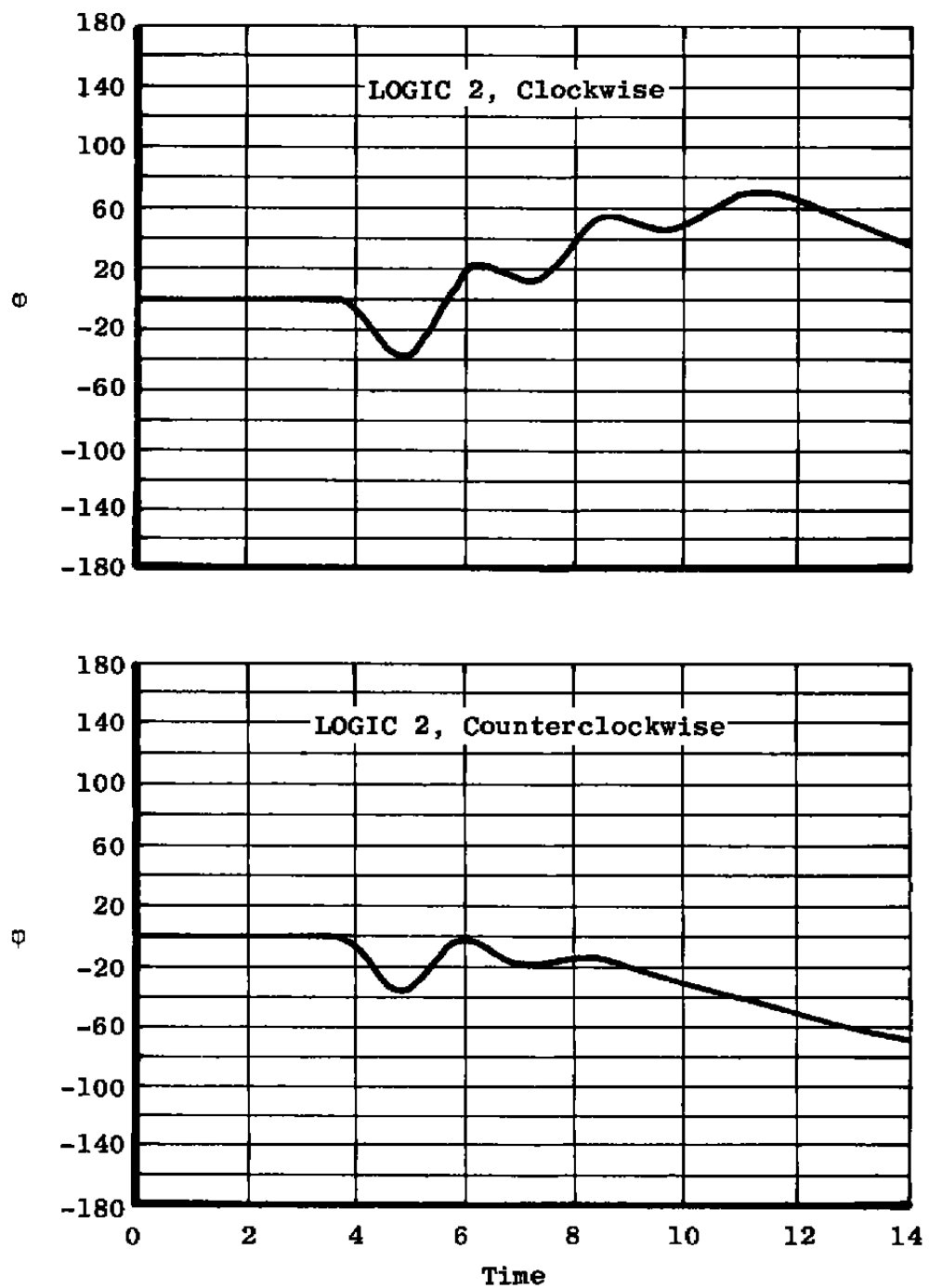


c. Concluded  
Figure 19. Continued.

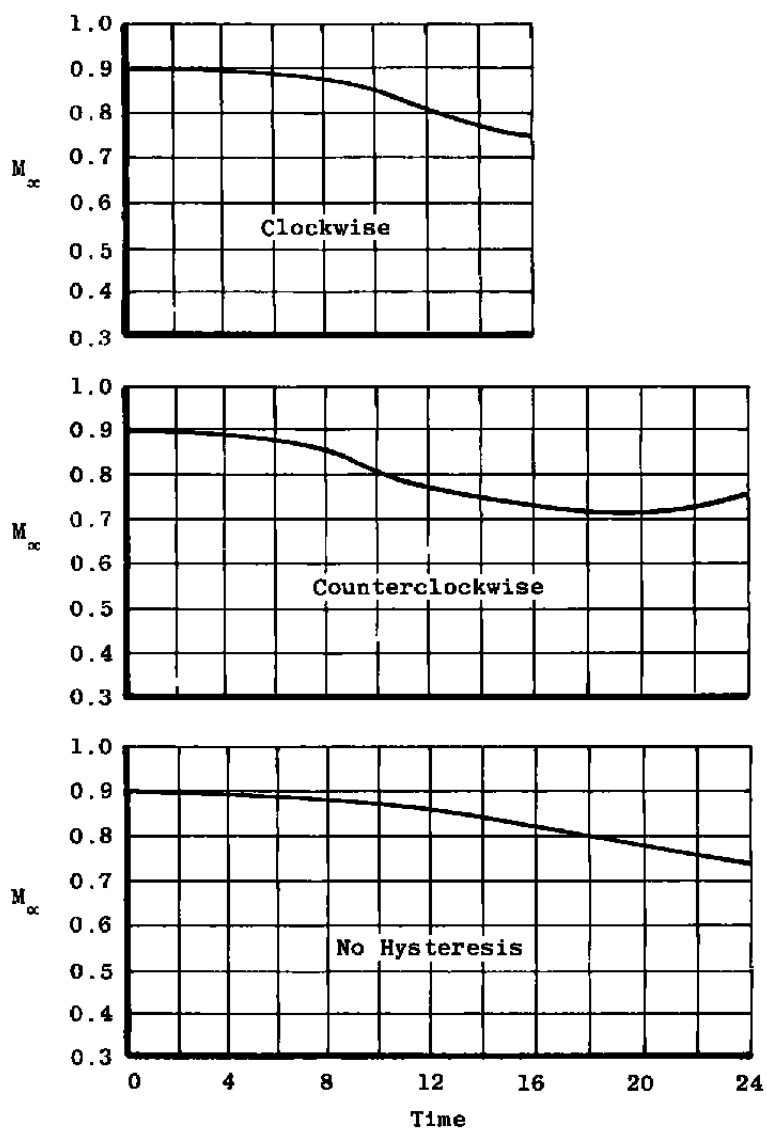




d. Roll angle  
Figure 19. Continued.

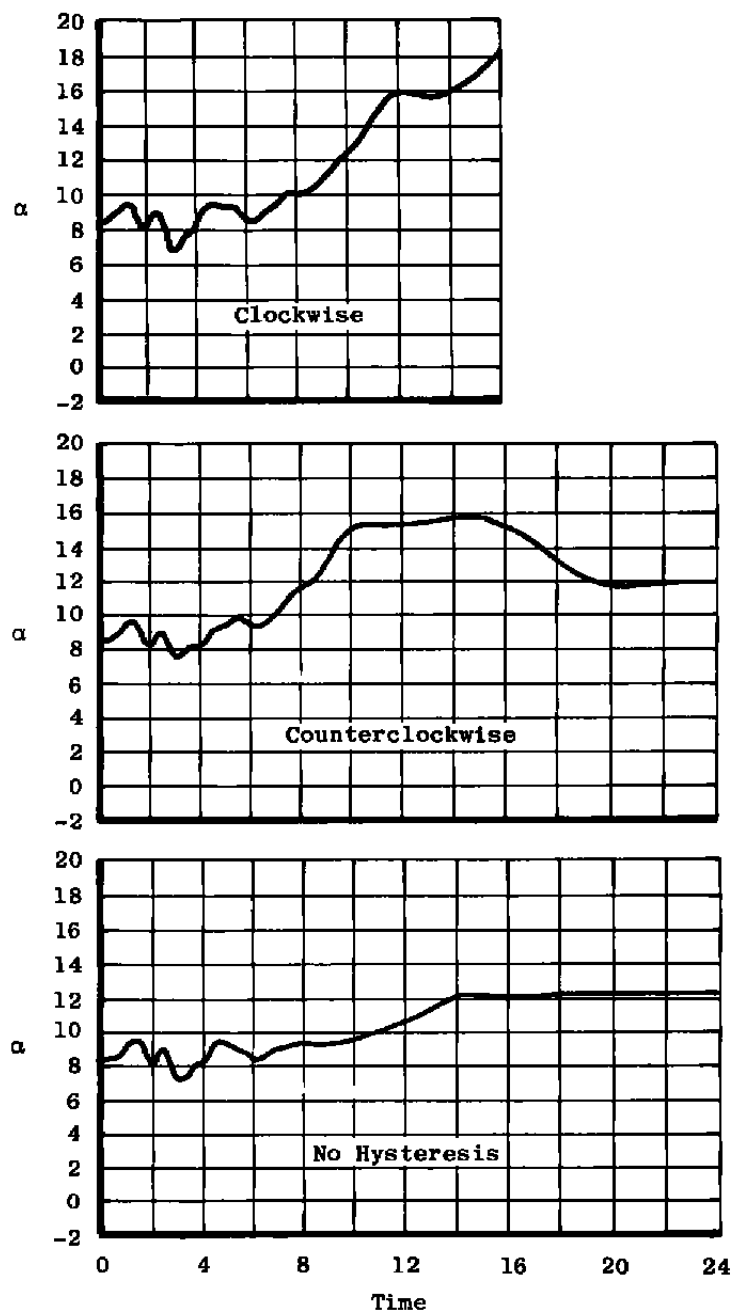


d. Concluded  
Figure 19. Concluded.

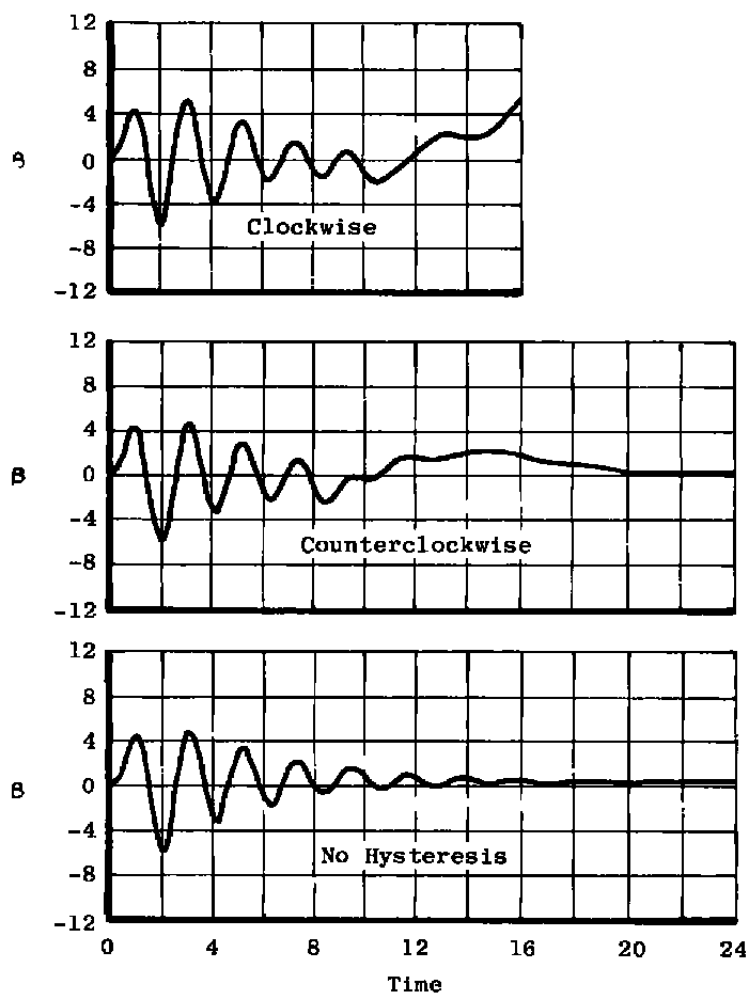


## a. Mach number

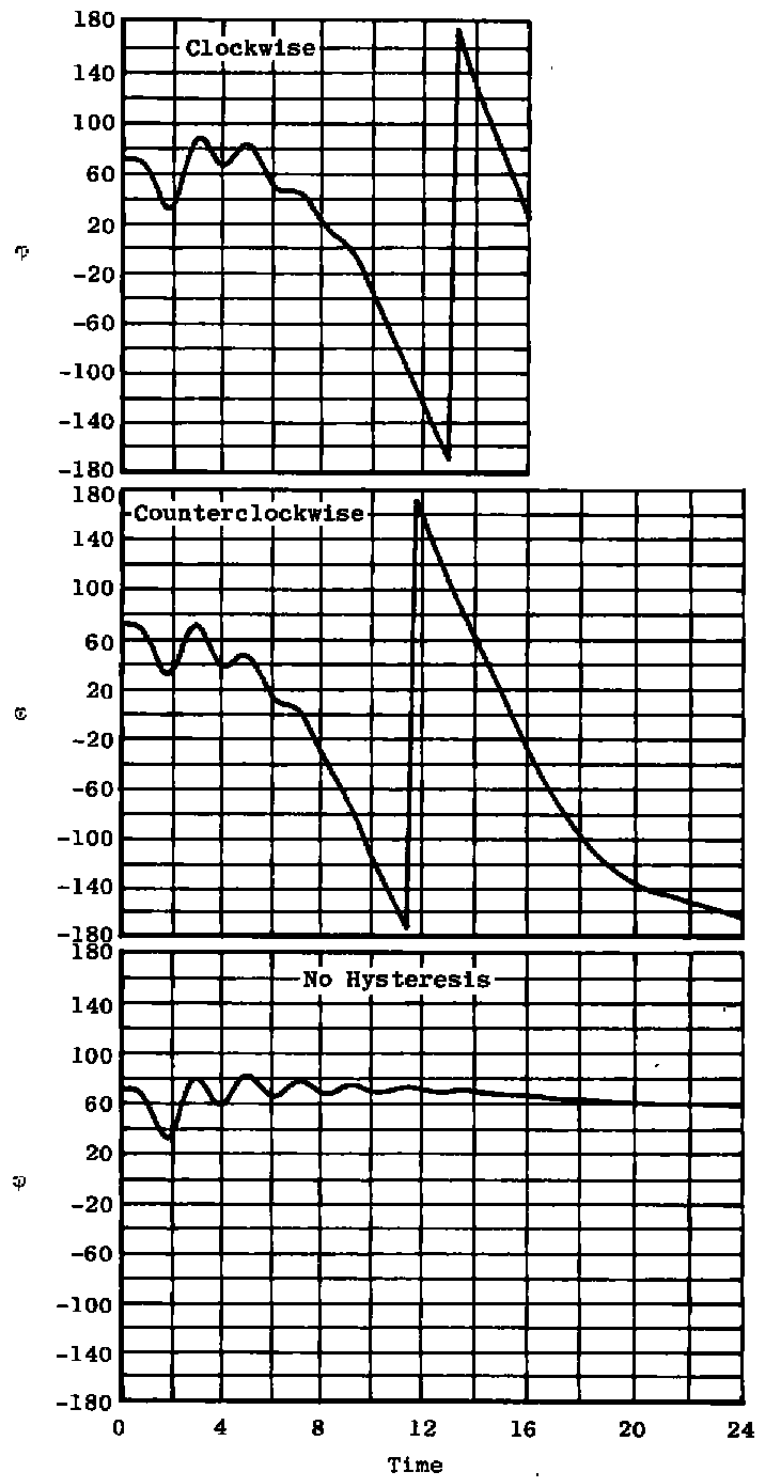
Figure 20. Effect of  $\Delta C_{\ell H}$  direction on the aircraft motion with LOGIC 1, 3-g turning flight.



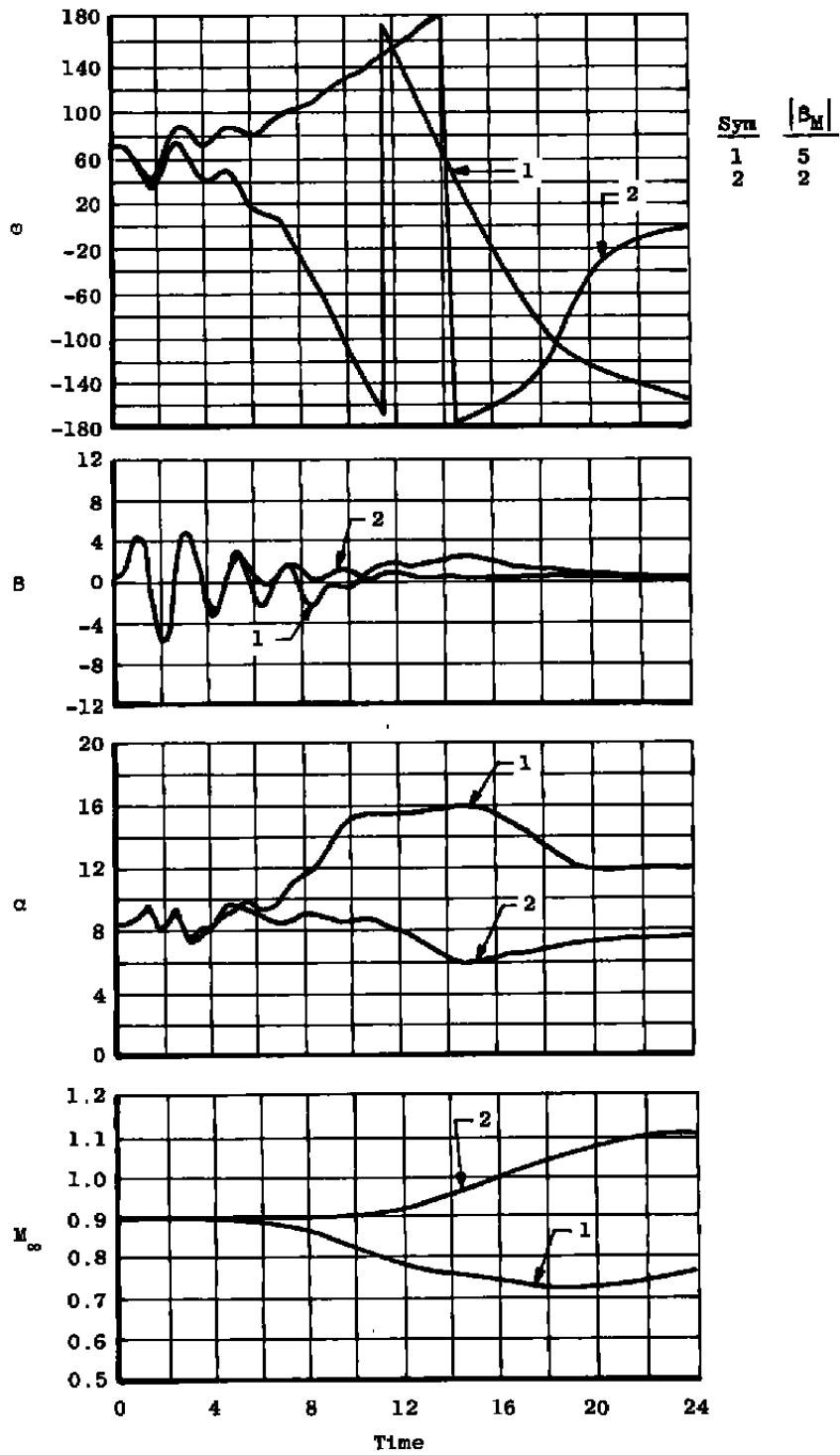
b. Angle of attack  
Figure 20. Continued.



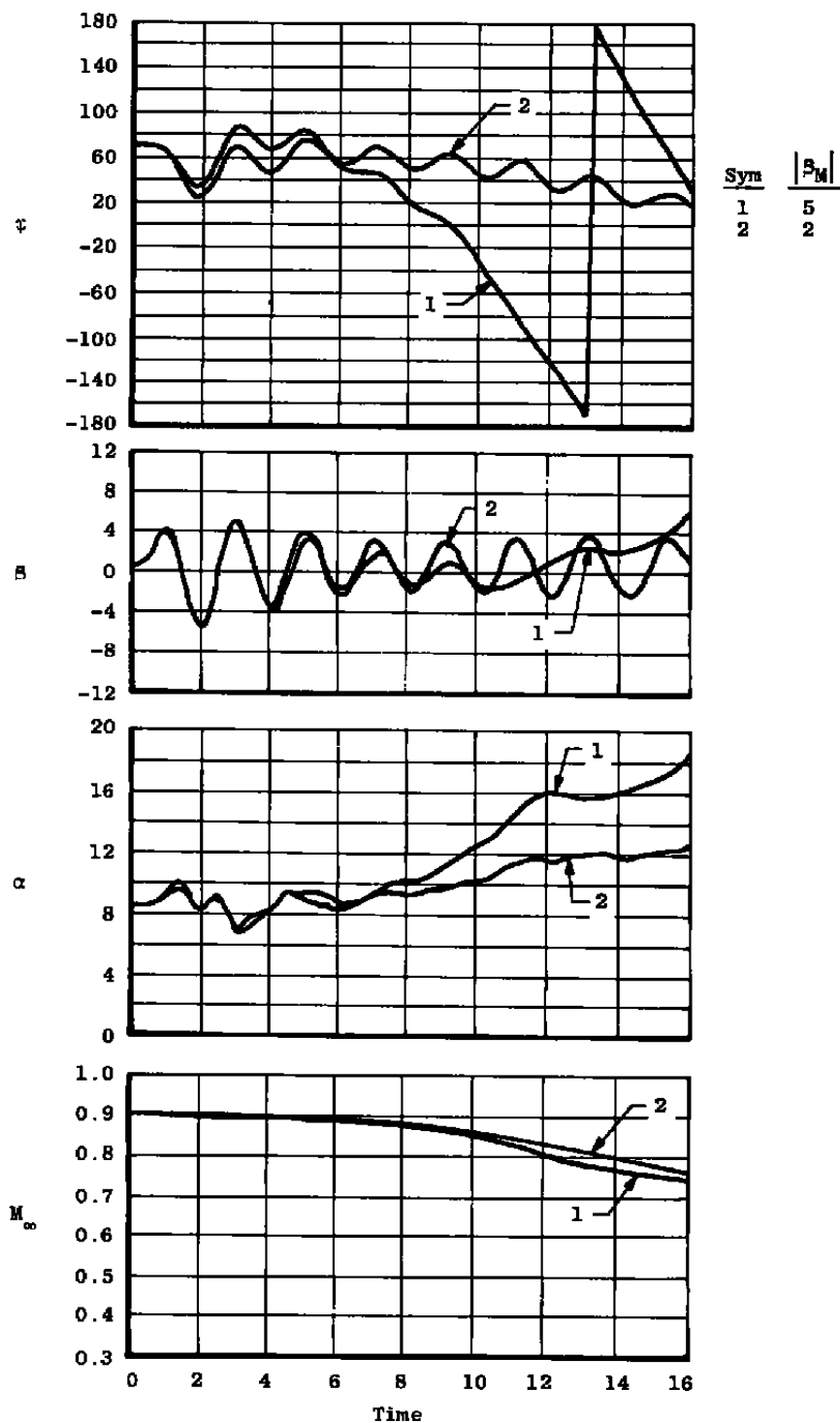
c. Sideslip angle  
Figure 20. Continued.



d. Roll angle  
Figure 20. Concluded.

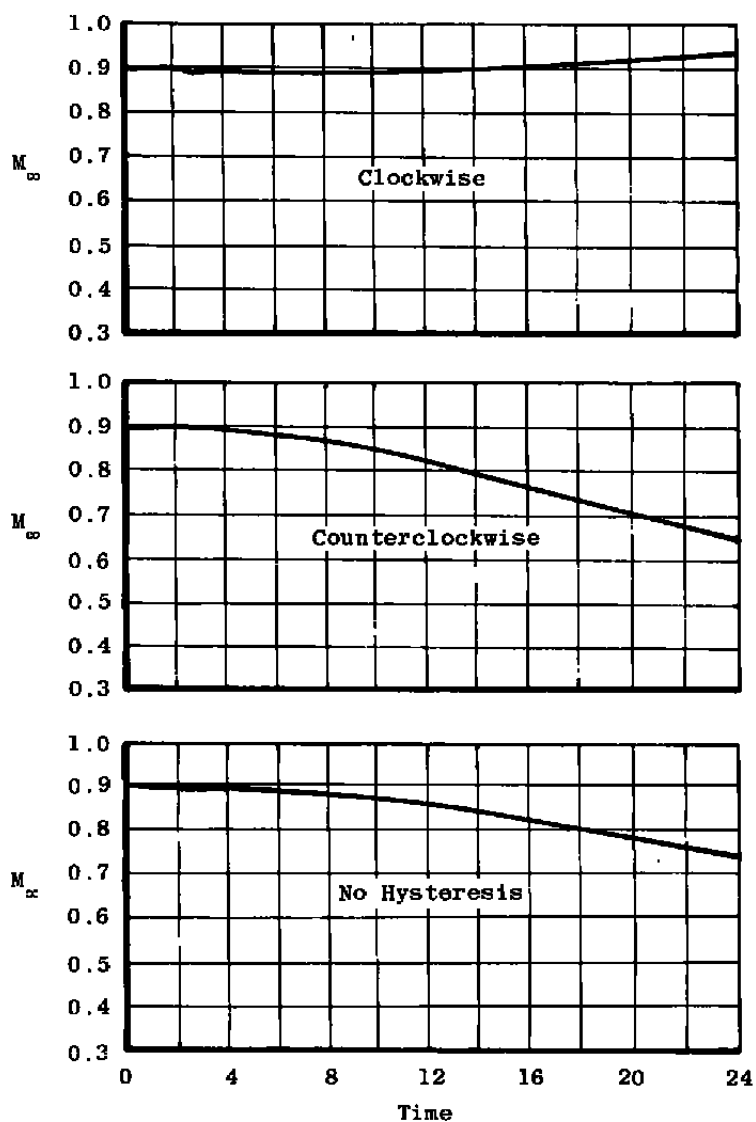


a. Counterclockwise  $\Delta C_{\ell_H}$   
Figure 21. Effect of  $\beta_M$  on the aircraft motion with LOGIC 1, 3-g turning flight.



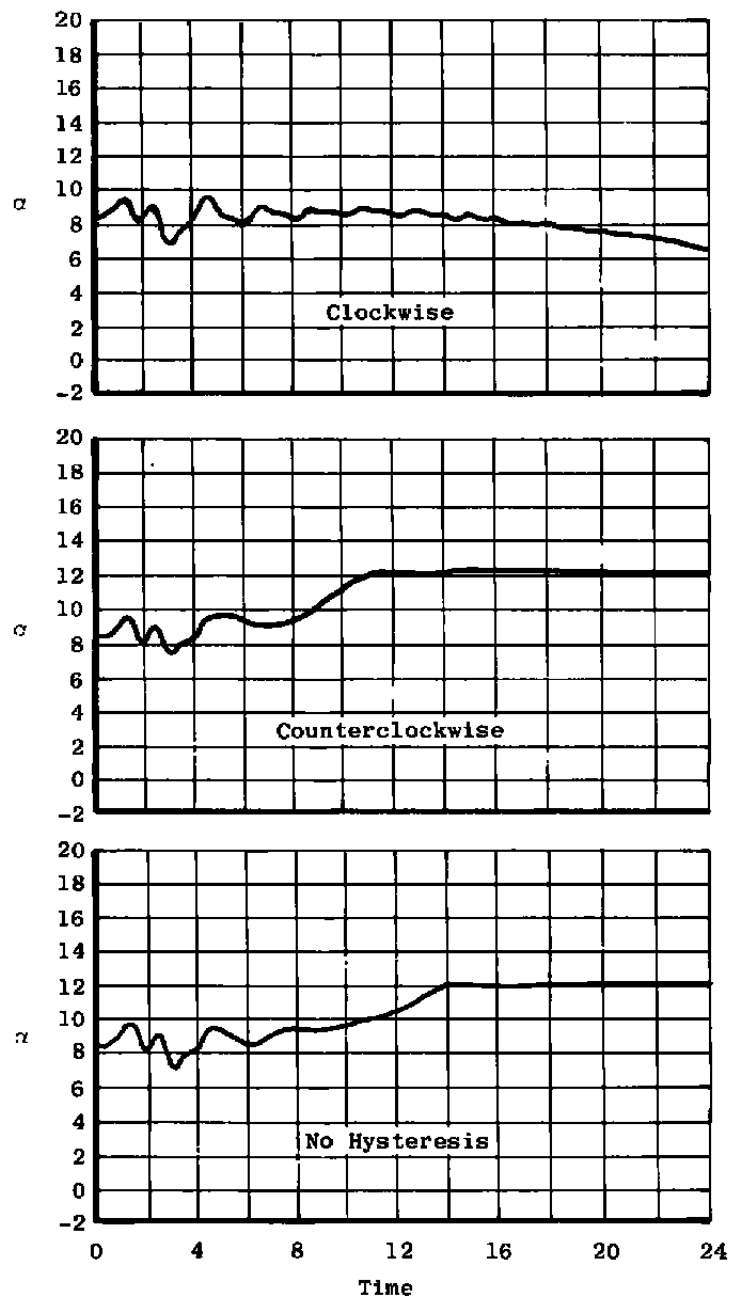
b. Clockwise  $\Delta C_{\ell H}$   
 Figure 21. Concluded.



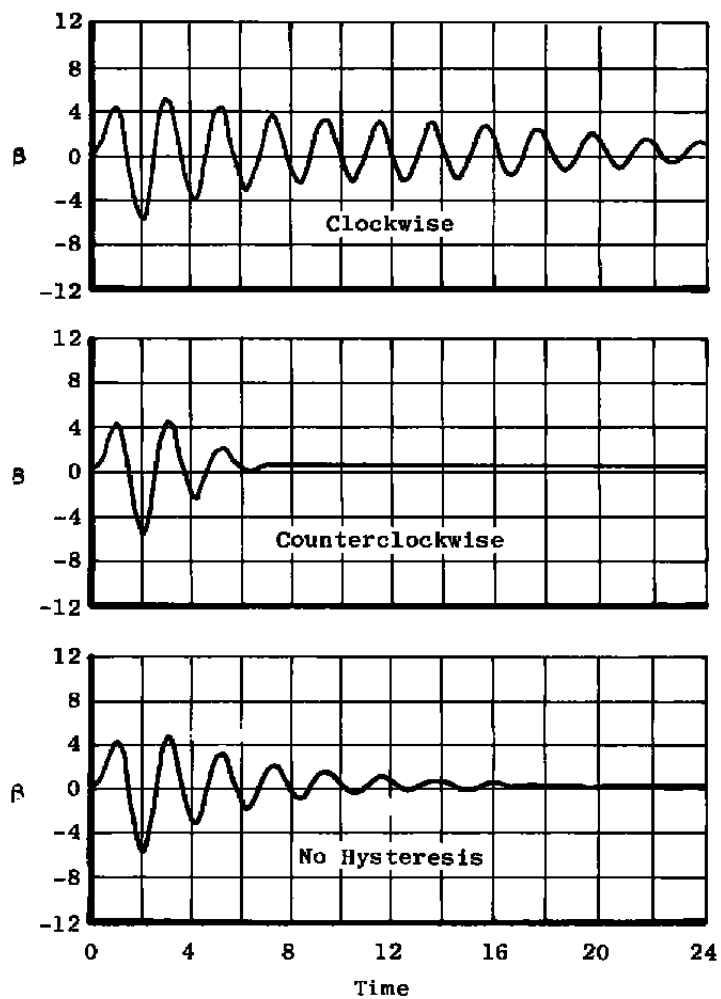


a. Mach number

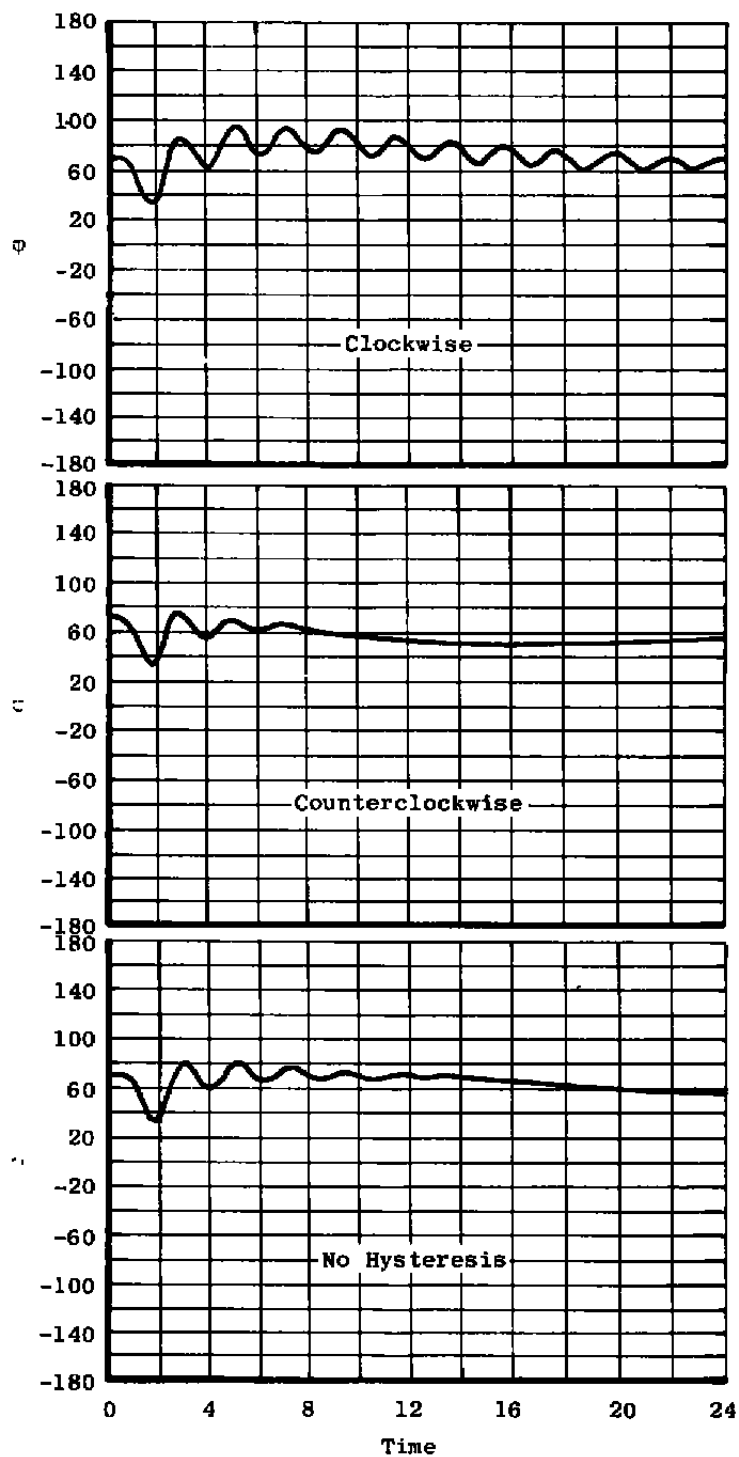
Figure 22. Effect of  $\Delta C_{\ell H}$  direction on the aircraft motion with LOGIC 2, 3-g turning flight.



b. Angle of attack  
Figure 22. Continued.



c. Sideslip angle  
Figure 22. Continued.



d. Roll angle  
Figure 22. Concluded.

Table 1. Configuration Identification

<u>Configuration Number</u>	<u>Configuration</u>
1	Clean F-4C model
2	F-4C with $S_1$ and $S_3$
3	F-4C with $S_3$
4	F-4C with $S_2$ (not tested - see Ref. 2)
5	F-4C with $S_1$ and $S_2$
6	F-4C with $S_1$

**Table 2. Mass, Inertia, and Dimensional Characteristics  
of the Full-Scale F-4 Aircraft**

Loading

Weight, lb.	36,950
Cg, percent Mean Aerodynamic Chord	33.0

Moments of Inertia, Slug-ft<sup>2</sup>

$I_X$	22,600
$I_Y$	163,100
$I_Z$	182,000
$I_{XZ}$	5,450

Wing

Span, ft	38.41
Area, ft <sup>2</sup>	538.34
Mean Aerodynamic Chord, ft	16.04

Inertia Coupling Terms

$$\begin{array}{ll} \frac{I_Y - I_Z}{I_X} = -0.836 & \frac{I_{XZ}}{I_X} = 0.241 \\ \frac{I_Z - I_X}{I_Y} = 0.977 & \frac{I_{XZ}}{I_Y} = 0.033 \\ \frac{I_X - I_Y}{I_Z} = -0.772 & \frac{I_{XZ}}{I_Z} = 0.030 \end{array}$$

**Table 3. Incremental Rolling-Moment Coefficient  
Attributable to Hysteresis**

Mach Number	Angle of attack, deg				
	0	5	10	15	20
0.7	0	0	0	0	0
0.8	0	0	0	0.005	0
0.85	0	0	0.001	0.009	0
0.9	0	0	0.002	0.006	0
0.95	0	0	0.001	0.005	0
1.1	0	0	0	0.002	0

## APPENDIX A EQUATIONS OF MOTION

### A-1.0 SIX-DEGREE-OF-FREEDOM, RIGID-BODY EQUATION OF MOTIONS

The dynamic equations required to specify the translational and rotational motions of a rigid body moving through space are described in this appendix. The six-degree-of-freedom nonlinear differential equations representing the linear and angular accelerations on a moving body axis system (Fig. A-2) whose origin is at the aircraft center of mass are given below.

Forces:

$$\dot{u} = rv - qw - g \sin \theta + \frac{F_x}{m} + \frac{T_x}{m}$$

$$\dot{v} = pw - ru + g \cos \theta \sin \phi + \frac{F_y}{m}$$

$$\dot{w} = qu - pv - g \cos \theta \cos \phi + \frac{F_z}{m} + \frac{T_z}{m}$$

Moments:

$$\dot{p} = \frac{I_y - I_z}{I_x} qr + \frac{I_{xz}}{I_x} (\dot{r} + pq) + \frac{M_x}{I_x}$$

$$\dot{q} = \frac{I_z - I_x}{I_y} pr + \frac{I_{xz}}{I_y} (r^2 - p^2) + \frac{M_y}{I_y} + \frac{M_{YT}}{I_y}$$

$$\dot{r} = \frac{I_x - I_y}{I_z} pq + \frac{I_{xz}}{I_z} (\dot{p} - qr) + \frac{M_z}{I_z}$$

The external forces and moments ( $F_x$ ,  $F_y$ ,  $F_z$ ,  $M_x$ ,  $M_y$ , and  $M_z$ ) in the equations are comprised of aerodynamic coefficients for the aircraft. The external force and moment contributions attributable to engine thrust are represented by  $T_x$ ,  $T_z$ , and  $M_{YT}$  and are developed in Section A-2.0. Development of the aerodynamic math model used is presented in Section A-3.0.



The auxiliary equations used in this analysis are the following:

$$\alpha = \tan^{-1} \left( \frac{w}{u} \right), \quad \beta = \sin^{-1} \left( \frac{v}{V} \right)$$

$$\dot{\alpha} = \frac{u\dot{w} - w\dot{u}}{u^2 + w^2}, \quad \dot{\beta} = \dot{v} - \frac{v}{V^2} \left( \frac{u\dot{u} + v\dot{v} + w\dot{w}}{\sqrt{u^2 + w^2}} \right)$$

$$V = \sqrt{u^2 + v^2 + w^2}, \quad \gamma = \tan^{-1} \left( \frac{\dot{h}}{\sqrt{\dot{x}^2 + \dot{y}^2}} \right)$$

$$\dot{\theta} = q \cos \phi - r \sin \phi$$

$$\dot{\phi} = p + \tan \theta (r \cos \phi + q \sin \phi)$$

$$\dot{\psi} = \frac{r \cos \phi + q \sin \phi}{\cos \theta}$$

The equations of motion are numerically integrated to provide time histories of the aircraft motion.

#### A-2.0 EQUATIONS DEFINING THE FORCE AND MOMENT CONTRIBUTIONS ATTRIBUTABLE TO ENGINE THRUST

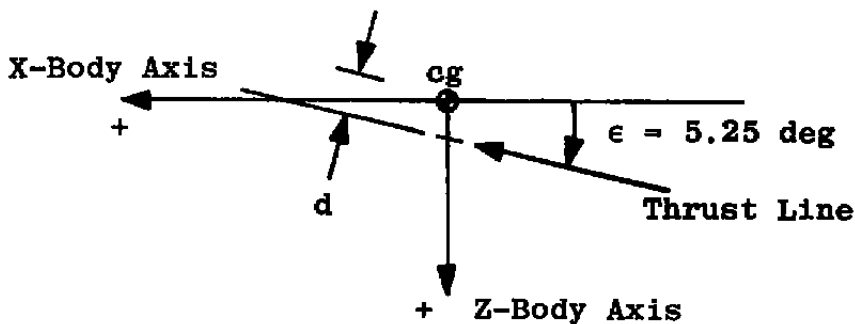


Figure A-1. External force and moment contributions attributable to engine thrust.

<u>Forces</u>	<u>Moments</u>
$T_X = T \cos \epsilon$	$M_{XT} = 0$
$T_Y = 0$	$M_{YT} = T(d)$
$T_Z = -T \sin \epsilon$	

where

$d$  = Distance between thrust line and CG

### Assumptions

1. Engine thrust line is parallel to X-Z plane.
2. There is no variation in Y and Z center of gravity location.

### A-3.0 EQUATIONS DEFINING THE TOTAL AERODYNAMIC DATA ALONG AND ABOUT EACH BODY AXIS

#### Longitudinal Axis Plane

$$F_X = q_\infty S \left\{ C_X(\alpha, \beta, M_\infty) + \Delta C_X(\alpha, M_\infty, \delta_H) + \left[ C_{X_q}(\alpha) \right] \frac{qC}{2V} \right\}$$

$$F_Z = q_\infty S \left\{ C_Z(\alpha, \beta, M_\infty) + \Delta C_Z(\alpha, M_\infty, \delta_H) + \left[ C_{Z_q}(M_\infty) q + C_{Z_{\dot{\alpha}}}(M_\infty) \dot{\alpha} \right] \frac{C}{2V} \right\}$$

$$M_Y = q_\infty S C \left\{ C_m(\alpha, \beta, M_\infty) + \Delta C_m(\alpha, M_\infty, \delta_H) + \left[ C_{m_q}(M_\infty) q + C_{m_{\dot{\alpha}}}(M_\infty) \dot{\alpha} \right] \frac{C}{2V} \right\}$$

#### Lateral-Directional Axis Plane

$$F_Y = q_\infty S \left\{ C_Y(\alpha, \beta, M_\infty) + \Delta C_Y(\alpha, M_\infty, \delta_H) + \Delta C_Y(\alpha, M_\infty, \delta_a) \right. \\ \left. + \left[ C_{Y_p}(\alpha, M_\infty) \right] \frac{Pb}{2V} + \left[ C_{Y_r}(\alpha, M_\infty) \right] \frac{rb}{2V} \right\}$$

$$M_Z = q_\infty S b \left\{ C_n(\alpha, \beta, M_\infty) + \Delta C_n(\alpha, M_\infty, \delta_r) + \Delta C_n(\alpha, M_\infty, \delta_a) \right. \\ \left. + \left[ C_{n_p}(\alpha, M_\infty) \right] \frac{Pb}{2V} + \left[ C_{n_r}(\alpha, M_\infty) \right] \frac{rb}{2V} \right\}$$

$$M_X = q_\infty S b \left\{ C_\ell(\alpha, \beta, M_\infty) + \Delta C_\ell(\alpha, \beta, \delta_a) + \Delta C_\ell(\alpha, \beta, \delta_r) \right. \\ \left. + \Delta C_{\ell_H}(\alpha, M_\infty) + \left[ C_{\ell_p}(\alpha, M_\infty) \right] \frac{Pb}{2V} - \left[ C_{\ell_r}(\alpha, M_\infty) \right] \frac{rb}{2V} \right\}$$

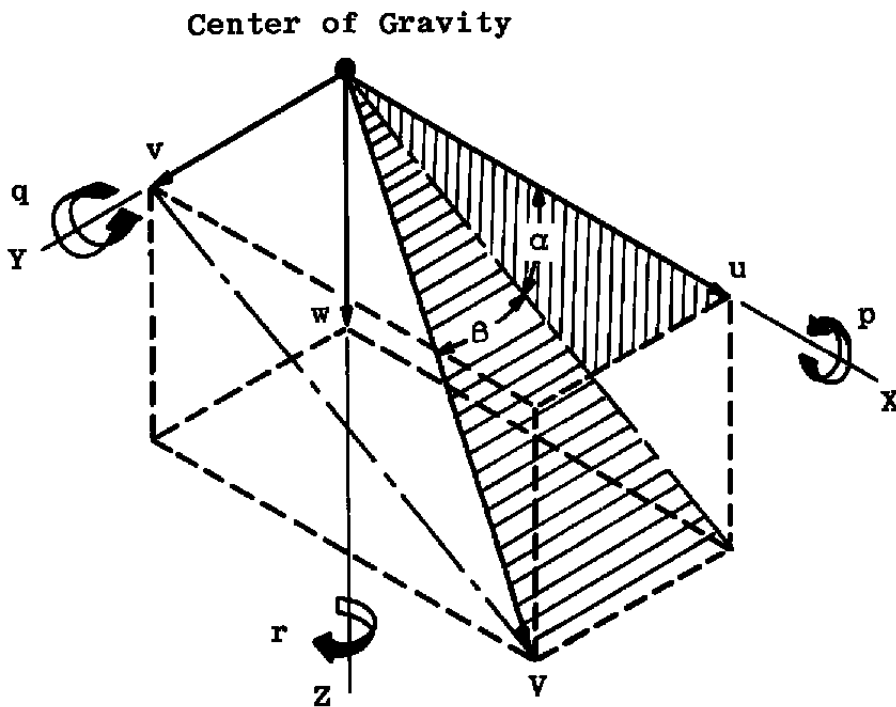


**Figure A-2. Body axial system.**

## NOMENCLATURE

BL	Buttline, in.
b	Wing span; model = 1.927 ft, full scale = 38.41 ft
$C_A$	Axial-force coefficient, measured axial-force/ $q_\infty S$
CG	Center-of-gravity location, percent chord
$C_L$	Centerline
$C_l$	Rolling-moment coefficient, rolling moment/ $q_\infty S b$
$C_{l_p}$	Derivative of rolling-moment coefficient with respect to roll rate, $\partial C_l / \partial (pb/2V)$ , per radian
$C_{l_r}$	Derivative of rolling-moment coefficient with respect to yaw rate, $\partial C_l / \partial (rb/2V)$ , per radian
$C_m$	Pitching-moment coefficient, pitching moment/ $q_\infty S b$
$C_{m_q}$	Derivative of pitching-moment coefficient with respect to pitch rate, $\partial C_m / \partial (q\bar{c}/2V)$ , per radian
$C_{m_{\dot{\alpha}}}$	Derivative of pitching moment with respect to $\dot{\alpha}$ , $\partial C_m / \partial (\dot{\alpha}\bar{c}/2V)$ , per radian
$C_N, C_Z$	Normal-force coefficient, ( $C_N = -C_Z$ ) normal force/ $q_\infty S$
$C_n$	Yawing-moment coefficient, yawing moment/ $q_\infty S b$
$C_{n_p}$	Derivative of yawing-moment coefficient with respect to roll rate, $\partial C_n / \partial (pb/2V)$ , per radian
$C_{n_r}$	Derivative of yawing-moment coefficient with respect to yaw rate, $\partial C_n / \partial (rb/2V)$ , per radian
$C_p$	Pressure coefficient, $p - P_\infty / q_\infty$
$C_X$	Longitudinal-force coefficient, longitudinal force/ $q_\infty S$
$C_{X_q}$	Derivative of longitudinal-force coefficient with respect to pitch rate, $\partial C_X / \partial (q\bar{c}/2V)$ , per radian
$C_Y$	Side-force coefficient, side force/ $q_\infty S$
$C_{Y_p}$	Derivative of side-force coefficient with respect to roll rate, $\partial C_Y / \partial (pb/2V)$ , per radian

$C_{Y_r}$	Derivative of side-force coefficient with respect to yaw rate, $\partial C_Y / \partial (rb/2V)$ , per radian
$C_{Z_q}$	Derivative of normal-force coefficient with respect to pitch rate, $\partial C_Z / \partial (q\bar{c}/2V)$ , per radian
$C_{Z_{\dot{\alpha}}}$	Derivative of normal-force coefficient with respect to $\dot{\alpha}$ , $\partial C_Z / \partial (\dot{\alpha}\bar{c}/2V)$ , per radian
$c$	Local wing chord
$\bar{c}$	Mean aerodynamic chord, scale model = 0.802 ft, full scale = 16.04 ft
$d$	Distance from thrust line to center of gravity, ft
FS	Fuselage station, in.
$F_X$	Force acting along X-body axis, lb
$F_Y$	Force acting along Y-body axis, lb
$F_Z$	Force acting along Z-body axis, lb
$g$	Acceleration due to gravity, ft/sec <sup>2</sup>
$h$	Altitude, ft
$I_X, I_Y, I_Z$	Moments of inertia about X-, Y-, and Z-body axes, respectively; slug-ft <sup>2</sup>
$I_{XZ}$	Product of inertia, slug-ft <sup>2</sup>
$M$	Mass, slugs
$M_X$	Moment acting about X-body axis, ft-lb
$M_Y$	Moment acting about Y-body axis, ft-lb
$M_{YT}$	Moment acting about Y-body axis caused by engine thrust, ft-lb
$M_Z$	Moment acting about Z-body axis, ft-lb
$M_\infty$	Free-stream Mach number
$p$	Local static pressure, psfa
$p, q, r$	Roll, pitch, and yaw rates about X-, Y-, and Z-body axes, respectively, radians/sec

$\dot{p}, \dot{q}, \dot{r}$	Roll, pitch, and yaw accelerations about X-, Y-, and Z-body axes, respectively; radians/sec <sup>2</sup>
$P_t$	Free-stream total pressure, psfa
$P_\infty$	Free-stream static pressure, psfa
$q_\infty$	Free-stream dynamic pressure, psf
$R_e$	Unit Reynolds number, per foot
$S$	Wing reference area; scale model = 1.325 ft <sup>2</sup> ; full scale = 538.34 ft <sup>2</sup>
$T$	Engine thrust, lb
$T_x$	Component of thrust along X-body axis, lb
$T_z$	Component of thrust along Z-body axis, lb
$u, v, w$	Components of total velocity along X-, Y-, and Z-body axes, respectively; ft/sec
$V$	Total velocity, ft/sec
$WL$	Waterline, in.
$X, Y, Z$	Body axes
$x, y, z$	Linear distance along X-, Y-, and Z-body axes, respectively, ft
$x/c$	Fraction of wing chord measured from the leading edge
$y/c$	Fraction of wing chord measured vertically from chord line
$\alpha$	Angle of attack referenced to model waterline, deg
$\beta$	Angle of sideslip, deg
$\beta_M$	Angle of sideslip at which hysteresis is present, deg
$\delta_a$	Aileron deflection (positive when trailing edge of right aileron is down), deg
$\delta_H$	Stabilator deflection (positive when trailing edge is down), deg
$\delta_r$	Rudder deflection (positive when trailing edge is left), deg
$\epsilon$	Angle between thrust line and X-body axis, deg

$\theta$	Angle between X-body axis and horizontal measured in vertical plane, deg
$\Delta C_{rH}$	Incremental rolling-moment coefficient attributable to hysteresis, incremental rolling moment/ $q_{\infty} S_b$
$\phi$	Angle between Y-body axis and horizontal measured in vertical plane, deg
$\psi$	Angle between Y-body axis and vertical measured in a horizontal plane, deg

# **SUBSCRIPT**

- Derivative with respect to time